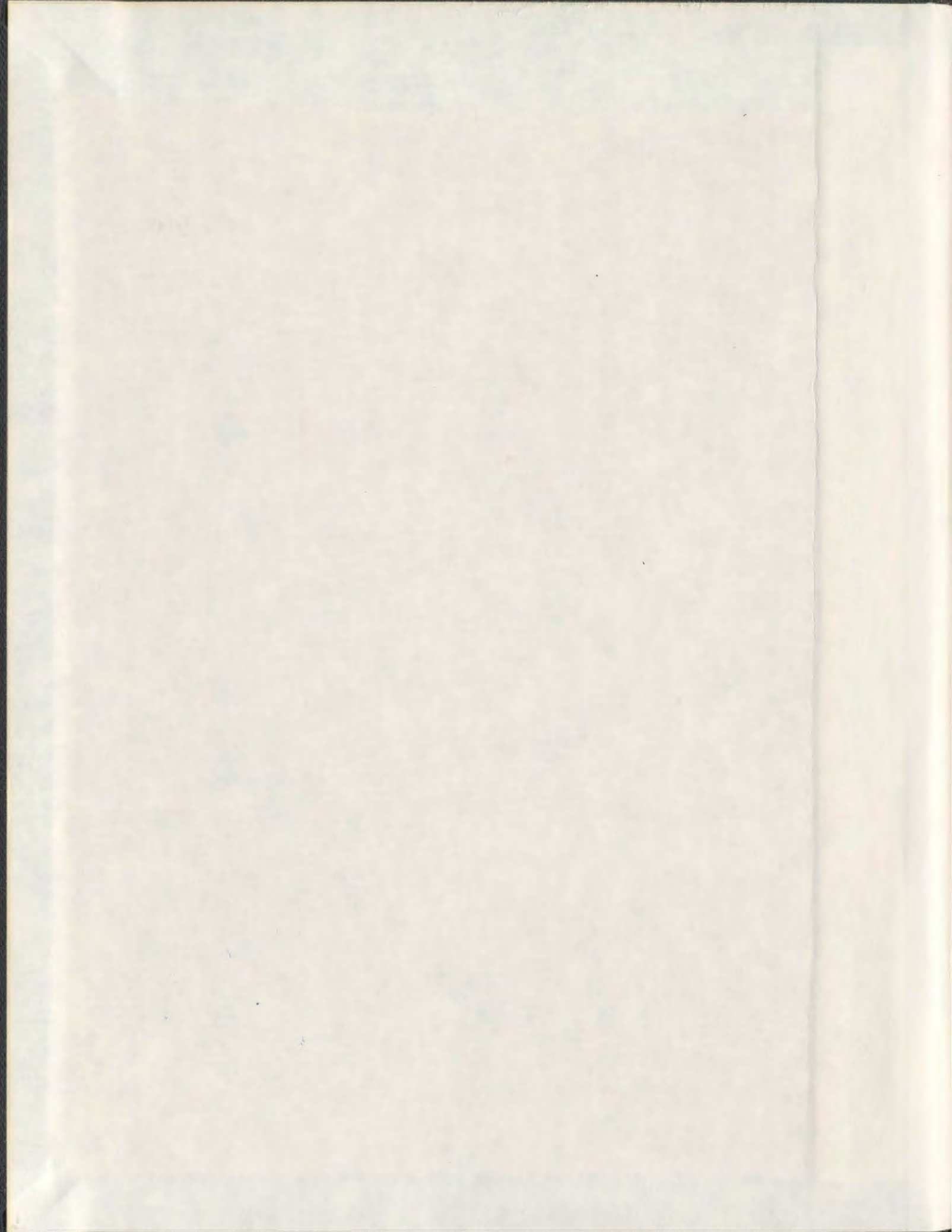
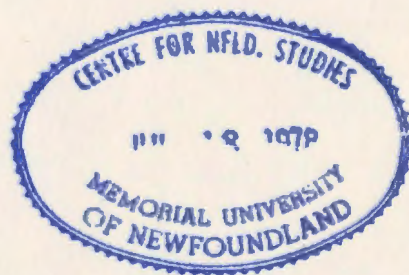


THE DEVELOPMENT OF NOVEL MARINE
COMMUNICATIONS CHANNEL MODELS USING
THEORETICALLY-BASED AND NUMERICAL
ELECTROMAGNETIC SIMULATION METHODS

IAN TIMMINS



001311



**The Development of Novel Marine
Communications Channel Models Using
Theoretically-Based and Numerical
Electromagnetic Simulation Methods**

by

©Ian Timmins

B.Sc., McMaster University, Hamilton, Ontario (1997)
M.Eng., McMaster University, Hamilton, Ontario (1999)

A thesis submitted to the
School of Graduate Studies
in partial fulfillment of the
requirements for the degree of
Doctor of Philosophy

Faculty of Engineering and Applied Science
Memorial University of Newfoundland

October 2010

St. John's

Newfoundland

The Development of Novel Marine Communications Channel Models Using Theoretically-Based and Numerical Electromagnetic Simulation Methods

by

Ian Timmins

Abstract

Maritime communications is fast becoming a growing area of interest. Use of a "commercial-off-the-shelf" (COTS) integration approach to system design, increasing interest in maritime security and demanding bandwidth requirements of sensors make understanding the effects of the sea on the communications channel an important design consideration when developing reliable and high bandwidth communications links. Conventional VHF communications are being replaced with SATCOM and cellular technologies for a variety of vehicular, sensor, life craft, and survival suit systems. Considering this occurrence, the marine communications channel and the effects of the sea surface have remained an area of limited study, particularly in comparison to the efforts placed on research for terrestrially-based communications channels. Urban environments, mountainous terrain, seasonal issues, and foliage are well studied in regard to effects on communications channels. To support design of systems for marine applications, the contribution of this research effort is the development of communications channel models by novel theoretical and numerical method-

ologies. The results of these efforts are models suitable for use in quantifying sea surface shadowing effects on communication channel performance in fully developed deep sea locations.

First, a theoretically-based marine geometrical theory of diffraction (Marine GTD) model is developed, whereby a diffraction methodology is devised specifically for single sea surface waves. For this segment, a sea surface wave is considered as an obstructing object between transmitter and receiver creating a shadowing condition. The physical sea surface attributes are studied using the modified Pierson-Moskowitz model for the north North Atlantic such that a novel Geometrical Theory of Diffraction wedge is synthesized based exclusively upon sea surface height. The wedge is thus physically representative of a fully-developed deep sea surface wave, and may be used to estimate diffraction loss. Complete formulations of the generalized model are given such that path loss effects due to diffraction are easily determined requiring only the height of the sea and the positions of the transmitter and receiver.

Second, a marine communications channel modeling methodology is developed using transient electromagnetic simulation methods to simulate overwater propagation of VHF to 3 GHz signals above a realistic fully developed random deep sea surface. The field of computational electromagnetics is focused upon use of numerical methods to obtain solutions to Maxwell's equations for problems not addressed easily analytically, or for which no analytic solution is possible. This is very much the case with the marine propagation environment. The complexity of the sea sur-

face makes analytical solutions extremely difficult, and the stochastic nature of the surface makes detailed knowledge of the sea over the entire physical channel at the precise time of measurement nearly impossible. The proposed methodology of using the Finite Difference - Time Domain (FDTD) method allows high accuracy propagation analysis over a well-known realistic random sea surface. In the post analysis segment of the FDTD simulation effort, conventional wireless communications channel measurement analysis methods are applied to characterize channel performance using the path loss equation. This proposed methodology solves the key historical problem of conducting marine propagation studies. Specifically, propagation analysis can hereafter be conducted whereby detailed knowledge of the sea surface over which propagation occurs is readily available. From the collective analysis of multiple communications channels consisting of various random sea surfaces, novel parameterized channel models are developed. The end result of the numerical segment of this research is compact generalized models that are functions of both frequency and wave height that quantify marine communications channel performance during sea surface shadowing conditions.

For both analytical and numerical methods, the Pierson-Moskowitz sea surface spectral functions are used to develop the required sea surface physical profile and subsequent random sea surfaces. Although this research effort has been conducted in support of the application of Unmanned Aerial Vehicles for maritime surveillance, the proposed methods may be used to estimate channel performance for any wire-

less technology operating in the marine environment, however, the Pieron-Moskowitz model is regionally specific to the north North Atlantic. The results are suitable within that geography for circumstances as outlined per the channel topology with considerations to the frequency limitations of the geometrical theory of diffraction and the conducted FDTD simulations. Both models are verified for validity by direct comparison to the well-known analytic knife edge diffraction model.

Acknowledgements

The author wishes to thank Dr. Siu O'Young for his support and guidance through this process.

The members of the RAVEN project at Memorial have been key in the support and execution of this endeavor, including Ronnie Lewis, Jim Millan, Mark Brophy, Jon Stevenson, Scott Xiang Fang and others.

I would also like to extend my thanks to the Supervisory Committee, and the Examination Committee, for their comments and feedback which have contributed to the end result of this research effort.

Most of all, I would like to thank my family, specifically my father, mother, brother and sister for their continued support.

List of Symbols

<i>FDTD</i>	Finite Difference - Time Domain
<i>AIS</i>	Automatic Identification System
<i>h</i>	Observable Sea Height
<i>t</i>	Time
<i>N</i>	Wedge Parameter
<i>H_s</i>	Significant Sea Height
<i>MoM</i>	Method of Moments
<i>GTD</i>	Geometrical Theory of Diffraction
<i>PM</i>	Pierson-Moskowitz
<i>V</i>	Windspeed at 19.4 m above the sea surface
<i>k</i>	Wavenumber
<i>g</i>	Acceleration due to gravity
λ	Wavelength
<i>E_{KE}</i>	Field at the RX location of the KE diffraction
<i>d₁</i>	Distance from TX to the KE/Marine GTD Peak Base
<i>d₂</i>	Distance from the KE/Marine GTD Peak Base to RX
<i>D</i>	Diffraction Coefficient
<i>s</i>	Distance from TX to the GTD Peak
<i>s'</i>	Distance from the GTD Peak to RX
<i>DFT</i>	Discrete Fourier Transform
<i>L_d</i>	Physical length of a sea surface wave
<i>QW</i>	Quarter wedge angle
<i>EW</i>	Exterior wedge angle
<i>n</i>	Wedge attribute pertaining to the GTD geometry
<i>L_s</i>	Link Budget Loss
<i>G_T</i>	Gain of Transmit Antenna

G_R	Gain of Receive Antenna
S_{RX}	Noise Factor of Receiver
Ω_t	Transmitted Power
M_{shad}	Link budget shadowing allowance
L_I	Link budget interferrance allowance
G_{HO}	Link budget hand-off gain
n	Path Loss Exponent
X_σ	Zero Mean Gaussian Random Variable Contributing to Path Loss
σ	Standard Deviation of X_σ
K	Rice Factor
MXS	Mean Excess Delay
RMS	Root Mean Square Delay
α_k	Multipath component magnitude
τ_k	Multipath component delay
\vec{E}	Electric field intensity (V/m)
\vec{H}	Magnetic field intensity (A/m)
\vec{D}	Electric flux density (Coul/m ²)
\vec{B}	Magnetic flux density (Wb/m ²)
\vec{M}	Magnetic current density (A/m ²) (Fictitious)
\vec{J}	Electric current density (V/m ²)
μ_o	permiability of free space
ϵ_o	permativity of free space
ρ	Electric charge density (Coul/m ³)
BW	Bandwidth

List of Abbreviations

<i>FDTD</i>	Finite Difference - Time Domain
<i>AIS</i>	Automatic Identification System
<i>MoM</i>	Method of Moments
<i>GTD</i>	Geometrical Theory of Diffraction
<i>PM</i>	Pierson-Moskowitz
<i>DFT</i>	Discrete Fourier Transform
<i>IDFT</i>	Inverse Discrete Fourier Transform
<i>MXS</i>	Mean Excess Delay
<i>RMS</i>	Root Mean Square Delay
<i>BW</i>	Bandwidth
<i>VHF</i>	Very High Frequency
<i>RF</i>	Radio Frequency
<i>KE</i>	Knife Edge
<i>TX</i>	Transmitter
<i>RX</i>	Receiver
<i>PCB</i>	Printed Circuit Board
<i>UAV</i>	Unmanned Aerial Vehicle

Contents

Abstract	iv
Acknowledgement	v
List of Symbols	vii
List of Abbreviations	viii
Contents	ix
List of Figures	xii
List of Tables	xx
1 Introduction	1
2 Literature Review	11
3 Marine Geometrical Theory of Diffraction	18
3.1 Theoretical Development of a Marine Propagation Channel Model . .	18
3.2 Pierson-Moskowitz Model Examination for Wave Physical Attributes	20
3.3 Overview of the Knife Edge and Conventional Geometrical Theory of Diffraction Models	22
3.4 Synthesis of the Diffraction Coefficient for the Marine GTD	27
3.5 Finalized form of the novel Marine Geometrical Theory of Diffraction	40

4	Marine GTD Numerical Results	42
4.1	Marine GTD and Knife Edge Comparison	42
4.2	Marine GTD Evaluation Summary	44
5	The Practice of Channel Modeling	48
5.1	Overview	48
5.2	Ideal Propagation in Free Space	50
5.3	Mobile Radio and Propagation in Terrestrial Environments	51
5.4	Large Scale Fading (Shadowing)	54
5.5	Small Scale Fading and Subsequent Transient Channel Effects	56
5.6	Summary of Channel Modeling Concepts	59
6	Development of a Novel Marine Electromagnetic Propagation Analysis Tool	60
6.1	The History of EM Simulation	60
6.2	Formulation of the Finite Difference - Time Domain Problem	65
6.3	Finite Elements of Space and Time	71
6.4	The Specifics of the north North Atlantic Ocean	75
6.5	Generating A Random Sea Surface as a Physical Channel Model Component	77
6.6	Shadowing Study Boundary Forcing Function	80
6.7	Input Pulse & Simulation Bandwidth	82
6.8	EM Simulation Development Summary	85
7	Knife Edge Validation of FDTD Simulation Engine	88
7.1	Validation of the FDTD EM Simulation Tool by Analytic Knife Edge Diffraction and Free Space Propagation Analysis	88
7.2	Numerical Knife Edge Diffraction Analysis	89
7.3	Validation of the FDTD EM Simulation by Propagation in Free Space	91
7.4	Knife Edge and Free Space Validation Summary	102

8 FDTD Marine Communications Channel Propagation Analysis and Modeling Results	105
8.1 Overview	105
8.2 Sea Surface Shadowing Propagation Analysis for Path Loss Evaluation and Frequency Domain Model Development	108
8.3 Sea Surface Shadowing Transient Analysis & Model Development . .	134
8.4 Inshore Measurement Outline	140
9 Conclusion	149
List of References	154

List of Figures

1-1	Theoretically-based model development.	9
1-2	Marine overwater propagation analysis methodology using the FDTD method.	10
3-1	Measured data of the significant wave height vs. wind speed off the coast of Newfoundland at the tail of the Grand Banks during the 1990 - 2007 time period.	22
3-2	Measured data of the significant wave height vs. peak period off the coast of Newfoundland at the tail of the Grand Banks during the 1990 - 2007 time period.	23
3-3	The knife edge topology.	24
3-4	The geometrical theory of diffraction topology.	26
3-5	Applying the GTD to the Sea Surface.	28
3-6	The modified Pierson Moskowitz spectral functions for increasing wave height.	29
3-7	Modified PM sea surface wave temporal point displacement.	30
3-8	Sea surface displacement for increasing wave height.	31
3-9	Period as a function of sea surface height.	32
3-10	Pierson-Moskowitz single sea surface wave form envelope.	33
3-11	Pierson-Moskowitz single waves.	34
3-12	Pierson-Moskowitz waveform envelope first derivatives.	35
3-13	Single Pierson-Moskowitz waveform envelope second derivatives.	36

3-14	PM single wave distance to 1st minimum.	36
3-15	Quarter Wedge Angle (QW) vs. Observable Wave Height.	37
3-16	Quarter Wedge angle and Polynomial Fitting Function (Blue) vs. Observable Wave Height.	37
3-17	Exterior Wedge angle (EW) vs. Observable Wave Height.	38
3-18	Exterior Wedge angle (EW) and Polynomial Fitting Function (Blue) vs. Observable Wave Height.	38
3-19	n for the calculated wedge representing a single sea surface wave vs. Observable Wave Height.	39
3-20	n and the Polynomial Fitting Function (Blue) vs. Observable Wave Height.	39
4-1	Proposed Marine GTD evaluation topology.	43
4-2	Marine GTD Diffraction Coefficient vs. Frequency.	43
4-3	KE and Marine GTD diffraction of a 25 m wave for perpendicular polarization.	44
4-4	KE and Marine GTD diffraction of a 25 m wave for parallel polarization.	45
4-5	Perpendicular and Parallel Marine GTD diffraction coefficients for a 10 m wave.	46
4-6	KE and Marine GTD diffraction loss of a 10 m wave for parallel polarization.	47
4-7	KE and Marine GTD diffraction loss of a 10 m wave for perpendicular polarization.	47
5-1	2-dimensional Electromagnetic Free Space Propagation Simulation	50
5-2	For a single narrow impulse, the time domain response of a channel is both time variant and dispersive.	57
6-1	The "leapfrog" modeling approach to the finite difference technique, illustrating the E and H fields interleaved in both time and space.	68

6-2	The 3-dimensional Yee cell illustrating the orientation of the \vec{E} and \vec{H} fields.	69
6-3	The stationary random Gaussian process has produced an arbitrary sea surface based on the modified Pierson-Moskowitz spectral functions as a function of time.	78
6-4	Sea surface boundary condition mask for the finite difference grid, implementing the sea surface boundary condition during the FDTD simulation.	79
6-5	The proposed Boundary Forcing Function (BFF) used for shadowing study of ocean waves, forcing the outer limits of the sea surface to nil wave height in an exponentially decaying fashion.	81
6-6	A sea surface boundary condition before application of the proposed boundary forcing function.	82
6-7	The same sea surface boundary condition after application of the proposed boundary forcing function.	83
6-8	Transient illustration of a Gaussian pulse with approximately 1 ns rise time.	84
6-9	Normalized spectral content of a Gaussian pulse with approximately 1 ns rise time.	85
6-10	Transient illustration of a Gaussian pulse with approximately 300 ps rise time.	86
6-11	Normalized spectral content of a Gaussian pulse with approximately 300 ps rise time.	87
7-1	The knife edge topology	89
7-2	FDTD boundary condition knife edge mask. The knife edge topology is also illustrated for clarity.	91
7-3	5.625 m knife edge diffraction FDTD and analytic results.	92
7-4	7.967 m knife edge diffraction FDTD and analytic results.	93

7-5	10.313 m knife edge diffraction FDTD and analytic results.	94
7-6	Free space FDTD simulation 20 % completed.	95
7-7	Free space FDTD simulation 40 % completed.	96
7-8	Free space FDTD simulation 60 % completed.	97
7-9	Free space FDTD Gaussian excitation pulse.	97
7-10	Free space FDTD received pulse.	98
7-11	Free space FDTD received pulse.	98
7-12	Globalstar (2.492 GHz) transmission loss through free space.	99
7-13	Iridium (1.621 GHz) transmission loss through free space.	99
7-14	AIS (162 MHz) transmission loss through free space.	100
7-15	Linear regression analysis of Globalstar (2.492 GHz) transmission loss through free space.	101
7-16	Linear regression analysis of Iridium (1.621 GHz) transmission loss through free space.	102
7-17	Linear regression analysis of AIS (162 MHz) transmission loss through free space.	103
7-18	Free space path loss exponent linear regression analysis summary. . .	103
8-1	Sea surface shadowing condition communications channel topology. .	109
8-2	Gaussian excitation pulse for the FDTD shadowing study.	110
8-3	Spectral content of the Gaussian excitation pulse.	110
8-4	Pierson Moskowitz spectral content for a single wave of a specified significant sea surface height.	111
8-5	Single sea surface wave obtained through DFT of Pierson Moskowitz spectral functions.	111
8-6	Sea surface subsection implemented as a boundary condition during propagation analysis.	112
8-7	Transient response at the RX location for a random sea surface simu- lation.	113

8-8	Transient response at the RX location for a random sea surface simulation.	114
8-9	Transient response at the RX location for a random sea surface simulation.	114
8-10	E_z field at 20 % completed simulation.	115
8-11	E_z field at 40 % completed simulation.	115
8-12	E_z field at 60 % completed simulation.	116
8-13	System transfer function between a TX and an RX location over a random sea surface showing attenuation from VHF to 3 GHz.	117
8-14	System transfer function between a TX and an RX location over a random sea surface showing attenuation from VHF to 3 GHz.	118
8-15	Path Loss between TX and RX locations for 433 MHz.	119
8-16	Path Loss between TX and RX locations for 1.621 GHz.	119
8-17	Path Loss between TX and RX locations for 2.492 GHz.	120
8-18	A localized region of optimization used for determining the path loss exponent and standard deviation.	121
8-19	A localized region of optimization used for determining the path loss exponent and standard deviation.	121
8-20	Path Loss Exponent vs. Observable Wave Height for 162 MHz with 95% confidence bounds.	122
8-21	Path Loss Exponent vs. Observable Wave Height for 433 MHz with 95% confidence bounds.	122
8-22	Path Loss Exponent vs. Observable Wave Height for 913 MHz with 95% confidence bounds.	123
8-23	Path Loss Exponent vs. Observable Wave Height for 1.62 GHz with 95% confidence bounds.	123
8-24	Path Loss Exponent vs. Observable Wave Height for 1.8 GHz with 95% confidence bounds.	124

8-25 Path Loss Exponent vs. Observable Wave Height for 2.5 GHz with 95% confidence bounds.	124
8-26 Path Loss Exponent vs. Observable Wave Height for 3.0 GHz with 95% confidence bounds.	125
8-27 Loss exponent linear regression analysis summary.	125
8-28 Path Loss Exponent per Wave Height (LE/m) vs. Frequency (GHz).	126
8-29 Path Loss Exponent per Wave Height (LE/m) vs. Log10(Frequency) (GHz) with 95% confidence bounds.	127
8-30 Standard Deviation vs. Observable Wave Height for 162 MHz with 95% confidence bounds.	128
8-31 Standard Deviation vs. Observable Wave Height for 433 MHz with 95% confidence bounds.	128
8-32 Standard Deviation vs. Observable Wave Height for 913 MHz with 95% confidence bounds.	129
8-33 Standard Deviation vs. Observable Wave Height for 1.62 GHz with 95% confidence bounds.	129
8-34 Standard Deviation vs. Observable Wave Height for 1.8 GHz with 95% confidence bounds.	130
8-35 Standard Deviation vs. Observable Wave Height for 2.5 GHz with 95% confidence bounds.	130
8-36 Standard Deviation vs. Observable Wave Height for 3.0 GHz with 95% confidence bounds.	131
8-37 Standard deviation linear regression analysis summary.	131
8-38 Shadowing study data set obtained through FDTD simulation for various randomly generated sea surfaces.	132
8-39 Standard Deviation per Wave Height (LE/m) vs. Frequency (GHz).	133
8-40 10 dB Delay Profile versus Observable Wave Height and corresponding data fit along with 95% statistical confidence bounds.	134

8-41	15 dB Delay Profile versus Observable Wave Height and corresponding data fit along with 95% statistical confidence bounds.	135
8-42	20 dB Delay Profile versus Observable Wave Height and corresponding data fit along with 95% statistical confidence bounds.	135
8-43	Linear Regression Analysis for delay profiles at 10 dB, 15 dB and 20 dB. The standard error, k , is given for a 95% statistical confidence level with respective lower and upper bounds.	136
8-44	Mean Excess Delay versus Observable Wave Height and corresponding linear regression analysis. The standard error for a 95% statistical confidence level is given with respective lower and upper bounds. . . .	137
8-45	Root Mean Square delay versus Observable Wave Height and corresponding linear regression analysis. The standard error for a 95% statistical confidence level is given with respective lower and upper bounds.	137
8-46	K factor versus sea height, and corresponding data fit function. The 95% lower and upper bounds are given.	138
8-47	Linear regression analysis summary for the mean excess, root mean square and Rice factor.	139
8-48	The gorge over which the transmitter (left peak) and receiver (right peak) are positioned for measurements.	141
8-49	A second perspective of the transmitter location above the communications channel.	142
8-50	The high gain RX Yagi antenna is fixed pointed at the transmitter location. The TX antenna is identical, located at the other side of the inlet.	142
8-51	An instantaneous random sea surface.	143
8-52	An second instantaneous random sea surface.	144
8-53	An third instantaneous random sea surface.	144

8-54	The 1 meter land based measurement used for standard calibration procedure of the path loss measurement.	146
8-55	Measured power and standard deviation of land calibration.	146
8-56	Measured Power and standard deviation of the fixed inlet link for 0.3 m and 1.0 m observable wave heights.	146
8-57	Standard deviation increase for the fixed inlet link at 0.3 m and 1.0 m observable wave heights calibration adjusted.	147
8-58	The raw standard deviation for the .3 m, 1 m observable wave heights compared to the standard deviation observed during the land based calibration process.	148
8-59	The standard deviation increase for the .3 m and 1 m observable wave heights adjusted by calibration results.	148

List of Tables

- 6.1 The sea state/observed wave height probability by for the North Atlantic, the north North Atlantic compared to worldwide locations. . 76

Chapter 1

Introduction

This research thrust is conducted to further understanding of the marine communications channel. This work presents two novel methodologies to model marine communications channel performance. A theoretically-based extension of the geometrical theory of diffraction (GTD), hereafter referred to as the marine geometric theory of diffraction (Marine GTD), will be given such that the diffraction around a fully developed single sea surface wave can be quantified based on the observable wave height and the positions of the transmitter and receiver. Second, a numerical methodology for marine propagation analysis is proposed and developed based on the Finite Difference - Time Domain (FDTD) method [1]. The FDTD approach overcomes the single most difficult aspect inhibiting the study of over water propagation. The proposed methodology allows propagation analysis to be conducted while retaining detailed knowledge of the sea surface over which the propagation occurs. This is accomplished by implementing a realistic random sea surface synthesized using the well-known Pierson-Moskowitz spectral functions whereby the sea surface functions as a perfect conducting boundary condition for the transient electromagnetic simulation. Post simulation analysis for a variety of random sea surfaces has produced novel models characterizing communications channel performance as functions of frequency and sea surface height in the north North Atlantic region. The models are valid from

VHF to 3 GHz and for sea surface waves up to 14 m. Comparison of the marine geometrical theory of diffraction to the well-known knife edge method of diffraction analysis is given, and the validation of the EM simulation tool in regard to the ability to accurately perform diffraction analysis is established by numerical simulation of a knife edge topology and then directly compared to the analytical knife edge equation for the same physical topology.

Increasing interest in maritime security is a global occurrence as acts of terrorism and piracy are commonly cited in the news. To increase situational awareness, modern sensors and video surveillance are finding implementation in the marine environment [2]. Life craft and life suits are also becoming increasingly sophisticated, incorporating transponders and communications equipment to assist mariners in the event of emergency. This research effort offers direct insight into application of wireless communications devices and their effectiveness in various sea state conditions when used specifically for such purpose. In support of such applications, it is necessary to increase understanding of the sea on marine communications channel and furthermore quantify the limitations of the "COTS integration" approach of system design in an accurate fashion. Channel performance estimation is an important design consideration and a fundamental step in the architecture and design process of every wireless system. For developing reliable and high bandwidth technologies for marine applications, this effort is focused on obtaining communications channel understanding specifically for the marine environment, such that the same design process can be used for marine applications as is used for terrestrially-based systems.

Conventional VHF communications links are being replaced with SATCOM [3],[4] and cellular technologies for a variety of vehicular, sensor, life craft, and survival suit systems [5]. This research thrust has been a supporting effort to an Unmanned Aerial Vehicles (UAV) program whereby efforts to control the vehicle using satellite communications systems is of concern during maritime surveillance operations [6]. The interest is driven for UAVs by a decrease in advanced modern computing and sensor

costs, whereby the sophisticated and costly systems of a previous generation of technology are widely available as low cost or even commodity products [7]. More often, these new systems are dependent upon a data uplink provided by cellular or satellite communications infrastructure. Current communications technology is a fundamental technology gap [8], [2] for the application of UAVs for general aviation purposes by the Federal Aviation Administration (FAA). Generally speaking, loss of communications link is perceived as loss of control of the vehicle. Visibility and transmission elevation angles are of particular concern when relying on a satellite communications network [9],[10]. Prediction algorithms have been devised to overcome outage and delay limitations of communications links [11] but prevention of link loss is ultimately the prime objective for vehicular control and safety. Multipath effects, a common source of outages, in wireless channels cannot be adaptively controlled in the same manner that transmission line system paths can be specified [12],[13] nor can reflections in the wireless channel be directly compensated as in PCB (printed circuit board) communications channels [14],[15] to offset adverse analog effects. The proposed methodologies developed in this work provide insight into the fading and shadowing effects that are often the cause of communication link loss. Understanding the communications channel is fundamental to understanding the limitations of the communications system for UAVs as well as any marine surface vessel or sensor. The objective of this research thrust is two fold. First, to develop a theoretically-based model to quantify sea surface shadow effects suitable for marine applications, and second, to devise a unique methodology using highly accurate numerical methods for computational electromagnetics to conduct overwater propagation analysis during sea surface shadowing conditions. Both these approaches have produced generalized performance models relevant to propagation in the marine communications channel. The models are practical and suitable for quantifying shadowing effects and benefit the link budget calculation component of the system design process.

The process of communications channel model development is significantly differ-

ent than those used for conventional RF circuit model development [16], [17], [18]. Considering the importance in understanding the effects of the sea surface on the reliability and performance of the wireless communications link, the marine communications channel and the effects of the sea surface have remained an area of limited study, particularly in comparison to the effort placed on research for terrestrially-based communications channels [19],[20],[21]. This aspect of maritime communications is stated explicitly by Ohmori [22] in 1985, when at that time it was cited that there were no investigations into fading effects and relations between the wave height and frequency, and furthermore obtaining such understanding would be highly desirable. Urban environments, mountainous terrain, seasonal issues, and foliage have all been heavily studied in regard to effect on wireless communications channels. Shadowing effects [23] in common terrestrial environments [24] is a problem that every mobile user is familiar with. However, solutions to these problems, such as fixed distributed antennas systems (DAS) [25] in the urban environment, are often not well suited to marine vessel or aircraft applications to mitigate sea surface shadowing conditions. Systems must be designed to operate within their respective environmental conditions.

Propagation analysis and channel modeling are conducted by one of two mechanisms. First, analytical and theoretical models which use fundamental theory to establish propagation effects serve as a common estimation means of channel performance. The knife edge model is a typical example of this approach [23]. Though the topologies of such models are not fully representative of the physical communications channel of interest, they often serve as reasonable approximations. Second, measurement of an actual channel for performance to develop a model independent of the physical structure is often accomplished using the path loss equation [26]. This method offers generalized parameters, such as the path loss exponent and standard deviation of power fading regardless of the physical channel topology. The parameters of the path loss equation are universal and well understood, as they provide insight into the typical behavior of a communications channel as propagation occurs.

The models are often developed based on regional studies, such as specific cities, or rural areas. Hata [19] devised one of the most utilized models for various urban environments based on this approach. This work will focus directly on marine communications with a methodology for numerical characterization of the path loss equation for various sea surface conditions for the north North Atlantic region. Through this work the prime historical difficulty that has inhibited the study of the marine channel is overcome through EM simulation. This method provides the unique advantage of conducting propagation analysis over a realistic sea surface for which the details of the physical attributes are fully known. Such details during previous measurement agendas [27] were not available, and the respective lack of knowledge was cited as a limiting factor during previous measurement efforts [22].

For the theoretically-based model development component of this work, a sea surface wave is considered as an obstructing object between transmitter and receiver, creating a shadowing condition. A path loss model is created to quantify marine communications channel diffraction effects as the peak of the waveform envelope is modeled as a perfectly conducting wedge typical of the geometrical theory of diffraction (GTD). Synthesis of the model begins by establishing that the single relevant parameter that effect the spectral content of the fully developed sea surface is exclusively the significant sea height. Theoretical analysis is demonstrated on the Pierson-Moskowitz spectral model [28] for the north North Atlantic region to eliminate the wind speed from the accepted form of the spectral functions. Analysis is conducted to establish the most appropriate approximation of a single sea surface wave such that it is effectively represented by an obstructing wedge as prescribed by the GTD [29]. Establishing the parameter models of the sea surface, and subsequently the establishment of a synthesis method for the GTD wedge, produces a novel and efficient extension of the GTD methodology for marine propagation analysis results that requires no knowledge of the sea surface with the exception of the sea surface height. The result and major theoretically-based contribution is the extension of the

GTD, the marine geometrical theory of diffraction, and its complete formulation for diffraction analysis may be easily implemented for estimation of sea surface shadowing effects in a marine communications channel for any wireless communications application.

The second significant contribution of this research effort is the development of an EM simulation methodology for marine communications channel overwater propagation analysis [1] using the Finite Difference - Time Domain method [30]. This approach, overcomes the inadequacies of the theoretical modeling approach by using highly accurate numerical methods to solve propagation effects of a random sea surface, thus producing results based on a realistic channel boundary condition. Typically, inadequacies in the theoretical models are the driving force behind conducting extensive measurement agendas for channel characterization of propagation environments. Numerical methods are often used to solve problems for which an analytic result is not possible or not easily attainable. This proposed method attempts to accomplish two objectives. First, to provide high accuracy analysis of overwater propagation for a known random sea surface during shadowing conditions. Second, to use the population of data analysis to produce generalized formulae of key performance parameters based on physical attributes of the known sea surface [1]. The complex and random nature of the sea surface makes application of numerical methods a very appealing mechanism to studying overwater radio propagation.

The FDTD numerical simulation produces direct solutions to Maxwell's equations using a central difference approximation [30] during transient analysis. This approach will provide higher accuracy solutions as they are obtained directly from Maxwell's equations, particularly when compared to conventional propagation analysis methods such as ray tracing [23]. Ray tracing provides propagation analysis by explicitly evaluating signals reflecting from various surfaces in the physical propagation channel. Typically, it does not account for higher order phenomenon such as diffraction or scattering. Using the FDTD method will overcome this deficiency, and in the process

create two primary technical challenges. First, the FDTD technique requires a discrete element representation of the physical communications channel. Each of these discrete elements represents a physical location whereby EM field solutions are calculated. The size of the physical channel in application of the FDTD method is limited by available computer memory. In this case, the size of the channel is on the order of one hundred metres, and is designated in an attempt to maximize the length of the physical channel. Allocating length of channel is favored over height. For this type of modeling, the total finite difference grid is large in comparison to typical RF circuit applications of the FDTD method [31]. For distributed circuits, the analysis is generally conducted over only a few wavelengths of the relevant frequency. In the channel modeling case, the size of the structure is several hundred wavelengths. This aspect alone poses a challenge to the computational abilities of modern computers, specifically with lengthy computation times, as well as numerical effects such as dispersion that increase with total grid size. Similar studies investigating indoor wireless local area networks [32] have demonstrated obtaining direct solutions of Maxwell's equations for a communications channel is possible, however, in these cases the physical channel is on the order of only several metres, and furthermore the boundary conditions are typically well defined. The second primary challenge in the development of the marine communications channel propagation analysis tool is the synthesis of a random sea surface to be used as a boundary condition. For this case, the surface will be generated using the modified Pierson-Moskowitz (PM) spectral model [33]. Since the modified PM was developed for specific representation of the north North Atlantic sea surface, the post analysis results are specific to that region. However, this suffices for demonstration of the novel methodology, and any realistic sea surface model suitable for a different region can be used for other areas of interest. This synthesized sea surface is enforced during the numerical analysis as a perfectly conducting boundary from which detailed knowledge of the sea surface during propagation is retained and readily available during post simulation analysis.

Once the simulation engine is established, a shadowing study is conducted to numerically evaluate communications channel performance when the ocean surface obstructs line of sight between a transmitter and receiver. The software for this effort is a completely custom development based on the proposed methodology and implemented in Matlab. The software does not use any existing commercially or privately available products. The sea surface is generated for various significant wave heights, emulating a random sea surface existing in deep water [28]. Subsequent novel models obtained from post simulation analysis quantify shadowing effects for frequencies from 162 MHz to 3 GHz as a function of observable sea surface height. These models can be used directly in the link budget calculations for any marine communications system using a wireless communications link. Figure 1-1 illustrates the conceptual development and analysis required to produce the marine geometrical theory of diffraction (Marine GTD) for diffraction analysis due to sea surface obstruction between transmitter and receiver and Figure 1-2 shows the development agenda of the FDTD simulator for overwater propagation analysis based on obtaining highly accurate solutions to Maxwell's equations.

The structure of this thesis will first include a review of related and relevant previous works. This is followed by the development of the proposed theoretically-based marine geometrical theory of diffraction, which is an extension of the well-known GTD, whereby the perfectly conducting wedge is synthesized based on the physical attributes of a single sea surface wave. The results of the Marine GTD are compared to an equivalent topology using the knife edge model for verification and validation. This work is followed by the development of the FDTD simulation methodology. Overwater propagation analysis is conducted using a Pierson-Moskowitz random deep sea surface. The accuracy of the FDTD simulation engine is also established by simulation of a knife edge topology, providing direct comparison of the FDTD numerical propagation and diffraction results to be directly compared to the well established knife edge diffraction equation for common topologies. Numerical valida-

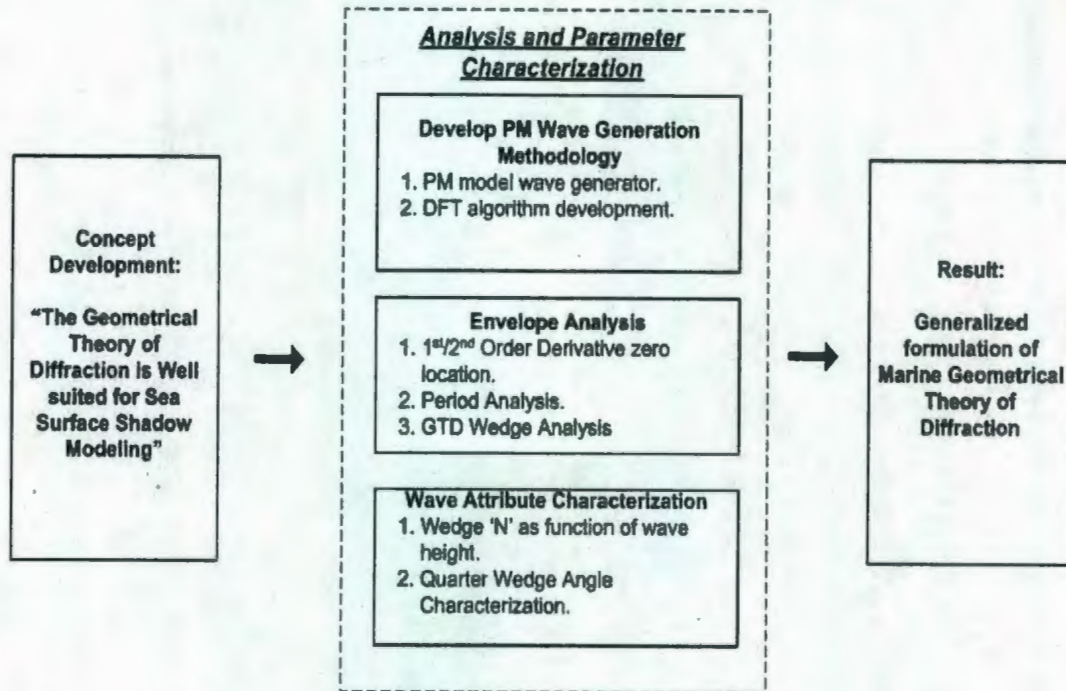


Figure 1-1: Theoretically-based model development.

tion of a simulation engine is often accomplished by simulation of analytical models, and this approach is used to verify the ability of the FDTD engine in conducting overwater propagation analysis during shadowing conditions by evaluation of knife edge diffraction loss. Propagation analysis using the FDTD transient simulation of various random sea surfaces is thereafter performed. Post simulation analysis of the numerical results for numerous random sea surface channels of various observable sea heights is used to synthesize general parameterized models for communications channel performance as functions of frequency and observable sea surface height. This includes path loss, standard deviation, mean excess delay, root mean square delay and rice factor. A brief measurement agenda is also performed at an inland location, between fixed transmitter and receiver. This measurement effort is not to validate all generalized models produced by the numerical study, but rather to support the general result that standard deviation of fading in the marine communications channel increases as sea height increases, which was suggested by the numerical results

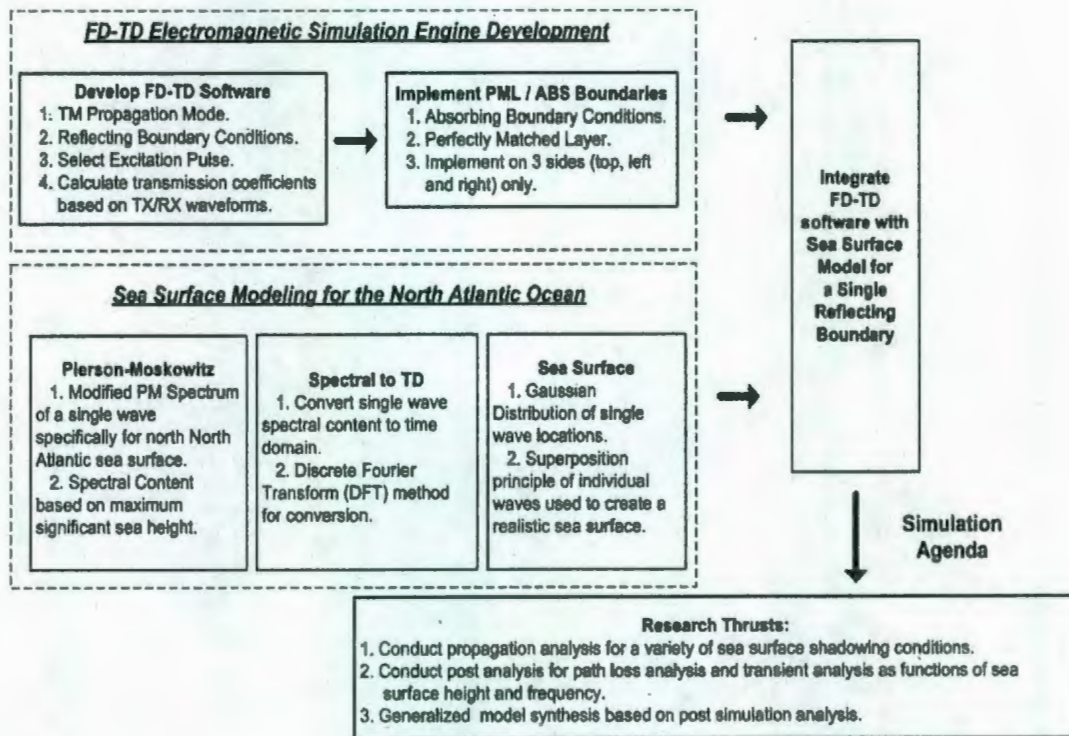


Figure 1-2: Marine overwater propagation analysis methodology using the FDTD method.

obtained for fully developed deep sea locations.

Chapter 2

Literature Review

The field of wireless communications is an extensive and well studied area, primarily because of the widespread use of commercial cellular systems. The application and subsequent research of this technology has been centered on supporting the typical end user. Terrestrially-based channel and propagation measurements for path loss studies are extremely common in published literature [34],[26],[35],[36], and [37]. Marine communications channel studies have had very few works conducted in comparison.

The lack of marine communications studies was stated explicitly by Ohmori [22] in 1985, when at that point in time there were no studies whatsoever in regard to the relations between the amount of fading and both the wave height and frequency. Although Ohmori's work demonstrated clear relationships between wave height and fading, it did not produce a generalized model suitable for wideband usage of channel performance as a function of both frequency and wave height. Furthermore, the study proceeded to state that the method of measurement of the sea surface during the experimental portion of their investigation was "objective." Another work by Karasawa [38] focused upon theoretical analysis of sea surface fading, also known as ducting, whereby the significance of the wave height was measured in regard to the level of fading. Unlike conventional transmission line communications systems that can be configured for distinct signal paths, [12],[13], the multipath effect in wireless marine

communications channels due to the sea surface can result in either a constructive or destructive effect and generally cannot be controlled. Karsawa's study resorted to statistical analysis as it investigated fading effects for maritime satellite communications. The importance of signal fade levels and quantifying the effect was cited in regard to the system design process. The degree of coherent and incoherent components in the transmission was of prime interest in this study. Once again, Karasawa's work did not produce a generic model suitable for usage in the link budget, and furthermore limited its studies to seas less than four metres in height. Other works state explicitly the difficulty of sea surface waveform measurements when conducting overwater communications channel measurements [39],[40]. Studies regarding the sea surface have previously focused on the coherent and incoherent signal components [41],[42] in which the fading is directly attributed to changes in the water surface [43]. Fresnel zones are often mentioned in these studies in regard to multipath effects, but are addressed only in concept and not in a quantitative fashion.

Channel modeling is typically accomplished by one of two mechanisms. First, analytical methods are employed to study propagation effects in proximity to ideal structures. This includes entities such as cylinders, spheres, or corners. One such common model for studying shadowing effects, or Fresnel zones, is known as knife edge diffraction [23], whereby an obstruction is approximated at the highest point by a straight perfectly conducting edge. Although this method provides fundamental understanding of underlying principles, very few structures within an actual physical propagation environment are well represented by such an ideal geometry. Pragmatically, the use of ideal structures in propagation analysis is typically for estimation by approximation of the genuine structure by an ideal equivalent. The second methodology commonly used for the study propagation effects is the development of the path loss model by direct measurement. Determining the generalized parameters of the path loss equation [44] results in a portable model of fixed form. The path loss equation is a generic representation of relevant parameters that is the defacto standard

to channel characterization through measurement. In this case, the relevant parameters do not provide any physical information about the propagation environment, but do provide pertinent information about what is experienced by signals propagating through the channel [45],[46]. Understanding of the path loss model is universal in the field of propagation analysis, and it's parameters give meaning to any propagation environment, with no need for physical knowledge of the channel whatsoever.

Each channel is unique in it's physical features, and typically channel performance is stochastic [47],[24]. For this reason relevant previous works towards the development of analytical methods and characterizing methods using the path loss equation will constitute a significant component of the literature review. As an alternative to a direct channel measurement approach, numerical methods will be developed and used in this work to conduct propagation analysis and provide characterization of the marine communications channel via the path loss equation [20]. Rappaport [44] is a key authority on this subject, and widely regarded as the leading expert in the field. For this effort the finite difference - time domain method will be used [30] in obtaining marine channel impulse responses such that evaluation of the parameters of the path loss equation for a known sea surface is possible. This approach is a novel methodology to conducting marine communication channel analysis and overwater propagation studies. It requires a sea surface boundary condition that retains detailed knowledge of the sea surface that would otherwise not be available during a measurement agenda [1],[48]. The best known formulation of a parameterized model based on measurement and which retains the form of the path loss equation was derived by Hata [19]. Developed for path loss estimation for a variety of terrestrial mobile communications channels, Hata's model was synthesized from measurements of various relevant physical parameters such as antenna height and frequency. Measurements were conducted in a number of geographic regions including urban, suburban and rural environments. The general form of Hata's model is heavily focused upon practical application for the link budget component of the system design process, and has retained prominent

significance in the field of mobile communications for terrestrial channels because of this practicality.

There are currently a limited number of papers in the IEEE database regarding EM simulation from a communications perspective focusing on marine applications [33],[49]. These studies focus specifically on the fading of a marine communications channel with respect to time. The efforts were conducted evaluating the fading effects of the marine communications channel using the method of moments approach of EM simulation [30]. Notably, in both of these cited studies the ocean surface is generated as a perfectly conducting surface. The uniqueness and difficulties of the marine communications channel are acknowledged by methods for mitigation of fading in a small number of publications [27],[50] regarding hardware design for surface vessels. Thus, the effects of channel degradation because of increased sea surface height is clearly a recognized phenomenon, yet compared to terrestrial channel fading, it is an understudied problem.

The concept of scattering from the ocean surface is, however, a well studied phenomenon from the perspective of radar systems [51],[52]. There have been numerous publications documenting backscatter at various frequencies of interest during various sea state conditions [53]. For example, a method of predicting wind conditions based on HF radar backscatter has been developed [54].

Modeling and synthesis of the random deep sea surface is a well known process [28]. In this case the modified Pierson-Moskowitz model for the north North Atlantic region is used, however any sea surface model would be applicable to the proposed methodology depending on the region of interest. For the subject of random sea surface generation, many of the recently published articles are focused on modern computer graphics rendering of sea surfaces [55]. These works demonstrate methods to render a realistically appearing sea surface for visual effects, whereby the actual spectral models developed by Pierson as a sea condition prediction tool are employed [28]. Although the study of the sea surface and scattering from the water surface is

a relatively mature field, the foundation of this work has not been for the purposes of communications channel characterization. This aspect makes this research effort a particularly unique endeavor.

The difference in all wireless communications channel studies is primarily the physical surroundings, or propagation environment, under which propagation effects are analyzed. For example, varying channel attributes such as antenna height or radiation pattern [20], as well as variations in the frequency of interest are controllable features of a propagation channel, whereas the effects of the environment for urban, suburban and rural areas [47],[24] tend to have drastically different effects on any wireless signals propagating in these regions. Regardless of these physical differences, the process of channel modeling to quantify the amount of attenuation, fading, and delay spread are all characterized in the same manner. These generalized parameters provide the system design or implementation engineers a generic language to directly compare the effects of the locale without knowing the details of the physical environment [56]. Understanding and quantifying the generalized behavior of path loss in cities, suburban or rural areas has been the historical focus [26],[35],[36] of research and measurement efforts. Moreover, path loss effects have attempted to characterize propagation in these regions also in proximity to specific terrain features common within those areas. This research effort attempts to add to this body of knowledge with the development of two novel methodologies of quantifying marine communications channel performance using theoretically-based and numerically-based models, such that diffraction effects experienced during sea surface shadowing conditions can be easily quantified in a manner that is pragmatic to the system level designer.

The geometrical theory of diffraction was developed in the mid-1970s by Kouyoumjian and Pathak [57] for high frequency diffraction analysis of an electromagnetic wave obliquely incident upon a smooth curved surface. The work was based on efforts originally by Keller for optical diffraction [58],[59]. In the early 1980s, Chamberlin and Luebbers [29] developed a subsequent methodology for quantifying path loss be-

tween transmitter and receiver based on actual physical terrain data implemented as obstructing "wedge" features between transmitter and receiver. The GTD model had some difficulties in calculations of particular physical occurrences for peaks of equal height in succession, moreover when one edge is illuminated by transition region fields diffracted by a preceding wedge [60], [61]. Overall, the GTD model generated excellent results and has found applications in a widespread variety of subsequent propagation analysis methods. Calculated results from a profile of hilly terrain for the GTD compared to measurements conducted on the same region proved to differ typically on the order of 5-10 dB [29]. Knife edge studies often produce greater discrepancies in comparison to GTD applications [62], due to the stronger physical resemblance of the wedge to a terrain feature than a straight vertical edge. The knife edge discrepancies compared to measurements are typically on the order of 10 to 20 dB [61]. Simulations using the method of moments [63] have also demonstrated extremely low levels of discrepancy when compared to analytical solutions obtained through GTD. More recently, the GTD has seen specific applications for propagation environments to support mobile communications platforms [64],[65]. Also, more detailed geometries such as material coatings [66] and evolved modeling methods for accurate analysis such as heuristics [67], [68] and parabolic equations [69] have been employed to aid in diffraction analysis.

The FDTD method is a numerical analysis technique using finite elements that has seen numerous applications in recent years. This method was proposed by Yee in 1966 [70], and the original paper illustrates the technique in full form. However, due to the computational resources required to implement any useful algorithm applying Yee's method, it is only in recent years that the method has been widely adopted by the electromagnetics community [30],[48]. This technique is not only applicable to electromagnetics, but to any circumstance where curl equations are involved and a central difference approximation can be applied. Other common applications include thermodynamics and acoustics [48]. The application of the FDTD method in

the field of electromagnetics has been primarily for conventional RF and microwave distributed circuit analysis [71], [72]. This includes common RF structures such as transmission lines, filters, and antennas [73],[74],[75]. However, a recent generalized thrust of applications of EM methods for channel modeling have used the FDTD method for propagation analysis. This includes propagation environments such as office and building space areas [32]. Unlike methods that use approximations such as ray tracing methods [23] to yield approximate propagation effects, the FDTD method can be employed to produce direct solutions based on Maxwell's equations. This approach provides high accuracy simulation results whereby the effects of reflection, diffraction and scattering are accurately modeled. Thus, it is advantageous to utilize any method which provides direct solutions to Maxwell's equations, where the computational resources make the effort feasible. The FDTD technique for this application is not limited by the physical size of the channel, as is the case with the other numerical methods that utilize a solution based on Green's functions. The Method of Moments [76] becomes increasingly prone to error with increased separation between discrete elements, and therefore use of the FDTD method for channel modeling is an emerging field taking advantage of low cost computational resources.

Chapter 3

Marine Geometrical Theory of Diffraction

3.1 Theoretical Development of a Marine Propagation Channel Model

The development of a novel theoretically-based model relevant to the marine communications channel is focused upon quantifying propagation losses during sea surface shadowing conditions. The objective is to produce a practical, generalized methodology to quantify diffraction effects for a fully-developed single deep sea wave obstructing line of sight between a transmitter and receiver. This work is an extension of the geometrical theory of diffraction. The formulation will be a unique and pragmatic mechanism whereby the methodology allows estimation of diffraction loss by approximating a single sea surface wave in the same fashion a conventional knife edge is used to represent terrain features on land, with the added accuracy of the perfectly conducting wedge as used in the GTD. This wedge bears closer physical resemblance to the physical form of a single sea surface wave than would a knife edge. The representation of the physical sea surface wave is innate to the proposed model, as only

the sea surface height within which the wireless communications system is specified to operate is required. The formulation thus alleviates the system designer from requiring any specific knowledge of the sea surface and respective wave geometries around which desired diffraction is to be quantified. It is important to realize that the case for the sea surface boundary is a fully-developed sea, such that the wind speed can be eliminated from the synthesis of the random sea surface. However, any sea surface synthesis procedure or measured data can be used in the presented methodology. Also, the analytical based extension of the GTD uses a worst case scenario to develop a waveform envelope, whereby the phase of the spectral content of the sea is formulated to add constructively. The subsequent method and formulation will be hereafter referred to as the marine geometrical theory of diffraction (Marine GTD). The process required for development of the novel Marine GTD will be carried out with the following milestones:

1. Pierson-Moskowitz model examination to demonstrate which physical attributes are relevant to the specification of a random sea surface.
2. Analysis of the GTD wedge model as a theoretical concept applied to the physical attributes of the single wave obtained from the PM model.
3. Finalized form of the newly devised marine geometrical theory of diffraction (Marine GTD) as an extension of the geometrical theory of diffraction.

Although this formulation will be based on the modified Pierson-Moskowitz spectral models due to the specific geographical interest of the north North Atlantic to the researcher, any other sea surface model deemed suitable for a different locale may be used with the proposed methodology. The process of the random sea surface generation is intended as a demonstration of the technique, and the reader is encouraged to use whatever model the best feel is appropriate, and resulting channel performance parameters for use in the wireless link budget calculations should be considered accordingly. An overview of the knife edge model for comparison purposes

to the proposed method is given such that the Marine GTD may be directly compared with a knife edge diffraction analytic result for a common physical channel topology.

3.2 Pierson-Moskowitz Model Examination for Wave Physical Attributes

The Pierson-Moskowitz model is based on the spectral content obtained by measurements for a fully developed random sea surface in a deep water location [28]. This investigation examines the parameters used in the PM spectral content model to establish if all parameters presented in the theory are relevant in specifying a sea surface. The premise of the modified Pierson Moskowitz model is based on the following parameters, A and B , whereby [28]:

$$A = 8.1 \cdot 10^{-3} g^2 \quad (3.1)$$

and

$$B = 0.74 \cdot \left(\frac{g}{V}\right)^4 \quad (3.2)$$

where g is acceleration due to gravity, and V is the wind velocity at 19.4 m. The significant wave height, H_s , can be expressed as a function of wind velocity for a fully developed sea in deep sea location as

$$H_s = 0.21 \cdot \frac{V^2}{g}, \quad (3.3)$$

which allows the previously defined constant B to be expressed in the form,

$$B = 0.0323 \cdot \left(\frac{g}{H_s}\right)^2 = \frac{3.11}{H_s^2}. \quad (3.4)$$

A and B are then used to generate the Pierson-Moskowitz spectral function,

$$S(\omega) = A\omega^{-5} \exp(-B\omega^{-4}). \quad (3.5)$$

As an alternate, the modified Pierson-Moskotwitz model specific to the north North Atlantic region is formulated as,

$$S_m(\omega) = \left[\frac{4 \cdot \pi^3 \cdot H_s^2}{T_z^4 \cdot \omega^5} \right] \cdot \exp\left(\frac{-16 \cdot \pi^3}{T_z^4 \omega^4}\right). \quad (3.6)$$

$$T_z = 2\pi \sqrt{\frac{m_0}{m_2}} \quad (3.7)$$

$$m_0 = \frac{A}{4 \cdot B} \quad (3.8)$$

and

$$m_2 = \frac{\sqrt{\pi} A}{4 \sqrt{B}}. \quad (3.9)$$

When simplified, the wind speed plays no role in magnitude of the spectral content for a fully developed sea surface. Once again, this approximation is for a fully-developed sea with infinite depth, no swell and unlimited fetch. Other models or methods for generation of a random sea surface may be used, and the formulation in this case is intended for demonstration of the proposed methodology. The reader is encourage to use any method they feel is better suited to the specific application at hand. Using this approximation allows us to conveniently characterize the diffraction exclusively as a function of a sea surface height. The assumption made in the synthesis of the random sea surface is the magnitude of the spectral function is used to generate the waveform envelope, and then the phase element is introduced by random distribution through spatial assignment. Alternatively, the random phase component can be introduced at the time the spectral function is generated.

To illustrate what measured data resembles compared to the aforementioned

Pierson-Moskowitz spectral functions, 3-1 illustrates the significant wave height vs. wind speed, while 3-2 illustrates significant wave height vs. peak period (<http://www.medsdmm.dfo-mpo.gc.ca/>).

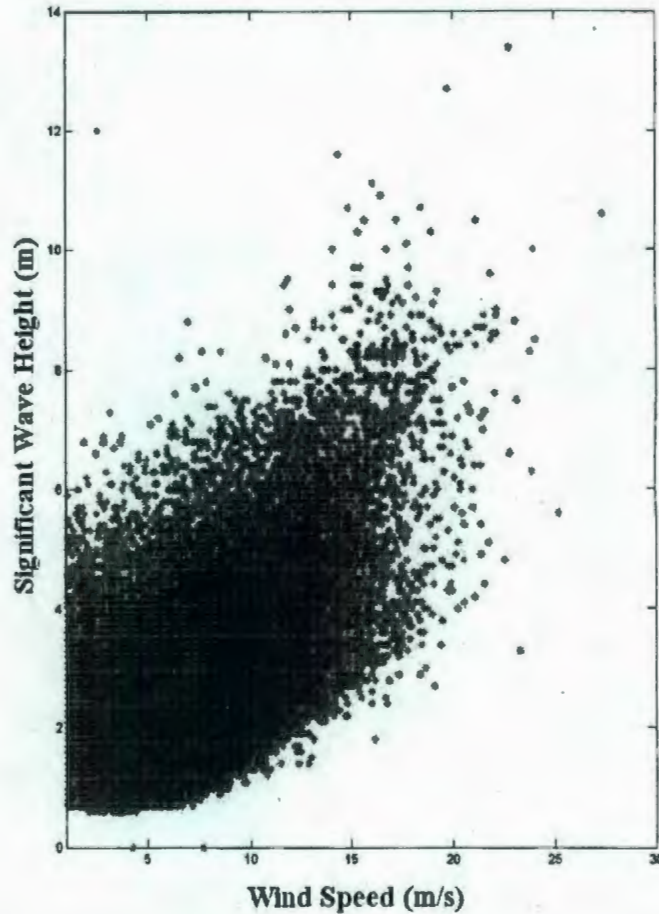


Figure 3-1: Measured data of the significant wave height vs. wind speed off the coast of Newfoundland at the tail of the Grand Banks during the 1990 - 2007 time period.

3.3 Overview of the Knife Edge and Conventional Geometrical Theory of Diffraction Models

The conventional forms of the knife edge (KE) model [23] and the geometrical theory

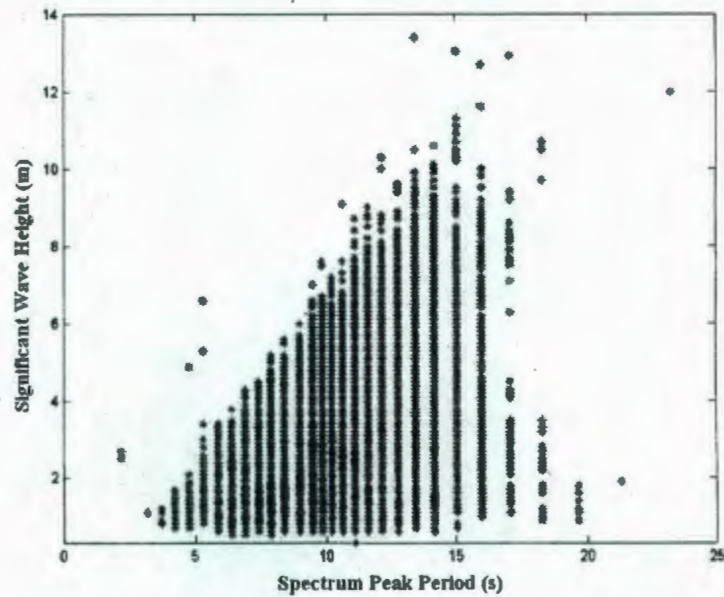


Figure 3-2: Measured data of the significant wave height vs. peak period off the coast of Newfoundland at the tail of the Grand Banks during the 1990 - 2007 time period.

of diffraction (GTD) model [57] are overviewed in this section. The KE model is a commonly used propagation model whereby an obstruction between transmitter and receiver is approximated by a perfectly conducting straight edge for which there is an analytical expression available and easily evaluated. The KE model will be used as a benchmark for the direct comparison between the analytic result for the KE and the proposed Marine GTD for diffraction calculations. The KE will also be used for a second purpose, to evaluate the accuracy of the FDTD simulation results by simulating a physical knife edge, and then comparing the analytic results with those obtained numerically through the FDTD simulation engine. The GTD propagation model provides a greater degree of physical approximation to the obstructing obstacle in comparison to the KE with the usage of a triangular wedge rather than a straight conducting body of equal height. This research effort proposes a novel formulation of the GTD model predisposed to sea surface shadowing conditions that is an extension of the GTD, and easily usable for diffraction analysis in the system design process.

The GTD model will be overviewed as a precursor to the newly proposed extension, the marine geometrical theory of diffraction model, as a key contribution of this work.

Shadowing can be quantified by the usage of the knife edge equation, whereby an obstructing body between a transmitter and receiver is approximated by a straight perfect conducting edge. Figure 3-3 illustrates the knife edge physical approximation for diffraction analysis. Typically, to estimate shadowing effects of common terrestrial obstructions, they are approximated by locating the conducting edge at the highest point of the obstructing object. In this case, the signal strength at the receiver, E_{KE} , due to incident field E_o is given as,

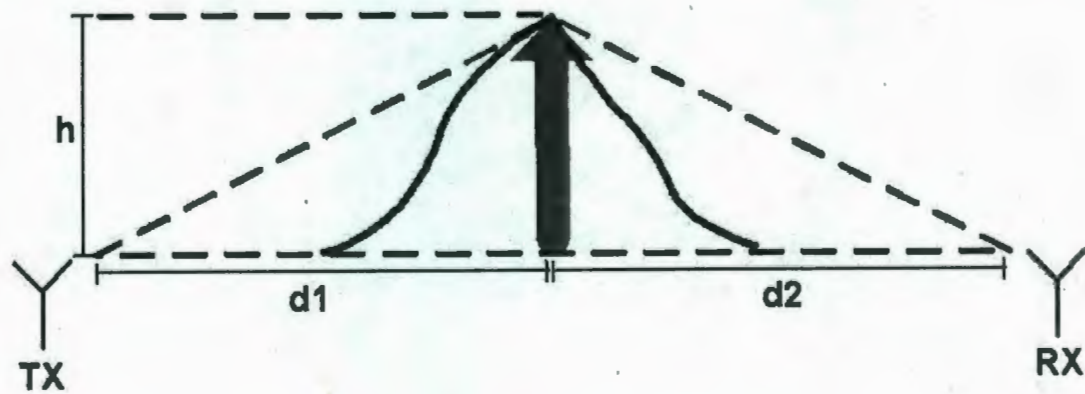


Figure 3-3: The knife edge topology.

$$E_{KE} = E_o \left(\frac{e^{-jk(d_1+d_2)}}{d_1 + d_2} \right) \cdot \left(\frac{1+j}{2} \right) \cdot \int_u^\infty e^{-j\pi\tau^2/2} d\tau \quad (3.10)$$

such that $u = h\sqrt{\frac{2(d_1+d_2)}{\lambda d_1 d_2}}$. For the knife edge equation, k is the wave number, λ is the wavelength and d_1 ; d_2 and h are dimensions as depicted in Figure 3-3. Clearly, E_{KE} is a function of wavelength, and thus need be calculated for all frequencies in the relevant band of interest.

Unfortunately, for the purposes of communications channel modeling, this widely accepted model does not account for the geometry of the actual obstruction, which has significant effect on the multipath propagation distance around the obstacle, and thus the delay spread for the channel. Previous efforts illustrate discrepancies in diffraction calculations for terrain features approximated by the KE model typically to be on the order of 10 - 20 dB [61] when compared to measurements. In actuality, a sea surface is a superposition of many single waves. Thus, in this effort we propose that for the purpose of communications channel modeling, a single wave can be approximated more accurately by a perfectly conducting wedge, rather than a knife edge. Though a combination of randomly positioned single waves is used to create a sea surface, it is difficult to evaluate diffraction effects for multiple waves simultaneously. Therefore, in an effort to produce a theoretically-based model that will provide a useful mechanism for diffraction analysis to the system designer, an extension of the geometrical theory of diffraction (GTD) is developed to provide insight into the diffraction around a single wave, which is predominantly a function of observable sea surface height, h , and is more physically representative than the knife edge approximation. The physical topology of the GTD is depicted in Figure 3-4 showing the wedge structure with the respective transmitter and receiver locations.

The generalized diffraction coefficient, D , as utilized for the GTD may be expressed as [29],

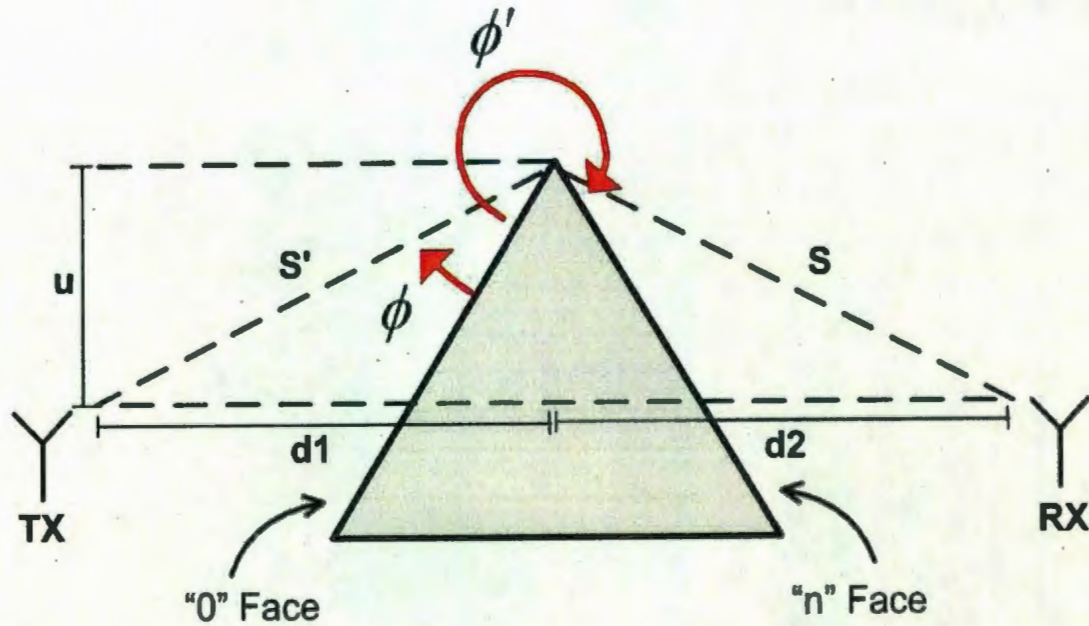


Figure 3-4: The geometrical theory of diffraction topology.

$$D = \frac{-e^{-j(\pi/4)}}{2n\sqrt{2\pi k}} \times \left[\begin{array}{l} \cot\left(\frac{\pi+(\phi-\phi')}{2n}\right) \cdot F(kLa^+(\phi-\phi')) + \cot\left(\frac{\pi-(\phi-\phi')}{2n}\right) \cdot F(kLa^-(\phi-\phi')) \\ + R_0 \cdot \cot\left(\frac{\pi-(\phi+\phi')}{2n}\right) \cdot F(kLa^-(\phi+\phi')) \\ + R_n \cdot \cot\left(\frac{\pi+(\phi+\phi')}{2n}\right) \cdot F(kLa^+(\phi+\phi')) \end{array} \right] \quad (3.11)$$

such that R_0 and R_n are the reflection coefficients for either the perpendicular or parallel polarizations of the "0" face, with incidence angle ϕ' and for the "n" face, reflection angle $n\pi - \phi$. Furthermore,

$$F(x) = 2j\sqrt{x}e^{jx} \int_{\sqrt{x}}^{\infty} \exp(-j\tau^2) d\tau \quad (3.12)$$

is a Fresnel integral such that $L = ss'/(s+s')$ and $a^\pm(\beta) = 2\cos^2\left(\frac{2n\pi N^\pm - \beta}{2}\right)$ such that $\beta = \phi \pm \phi'$. s and s' are depicted in Figure 3-4. N are the integers that satisfy or nearly satisfy $2n\pi N^+ - \beta = \pi$ or $2n\pi N^- - \beta = -\pi$. In the case of $n \approx 2$, the GTD

result and the knife edge result are almost identical.

For a perfectly conducting wedge, where the transmitter and receiver are not close to either a shadow or reflection boundary, the diffraction coefficient is given in a simplified form as [77],

$$D = \frac{e^{-j(\pi/4) \sin(\pi/n)}}{n\sqrt{2\pi k}} \left[\frac{1}{\cos(\pi/n) - \cos\left(\frac{\phi-\phi'}{n}\right)} \mp \frac{1}{\cos(\pi/n) - \cos\left(\frac{\phi+\phi'}{n}\right)} \right] \quad (3.13)$$

where k is the wave number, ϕ is the angle of diffraction, and ϕ' is the angle of incidence as illustrated in 3-4. $n\pi$ is the exterior wedge angle. The \mp term is dependent upon the polarization of the incident wave, for either perpendicular or parallel respectively. Since the sea surface is commonly approximated as a perfectly conducting surface, this simplified formulation of the diffraction coefficient is most suited for the development of a generalized marine geometrical theory of diffraction model.

3.4 Synthesis of the Diffraction Coefficient for the Marine GTD

In examination of the sea surface, it is proposed that the GTD wedge model can be applied to a single sea surface wave and be furthermore used in a similar capacity to which it is used for the evaluation of propagation around fixed terrestrial objects such as hills and buildings. For the purpose of the marine communications channel, the perfect conducting wedge is acceptable because of the salt water sea surface that comprises the wedge. This designation of the sea surface as a perfect conducting surface is a commonly used approximation [33]. As the peak of the sea surface is also assumed to be the most dominant physical feature of the single sea surface wave effecting the propagation diffraction in the marine communications channel, it is thus proposed that the physical application of the wedge topology to the single sea surface

wave will be applied in such a way as is illustrated in Figure 3-5.

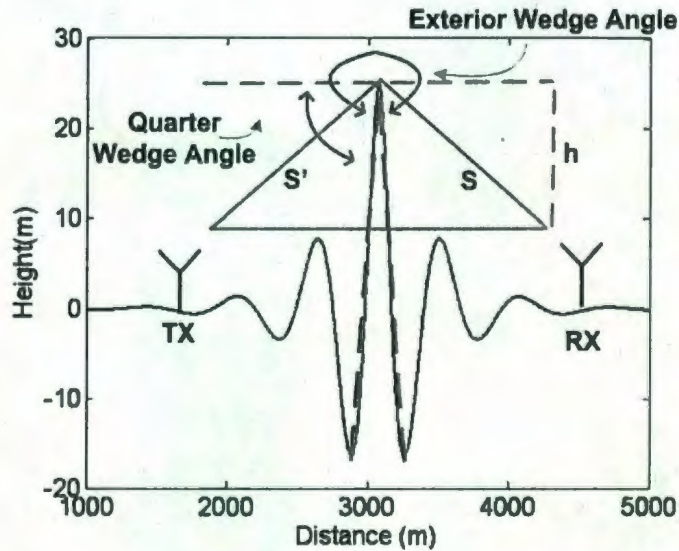


Figure 3-5: Applying the GTD to the Sea Surface.

For a field point not near the shadow or reflection boundary with a perfectly conducting wedge, which is an appropriate approximation for the sea surface, the field given by the diffraction around the wedge peak is given by E_{GTD} [77], where,

$$E_{GTD} = E_o \frac{e^{-jks'}}{s'} \cdot D \cdot \sqrt{\frac{s'}{s(s+s')}} \cdot e^{-jks} \quad (3.14)$$

whereby D is the diffraction coefficient and was previously defined for a perfectly conducting wedge in the previous section. Since it has been previously established that the only parameter that plays significant role in the frequency spectrum of the fully developed sea surface in a deep sea location is the wave height, we will develop a novel theoretically-based model as per the physical attributes of the single sea surface wave that is created by application of a wedge structure suitable for GTD diffraction analysis to the form of a single sea surface wave. This generalized formulation can then be used for link budget analysis during the system design process whereby no further detailed knowledge of the physical attributes of the sea are required other than observable sea surface height. Thus, as a theoretically-based model development

component of this research, the Marine GTD methodology may be used as a diffraction estimation tool in the same manner as the knife edge is used to approximate an obstruction between transmitter and receiver, with the added advantage of the higher accuracy of the geometrical theory of diffraction, and without the difficulty in establishing the wedge geometry of a single sea surface wave. The first segment of this development process is to evaluate the sea surface attributes with changing sea surface height. The modified Pierson-Moskowitz (PM) spectral functions are the basis of this analysis. Figure 3-6 illustrates the magnitude versus frequency for the modified Pierson-Moskowitz spectral functions with varying sea surface heights from 1 m to 25 m. The lower sea height spectral functions have higher frequency domain content, whereby the lower frequency content increases for each spectral function as illustrated. Clearly, lower spectral content increases in magnitude as wave height increases.

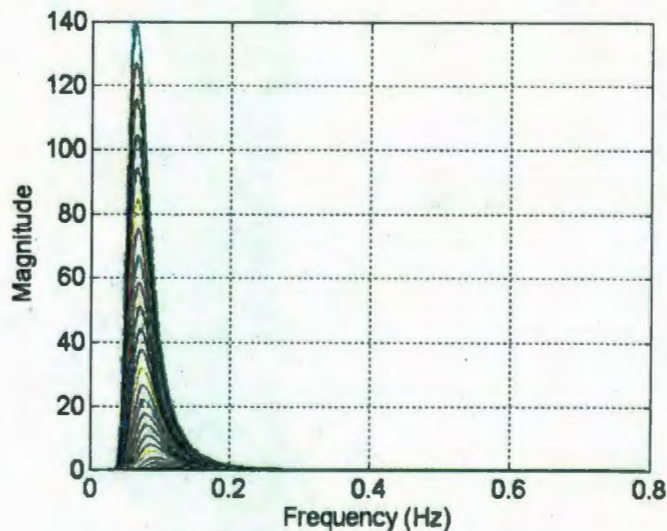


Figure 3-6: The modified Pierson Moskowitz spectral functions for increasing wave height.

The peak of the magnitude of the PM model can be seen to be lower in frequency as the sea surface height increases. Performing an Inverse Discrete Fourier Transform

(IDFT) on this spectral content [78], the transient displacement of a single point because of a single sea surface wave can be numerically determined. Figure 3-7 illustrates the transient displacement of the sea surface as per a single sea surface wave obtained from the modified Pierson-Moskowitz spectrum model and Figure 3-8 illustrate the effects on the displacement of the sea surface over time as well as the temporal spreading of the sea surface peak structure.

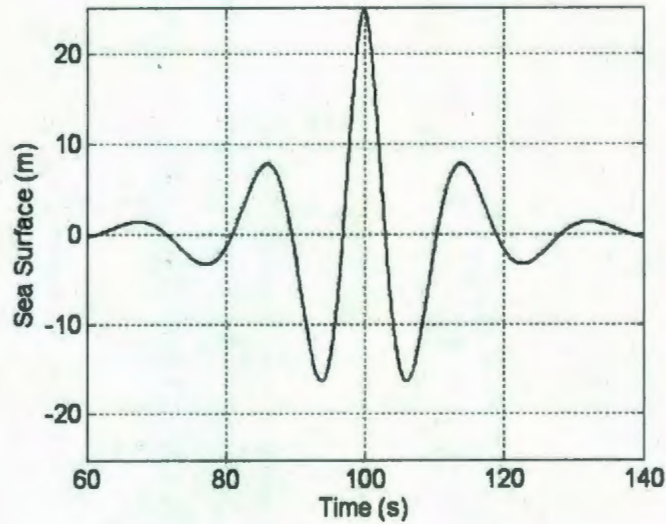


Figure 3-7: Modified PM sea surface wave temporal point displacement.

Once the transient displacement of the sea surface is obtained, assuming that the wave does not change its waveform envelope as it travels spatially, leads to the physical wave over distance [79]. The length of this physical wave, L_d , is determined using classical wave theory, whereby the length of the wave is dependent upon the period [79].

$$L_d = \left(\frac{g}{2 \cdot \pi} \right) \cdot T_p^2 \quad (3.15)$$

The period of the single wave also increases as a function of sea surface height. Figure 3-9 depicts this relationship.

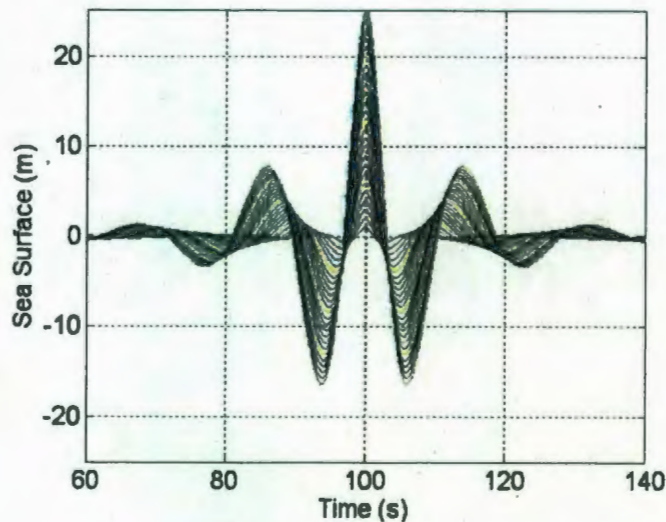


Figure 3-8: Sea surface displacement for increasing wave height.

The period of each wave is then used to extrapolate the spatial form of a single wave. Figure 3-10 shows the waveform envelope of a single sea surface wave as obtained from the Pierson-Moskowitz spectrum model with the length determined based on the period.

Figure 3-11 illustrates single waves of various heights from 1 m to 25 m obtained by DFT analysis. The sea surface waveforms of single waves are co-centered at each peak for closer examination and comparison of the changing attributes of single waves with changing peak heights.

Once the single waves for a variety of sea surface heights are obtained by numerical analysis, the attributes of each wave are quantified with the assistance of the 1st and 2nd derivatives, illustrated in Figures 3-12 and 3-13 respectively. The derivatives are evaluated numerically such that the 1st and 2nd zeros can be used in applying the proposed wedge approximation at the top of the highest peak for each observable wave. Figure 3-14 illustrates this.

Once the distance to each peak has been established, it is possible to calculate the attributes of the wedge as they pertain to the geometrical theory of diffraction.

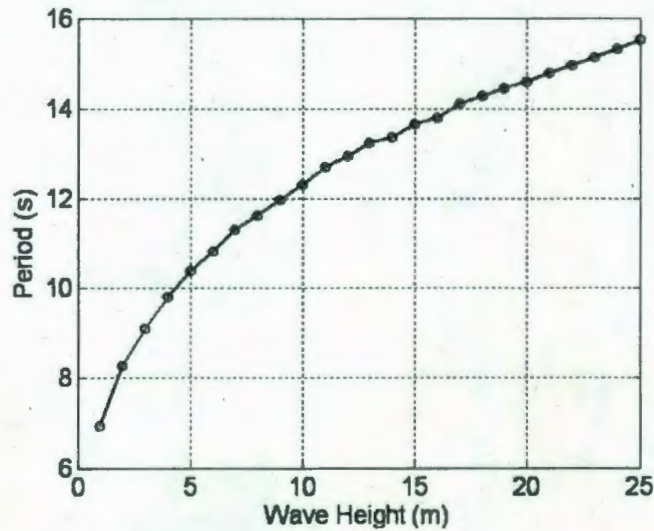


Figure 3-9: Period as a function of sea surface height.

The wedge angle from a normal perpendicular to the vertical vector of the wave is first determined in this process. Figure 3-15 illustrates this result.

The analysis leads to a polynomial function for the quarter wedge angle, QW as a function of sea surface height, h :

$$QW(h) = 3.027 \times 10^{-4}h^3 - 1.773 \times 10^{-2}h^2 + 0.514h + 1.135. \quad (3.16)$$

The polynomial fit compared to the original data is excellent, as illustrated in Figure 3-16.

Similarly, the exterior wedge angle (EW) can be examined as a function of observable sea surface height. The exterior angle is more explicitly described as the outside angle from the rising edge sea surface wave to the falling edge. Figure 3-17 illustrates that the exterior wedge angle increases as the observable wave height increases.

Similarly, this physical attribute can be characterized through a polynomial function fitted to the analysis results as a function of observable sea surface height. The exterior wedge angle and the polynomial fitting function are given in Figure 3-18 as functions of observable sea surface height.

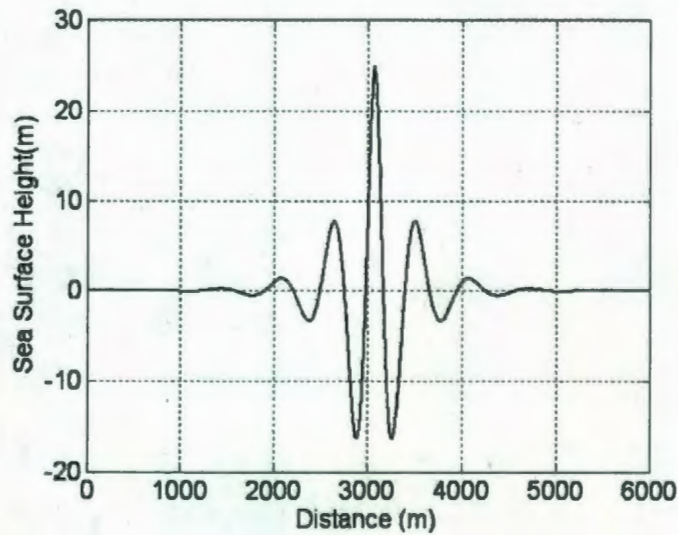


Figure 3-10: Pierson-Moskowitz single sea surface wave form envelope.

$$EW(h) = 6.054 \times 10^{-4}h^3 - 0.0354h^2 + 1.028h + 182.27 \quad (3.17)$$

Once the exterior wedge angle is determined, the n value for the GTD is calculated as,

$$n = EW/\pi, \quad (3.18)$$

where the exterior angle, EW , increases as the wave peak increases. Therefore, for a flat surface, $n = 1$, and n is observed to increase as the wave peak height increases. The n value can be calculated by applying the wedge geometry to the peak of the single wave obtained from the Fourier Transform of the modified Pierson-Moskowitz spectral model. Thus, n is determined for the range of single waves from 1 m to 25 m as illustrated in Figure 3-19.

The wedge n value is thus determined through regression analysis of single waves from 1 m to 25 m in height to be of the form:

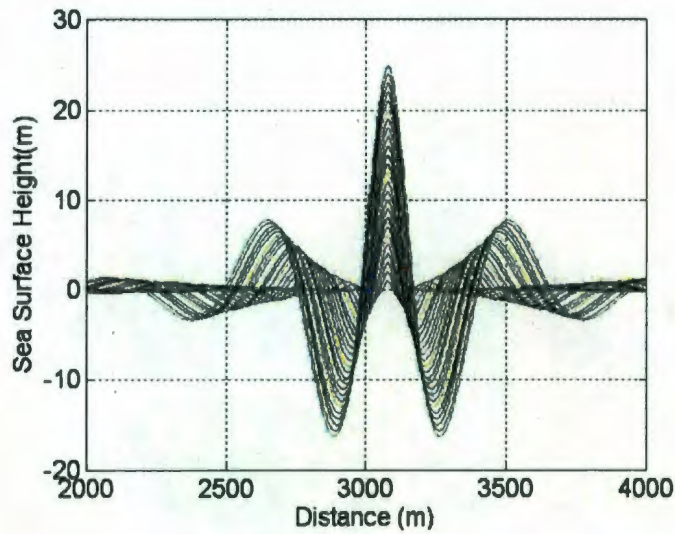


Figure 3-11: Pierson-Moskowitz single waves.

$$n(h) = -3.363 \times 10^{-6}h^3 + 1.970 \times 10^{-4}h^2 - 5.712 \times 10^{-3}h + 0.987 \quad (3.19)$$

Figure 3-20 illustrates the relationship between n observable sea surface height with the polynomial fitting function. Clearly, for a flat sea surface, $n = 1$, and n subsequently increases as sea surface wave height increases.

The polynomial fitting function has excellent agreement when compared to the numerically determined values from the aforementioned process. This model of n can now be used to apply the geometrical theory of diffraction to a single sea surface wave for propagation analysis based exclusively on the observable sea surface height. The proposed methodology requires only calculation of the n values for the perfectly conducting wedge and the quarter wave angles based on the transmitter and receiver locations in proximity to the wedge peak. It provides an easy mechanism for the designer to estimate diffraction loss in the system design process without requiring further knowledge of the physical sea surface, only the observable sea surface height.

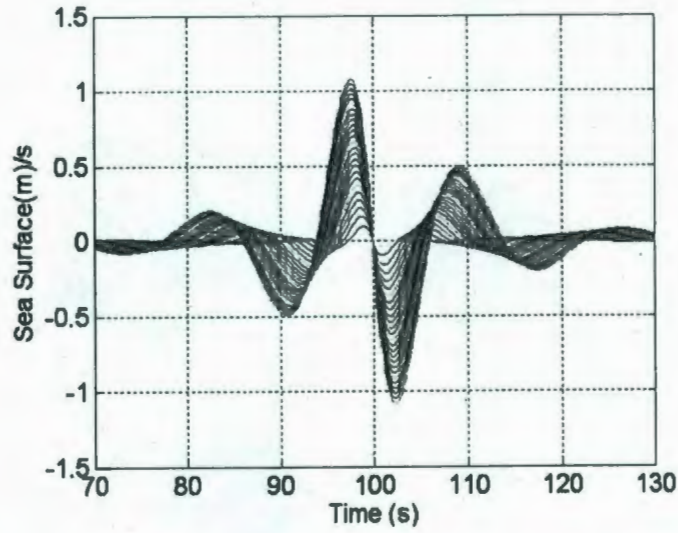


Figure 3-12: Pierson-Moskowitz waveform envelope first derivatives.

The polynomial function modeling the quarter wave angle (QW) can then be used to directly determine the ϕ and ϕ' in conjunction with the position of the TX and RX locations providing estimation of diffraction loss in the marine communications channel due a single obstructing sea surface wave.

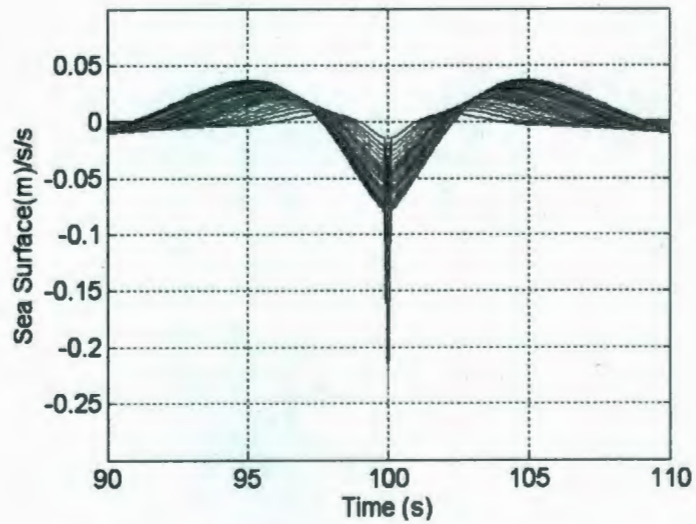


Figure 3-13: Single Pierson-Moskowitz waveform envelope second derivatives.

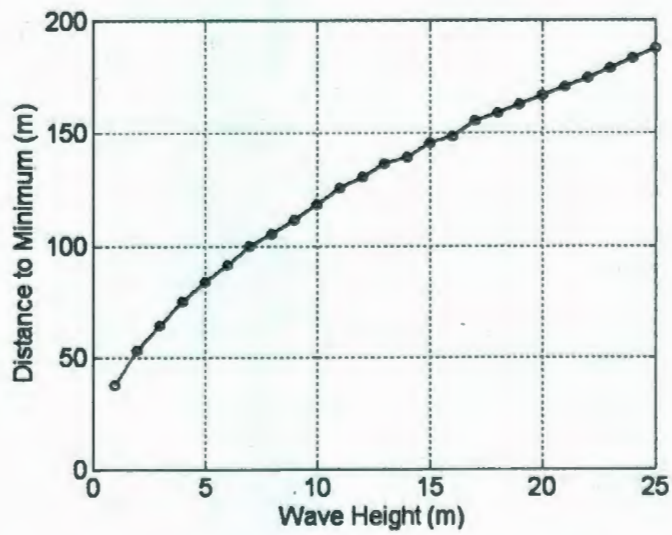


Figure 3-14: PM single wave distance to 1st minimum.

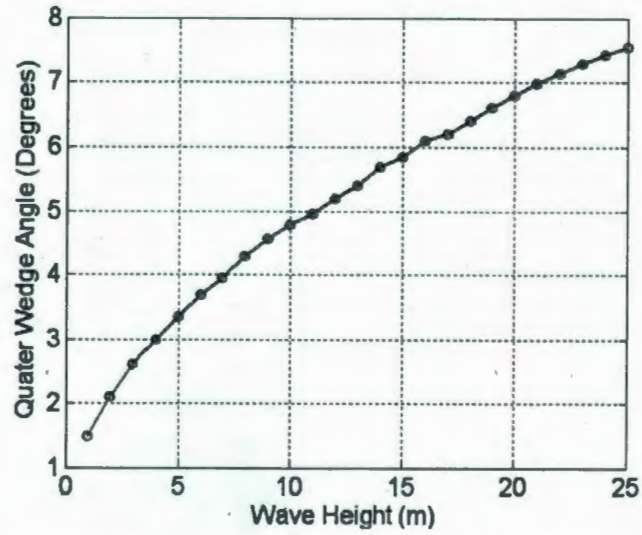


Figure 3-15: Quarter Wedge Angle (QW) vs. Observable Wave Height.

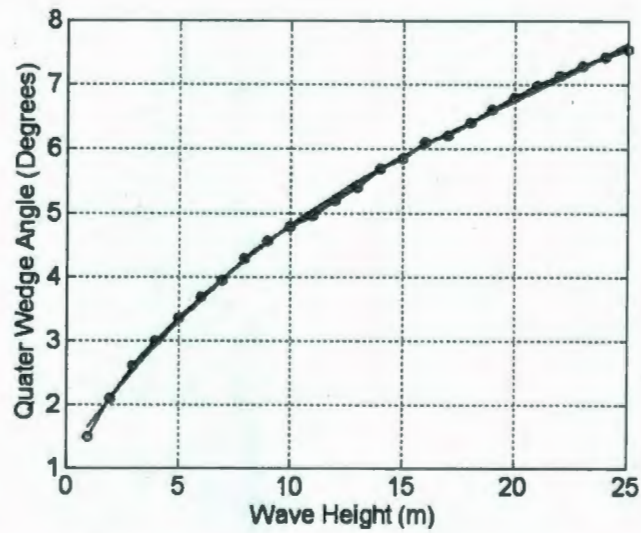


Figure 3-16: Quarter Wedge angle and Polynomial Fitting Function (Blue) vs. Observable Wave Height.

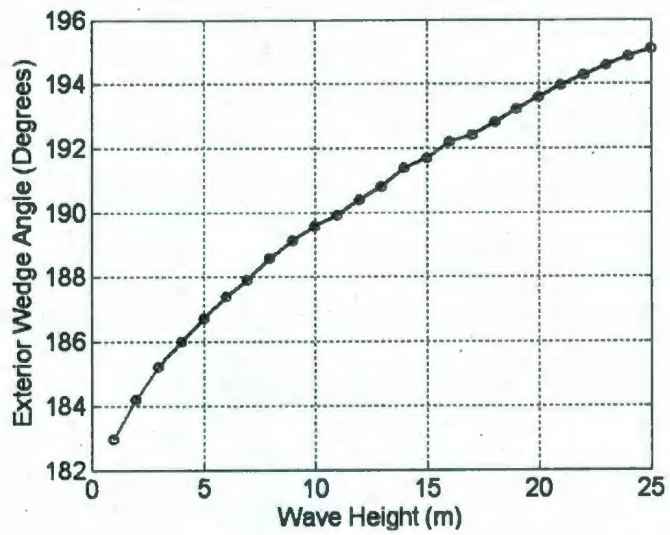


Figure 3-17: Exterior Wedge angle (EW) vs. Observable Wave Height.

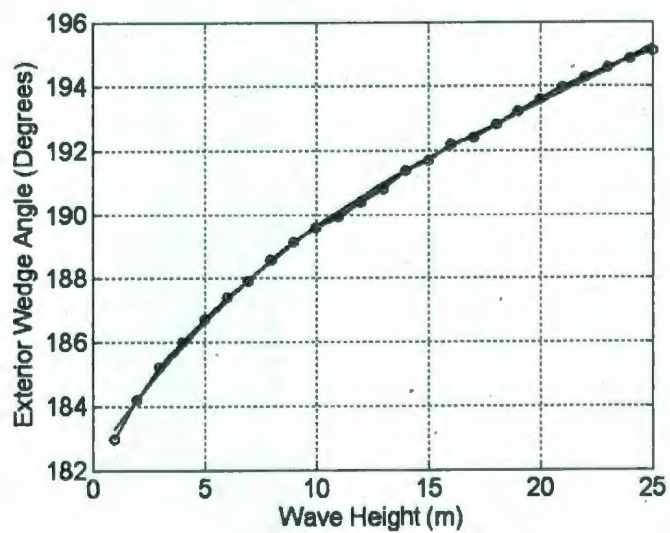


Figure 3-18: Exterior Wedge angle (EW) and Polynomial Fitting Function (Blue) vs. Observable Wave Height.

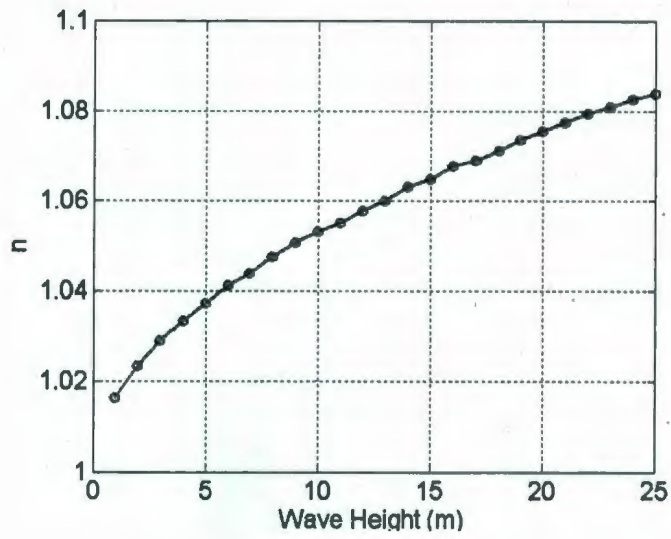


Figure 3-19: n for the calculated wedge representing a single sea surface wave vs. Observable Wave Height.

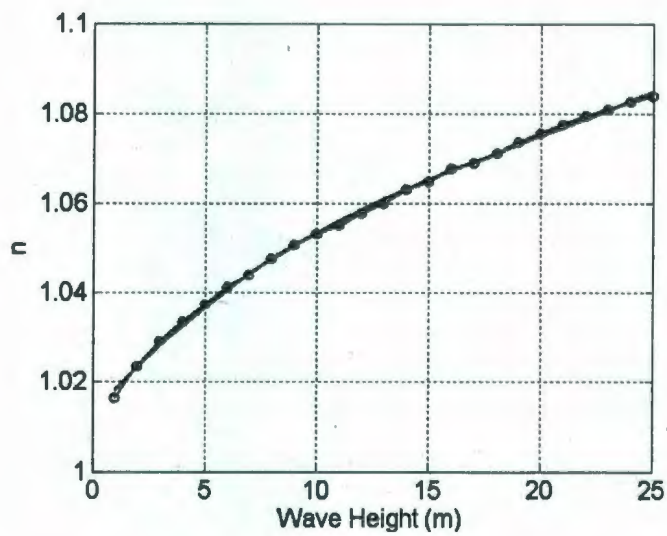


Figure 3-20: n and the Polynomial Fitting Function (Blue) vs. Observable Wave Height.

3.5 Finalized form of the novel Marine Geometrical Theory of Diffraction

The proposed marine geometrical theory of diffraction model takes the following form:

$$D(h) = \frac{\exp\left(\frac{-j\pi}{4} \sin\left(\frac{\pi}{-3.363 \times 10^{-6}h^4 + 1.970 \times 10^{-4}h^3 - 5.712 \times 10^{-3}h + 0.987}\right)\right)}{(-3.363 \times 10^{-6}h^4 + 1.970 \times 10^{-4}h^3 - 5.712 \times 10^{-3}h + 0.987)\sqrt{2\pi k}} \times F \quad (3.20)$$

such that

$$F = \left[\frac{1}{A-B} \mp \frac{1}{A-C} \right] \quad (3.21)$$

whereby,

$$A = \cos\left(\frac{\pi}{-3.363 \times 10^{-6}h^4 + 1.970 \times 10^{-4}h^3 - 5.712 \times 10^{-3}h + 0.987}\right) \quad (3.22)$$

$$B = \cos\left(\frac{\phi - \phi'}{-3.363 \times 10^{-6}h^4 + 1.970 \times 10^{-4}h^3 - 5.712 \times 10^{-3}h + 0.987}\right) \quad (3.23)$$

$$C = \cos\left(\frac{\phi + \phi'}{-3.363 \times 10^{-6}h^4 + 1.970 \times 10^{-4}h^3 - 5.712 \times 10^{-3}h + 0.987}\right) \quad (3.24)$$

The quarter wedge angle for the symmetrical sea surface wedge is determined by

$$QW(h) = 3.027 \times 10^{-4}h^3 - 1.773 \times 10^{-2}h^2 + 0.514h + 1.135. \quad (3.25)$$

The TX and RX, QW_{TX} and QW_{RX} positions may be determined through the trigono-

metric relations,

$$QW_{TX} = \tan^{-1} \left(\frac{h - TX_h}{d_1} \right) \quad (3.26)$$

and

$$QW_{RX} = \tan^{-1} \left(\frac{h - RX_h}{d_2} \right). \quad (3.27)$$

Thus ϕ and ϕ' are given by:

$$\phi = QW(h) + 180 + QW_{RX} \quad (3.28)$$

and

$$\phi' = QW - QW_{TX}. \quad (3.29)$$

Through the usage of the marine geometrical theory of diffraction model, the loss because of diffraction from a transmitter and receiver during sea surface shadowing conditions can be easily approximated for a single fully developed deep sea wave, requiring only the sea surface height and the relative positions of the TX and RX locations. This methodology offers a unique and pragmatic mechanism for the system designer, whereby the theoretically-based marine geometrical theory of diffraction allows estimation of loss because of diffraction by approximating a single sea surface wave in the same fashion a conventional knife edge is used, with the added accuracy of the geometrical theory of diffraction representing the physical waveform. No further knowledge of the sea surface physical geometry is required in using this process. The system designer need only know the sea surface height in which his wireless communications system is designed to operate.

Chapter 4

Marine GTD Numerical Results

4.1 Marine GTD and Knife Edge Comparison

The marine geometrical theory of diffraction (Marine GTD) is evaluated for validity by direct comparison to the knife edge diffraction result. The knife edge is one of the most commonly used approximations for diffraction estimation. The objective for the development of the Marine GTD is to provide a pragmatic formulation with which a system designer can evaluate diffraction loss in the marine communications channel during sea surface shadowing conditions without requiring detailed knowledge of the sea surface profile around which propagation occurs. The only knowledge required in this novel formulation is the observable wave height, such that diffraction analysis may be conducted in the same fashion that a knife edge approximation is used, with a formulation that is more representative of the physical obstructions experienced in the physical channel, and hence more accurate [29]. This is advantageous, as in the published literature the knife edge diffraction estimation demonstrated larger discrepancies during comparative studies [62] than observed when compared to the highly accurate GTD results for terrestrial propagation environments. An example of a communications channel of the physical topology whereby the proposed methodology is

applied is given in Figure 4-1.

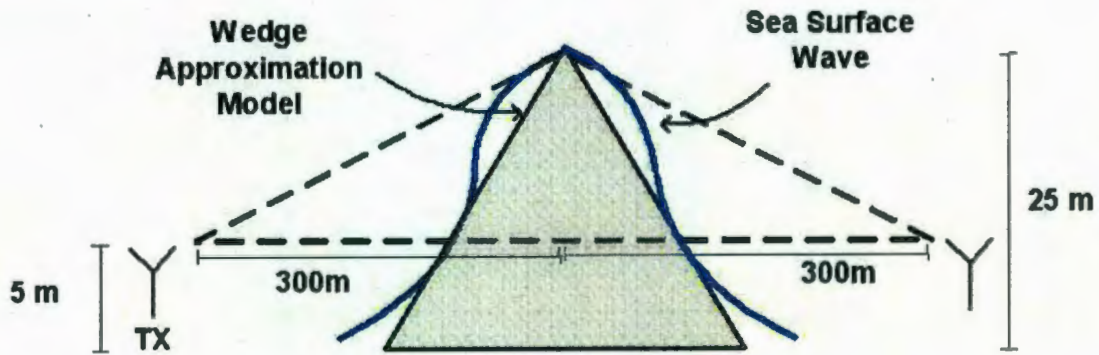


Figure 4-1: Proposed Marine GTD evaluation topology.

Applying the newly proposed marine geometrical theory of diffraction, the diffraction coefficients are determined numerically and illustrated in Figure 4-2 for perpendicular and parallel polarizations of the evaluation topology, as per Figure 4-1.

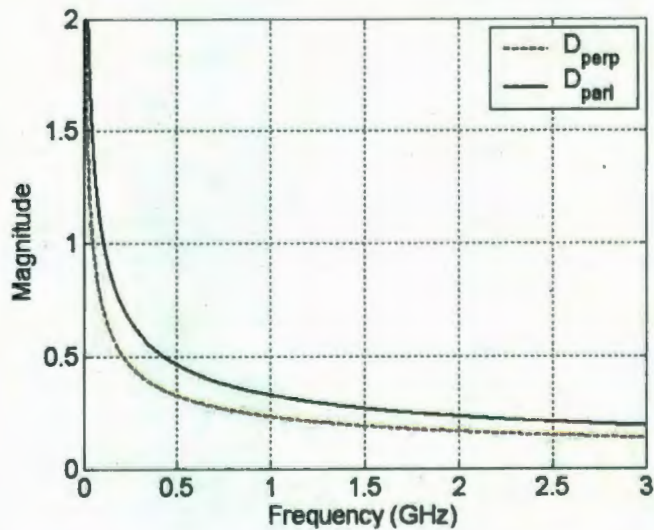


Figure 4-2: Marine GTD Diffraction Coefficient vs. Frequency.

Figure 4-2 illustrates the results for a channel topology with a 25 m wave, with the transmitter and receiver located at 5 m height, both of which are positioned an equal 300 m distance from the base of the peak. Figure 4-3 and Figure 4-4 compare the

diffraction loss calculation for perpendicular and parallel polarizations of the Marine GTD to the knife edge diffraction calculation.

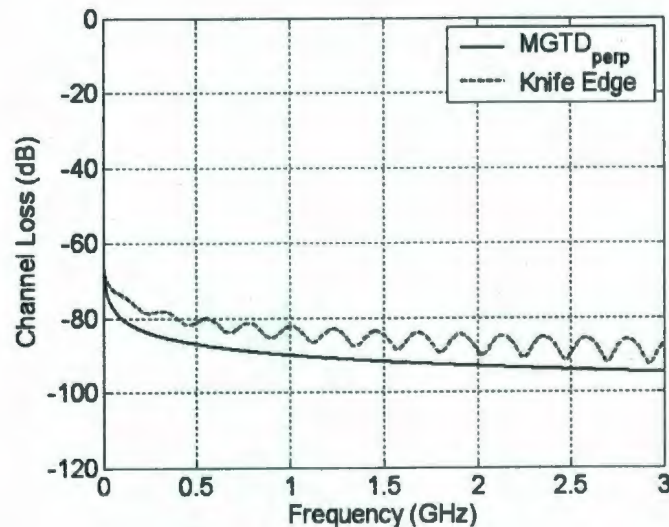


Figure 4-3: KE and Marine GTD diffraction of a 25 m wave for perpendicular polarization.

Similarly, calculations with a sea surface height of 10 m are performed. The transmitter and receiver located at 300 m from the base of the peak. The diffraction coefficient is observed in Figure 4-5 to be of higher order in magnitude. Intuitively, the diffraction loss is observed to be significantly less.

Figures 4-6 and 4-7 illustrate the diffraction loss parallel and perpendicular polarizations compared to the knife edge diffraction of a 10 m wave, with the transmitter and receiver located at 300 m from the base of the peak. Less diffraction loss is observed than for the 25 m high wave channel topology.

4.2 Marine GTD Evaluation Summary

In closing, the marine geometrical theory of diffraction has been developed and presented in generalized form. This approach, which is an extension of the generalized GTD, provides an easy mechanism for the estimation of path loss due to diffraction

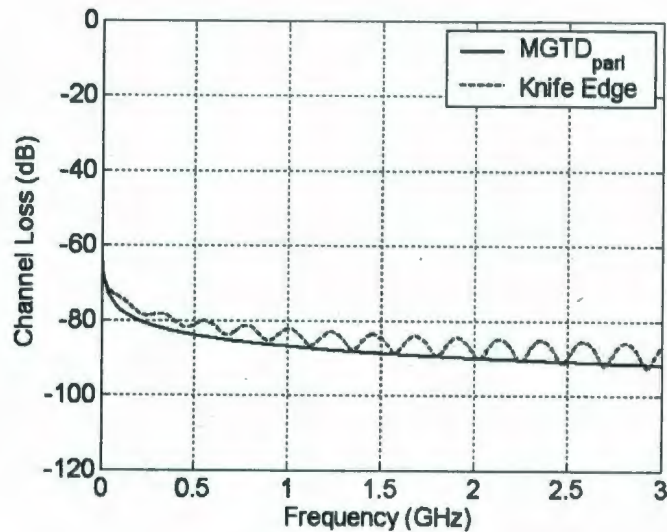


Figure 4-4: KE and Marine GTD diffraction of a 25 m wave for parallel polarization.

around a single obstructing wave in a marine communications channel during sea surface shadowing conditions. Unlike the knife edge approximation, which is commonly used for typical terrestrial obstructions, the Marine GTD is devised to retain a closer form to the physical attributes of the obstruction, as opposed to the straight vertical perfectly conducting knife edge. The knife edge is located at the peak of the obstruction, and more often than not bears little or no resemblance to the obstructing feature with the exception of the overall height. The Marine GTD method was developed using the physical attributes of a single sea surface wave obtained by analysis of the modified Pierson-Moskowitz spectral model. Although the sea surface is composed of a superposition of multiple waves, this theoretically-based concept provides a direct means to estimate diffraction loss based on only the topology of the transmitter/receiver locations and the sea surface wave height in the same manner as the knife edge diffraction model is used where the location of the tallest wave is approximated by the peak of the Marine GTD. Comparison of the calculated results by the Marine GTD prove to be very close to those obtained from a direct knife edge application for both perpendicular and parallel polarizations. With the well established record of highly

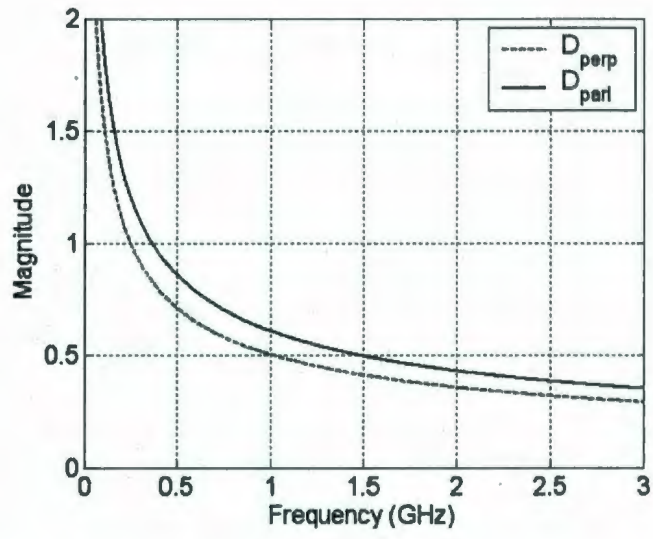


Figure 4-5: Perpendicular and Parallel Marine GTD diffraction coefficients for a 10 m wave.

accurate GTD calculations in comparison to diffraction measurements over known physical terrain features [29], the typical discrepancies observed between the knife edge calculations and the Marine GTD formulation in this study support validity of the proposed marine geometrical theory of diffraction.

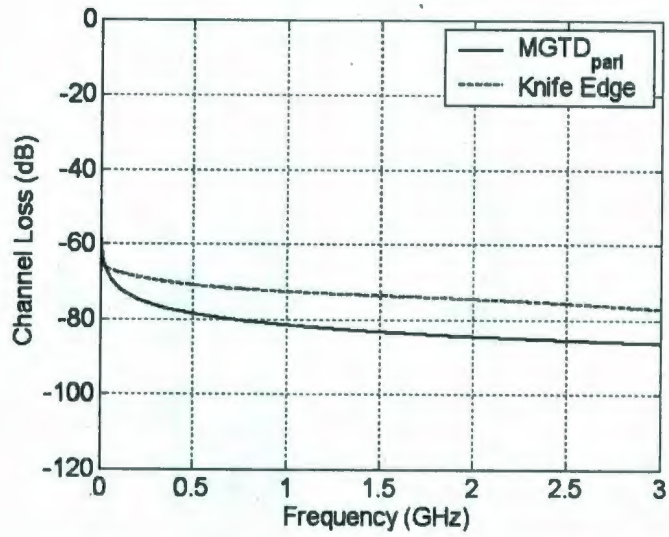


Figure 4-6: KE and Marine GTD diffraction loss of a 10 m wave for parallel polarization.

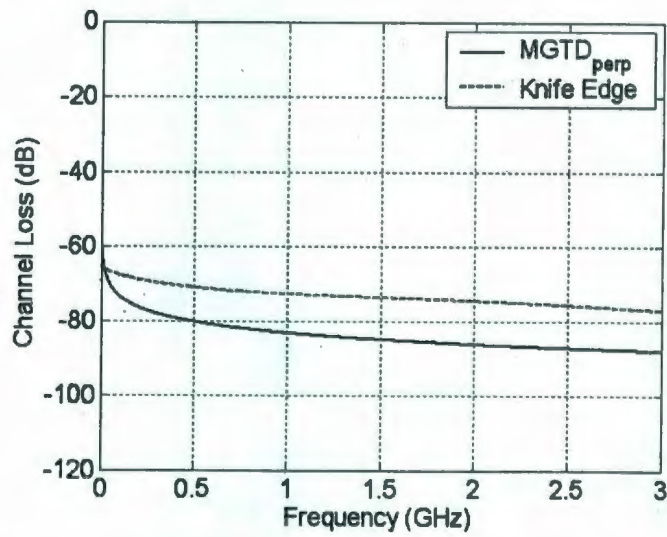


Figure 4-7: KE and Marine GTD diffraction loss of a 10 m wave for perpendicular polarization.

Chapter 5

The Practice of Channel Modeling

5.1 Overview

Modern wireless communications systems employed in the marine environment primarily use either VHF, cellular or satellite technologies [3]. As is the case with most commercial personal communications systems, the relevant frequency range currently used for these devices is approximately 100 MHz (VHF) to 3 GHz (Microwave). The objective of this segment of research is to provide a novel numerical modeling methodology to study overwater radio propagation over a random sea surface. Measurements conducted to characterize channel performance is typically accomplished through obtaining parameters of the path loss equation [45] for terrestrially-based mobile communications channels. The same form path loss equation will be used in this case to generate novel parameterized models characterizing the marine communications channel performance over random sea surfaces during post FDTD simulation analysis. Path loss and multipath effects, from which communications degradation results [9] in the form of either signal fading or intersymbol interference are quantified as functions of frequency and observable wave height. In this effort, the novel approach of replacing the typical measurement segment of the process with FDTD overwater propagation analysis offers the distinct advantage of retaining with detail

the physical attributes of the random sea surface over which the propagation occurs. Determination of the path loss exponent, characterizing the random fading contribution, as well as the mean excess delay and root mean square (RMS) delay can be accomplished with a detailed profile of the random sea surface. In previous works, this lack of knowledge of the sea surface during measurements has been the most difficult aspect in establishing parameterized relationships between channel performance and sea surface height while conducting measurement studies for overwater radio propagation [39],[40],[22]. For the system level designer, high accuracy parameterized models developed as functions of both frequency and observable wave height offer a distinct advantage in the link budget and timing analysis segment of the system design process for any marine communications application. This chapter will overview the standard parameters used to characterize communications channel performance [46]. Since these formulae are well established and universally accepted in the channel modeling field, the formulae are simply presented such that they are readily available to the reader due to their importance to this work.

This chapter begins by providing an overview of ideal propagation in free space. Free space propagation provides the theoretical foundation for understanding the path loss exponent. Propagation phenomenon affecting the received signal including power loss as well as fast and slow fading are given as relevant background in this work. The path loss equation [20], which is the most commonly used means of channel characterization is given in detail, as well as time delay methods of channel performance characterization. During post simulation analysis of overwater propagation studies conducted by FDTD method in this work, novel parameterized channel performance models as functions of both frequency and observable wave height will be derived in demonstration of the proposed methodology for conducting propagation analysis in the marine communications channel as the basis for this research effort.

5.2 Ideal Propagation in Free Space

The fundamental aspect of radio frequency propagation analysis may be summarized as free space path loss. Specifically, this occurs when propagation is completely uninfluenced by any physical body. In this case, the attenuation experienced by a radio signal as it spreads outwardly from a point source is analytic in nature. This is generally atypical of any practical communications channel on earth. Free space path loss may be illustrated through 2-dimensional electromagnetic (EM) simulation graphically with Gaussian excitation, as in Figure 5-1, illustrating the same point excitation at two different points in time. The right illustration shows the E-field at a later time of reference than the left.

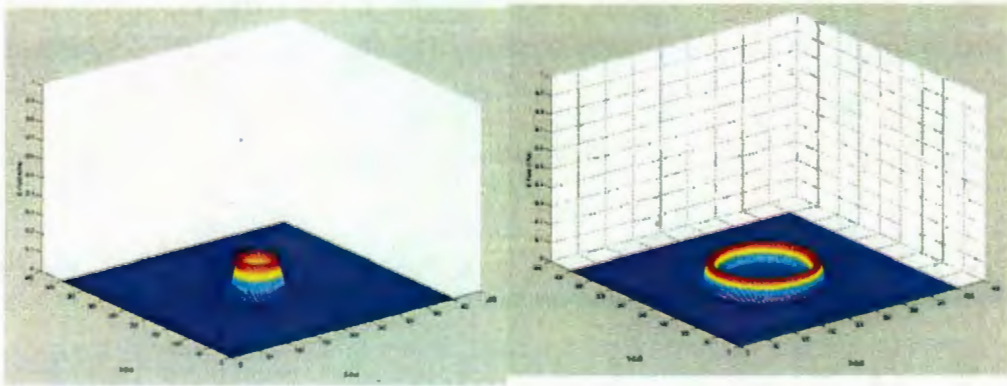


Figure 5-1: 2-dimensional Electromagnetic Free Space Propagation Simulation

As the RF energy radiates away from the source, the amplitude decreases as free space loss, L_s , is observed. Mathematically, this free space loss equation is commonly known to follow the form [23],

$$L_s(d) = \left(\frac{4\pi d}{\lambda} \right)^2 \quad (5.1)$$

where d is the distance of separation between the transmitter and receiver, and λ is the wavelength of the propagating signal.

Free space loss assumes that the channel path between the transmitter and re-

ceiver is free from all objects that may result in further levels of attenuation or multipath effects. It is easily understandable that this circumstance is not the case for any terrestrial application, whereby at minimum, even for airborne applications, the ground acts as a reflecting surface between any transmitter and receiver locations. In other words, transmission occurs such that propagation between two points results in multiple signal pathways that are a result of these reflections. This phenomenon is commonly referred to as multipath propagation. Multipath effects generally result in the inadequacy of the free space path loss equation to be used for quantification of terrestrial communications channel loss. It is noteworthy that the equivalent path loss exponent for free space as it pertains to the path loss equation, is 2. This is because of the exponent in the free space loss equation.

5.3 Mobile Radio and Propagation in Terrestrial Environments

Communications channels rarely adhere to any analytical form. The path loss equation [44] offers a means to characterize propagation and channel performance independent of the physical features of a channel. Mobile radio and the study of channel modeling is typically an empirical and measurement-based science [23],[20],[21]. This has resulted in a more generalized approach to characterizing channel performance in a variety of typical environments [56]. With the advent of wireless communications from a PCS and WLAN perspective, these studies have focused heavily on urban environments [46] for mobile cellular applications. Furthermore, increasing acceptance of WLAN technology within office and residential environments [32] has also contributed to the overall body of work. However, no two communications channels are identical, and furthermore environments that appear physically similar in topology may perform radically different with respect to their wireless communications chan-

nel performance [24]. Many communications channels are also heavily stochastic in nature. That is, their propagation characteristics change with time. This may be due to changing multipath effects in the environment such as moving vehicles or weather conditions that change during wireless communications operations. Nonetheless, it is widely accepted that propagation in any wireless channel is influenced in its performance by three distinct mechanisms: [47],[80].

1. Reflection - Occurs whenever a signal is incident upon an electrically large structure in comparison to the wavelength of the propagating signal.
2. Diffraction - When an electrically large body shadows the receiver from the transmitter, and secondary waves are formed behind the obstructing object such that some signal reaches the receiver without a line of sight path to the transmitter.
3. Scattering - Is relevant when obstructions exist between the transmitter and receiver that are of physical size on the order of the electrical wavelength of the propagating signal or smaller. In this circumstance, energy is scattered outwardly in all directions from these objects.

These phenomena each contribute directly to the received waveform envelope. Such effects are typical of transmissions between a mobile subscriber and a base station, and vice versa. The degree to which each effect contributes is highly dependent upon the frequency of the signal, and the physical features through which the signal propagates [44]. When evaluating the power delivered to a receiver from a transmitter through a physical environment these mechanisms manifest themselves in three propagation phenomena:

1. Path loss and variation of signal strength with distance.
2. Slow fading, which is observed in the form of a lognormal distribution of received signal strength.

3. Fast fading, which may contribute largely to overall measured signal strength as a result of multiple signal paths and their constructive or destructive interference effects between the transmitter and receiver. This is experienced most often when scattering occurs in the region of the receiver.

The effects of these phenomena on received signal power contribute directly in the system design process to the establishment of the link budget. Establishing the link budget is often the first step in the system design process, as it leads to the specification of system performance parameters such as transmitter power and antenna gain to provide efficient and simultaneously effective wireless communications between transmitter and receiver locations. Understanding the effects of path loss, slow and fast fading and furthermore the capability of quantifying these effects accurately for a specific communications channel is a distinct advantage in the specification and design of a wireless communications system. The relevant system parameters can be quantified and then used to determine the maximum allowable path loss in the system to sustain a predetermined quality of service. The path loss of the channel is primary in defining the system performance requirements. For example, the acceptable losses, L_p , in a channel may be defined through a basic link budget which may take the form,

$$L_p(dB) = \Omega_t + G_T + G_R - S_{Rx}, \quad (5.2)$$

where the acceptable path loss, in dB is equal to the combination of the transmitted power (Ω_t) the gain of both the transmitting and receiving antennas (G_T, G_R respectively). The ability of the receiver to detect signals in the presence of noise is also included in the link budget and defined as (S_{Rx}). Other parameters are relevant and may also be included depending on the specific circumstances. For example,

$$L_p(dB) = \Omega_t + G_T + G_R - S_{Rx} - M_{shad} - L_{Slow} - L_{Fast} - L_I + G_{HO}, \quad (5.3)$$

where channel slow fading loss, L_{Slow} , fast fading, L_{Fast} , shadowing, M_{shad} , and interference loading, L_I , reduce the link budget whereas G_{HO} , the handoff gain, increases the maximum allowable path loss.

The contributions of slow fading, shadowing and fast fading due to multipath effect are often the most difficult aspects of the link budget to quantify. Furthermore, they are often the most detrimental to maintaining a communications link. Multipath effects causing fading and ducting [43] is a predominantly studied topic in the field of marine communications. They are highly regarded as a detrimental factor in channel performance as changing multipaths [41],[42] are generated by a changing sea surface. This effect is also observed to worsen with increasing sea surface height [38],[81] and roughness. For this reason, in this effort we seek novel methods to quantify these detrimental effects in a pragmatic fashion suitable to aid in the link budget calculations of the system design process.

The link budget may also be used to provide insight into mitigation of communications problems. For example, the consideration of increasing the transmitted power, or replacing either antennas with one of a higher gain can be directly evaluated as a solution possibility to a poor quality of service communications link by re-examination of the link budget. However, if more detailed knowledge about the communications channel performance is available during the preliminary design process, it is a clear advantage to the system designer as quality of service problems can be innately avoided in the original system architecture.

5.4 Large Scale Fading (Shadowing)

Large scale fading, or shadowing, is referred to as the average loss of signal power over large areas, that is, the result of either path loss or attenuation within propagating mediums [23]. Unlike multipath fading, shadowing is caused by large terrain features located between the base station and the mobile subscriber. Typically, these

large objects include terrain features such as hills or mountains [61], trees, and buildings [82],[21]. In short, the receiver can be described as being "shadowed" by these large sized geographical features. The signal strength that is received, E , at an antenna from a source E_o , may then be expressed as,

$$E = E_o F e^{j\Delta\varphi}, \quad (5.4)$$

where F is an attenuation coefficient and $\Delta\varphi$ is a phase shift corresponding to the electrical length of each signal path. Using the path loss equation, it has been determined for non-ideal propagation paths the loss could be expressed generically as [83],

$$L_p(d) = L_s(d_o) + 10n \log(d/d_o), \quad (5.5)$$

where d is distance and d_o is a measured value of reference to a point taken in the far field of the antenna. The value of the loss exponent, n , commonly referred to as the path loss exponent, is dependent on physical attributes such as antenna heights, the wavelength, and the physical propagation environment. Normally n varies between 2 and 4, however in urban environments [21] in which streets can have a "waveguide" effect, the value of n can be less than 2 [20]. This is particularly interesting as in these circumstances the loss experienced in the propagation environment as a function of distance is actually less than that of free space loss.

The path loss as expressed above represents only the average value of attenuation. Realistically, a random contribution to the total loss is observed. To include this effect, the path loss equation is modified to become,

$$L_p(d) = L_s(d_o) + 10n \log(d/d_o) + X_\sigma, \quad (5.6)$$

where X_σ represents the zero mean Gaussian random variable with standard deviation of σ . The random contributions in typical mobile user propagation environments

[26],[84] of this term can contribute as much as 10 dB to the total path loss [24]. This formulation constitutes the primary objective for wireless communications channel modeling, whereby measurements are conducted to determine explicitly both n and X_σ . This study will also be the case, whereby these parameters will be determined based on numerical simulation of a marine communications channel under a sea surface shadowing condition for a variety of random sea surfaces. The novelty in this segment of work is utilizing the FDTD simulation method to establish path loss parameters with the advantage of a known sea surface using the same methodology whereby measurements are normally conducted and for the marine case the details of the sea surface are relatively unknown. This novel approach to the study of marine communications channels is a distinct solution to explicitly evaluating the contributions of shadowing and multipath fading of a specific sea surface as experienced during communications channel measurement studies [38].

5.5 Small Scale Fading and Subsequent Transient Channel Effects

Small scale fading is commonly referred to as fast fading and is typically a result of multipath effects in proximity to the receiver. Slight spatial motion, on the order of a wavelength, can dramatically effect the received signal amplitude and phase. It is a common problem for terrestrial mobile communications [24]. Satellite communications systems usually stipulate that a line of site be maintained to the sky, whereby the line of site signal component normally dominates the amplitude of the received signal [4],[10]. However, for typical terrestrial based commercial cellular systems it is rare that a line of sight condition exists between the base station and the mobile user. Moreoften, the receiver is not within a visible path to the transmitter, particularly in urban environments [44]. In the case where no line of sight exists, small scale fading, or Rayleigh fading, is observed to occur. Spatial variation on the order of partial

wavelengths between the transmitter and receiver can result in significant changes in the received signal amplitude and phase. This is due to the individual multipath signals contributing either constructively or destructively at the physical location of the receiver. Each specific multipath component will experience a specific phase shift and attenuation resulting from its respective signal propagation path. This is illustrated in 5-2, whereby the magnitude and latency of each multipath changes in time. Ultimately, the small fading phenomenon has two distinct effects on signals propagating through the wireless channel [26]:

1. Signal dispersion, which also may be described as spreading in time.
2. The channel fading is stochastic. That is, the small fading effect changes with time. This case is illustrated in Figure 5-2.

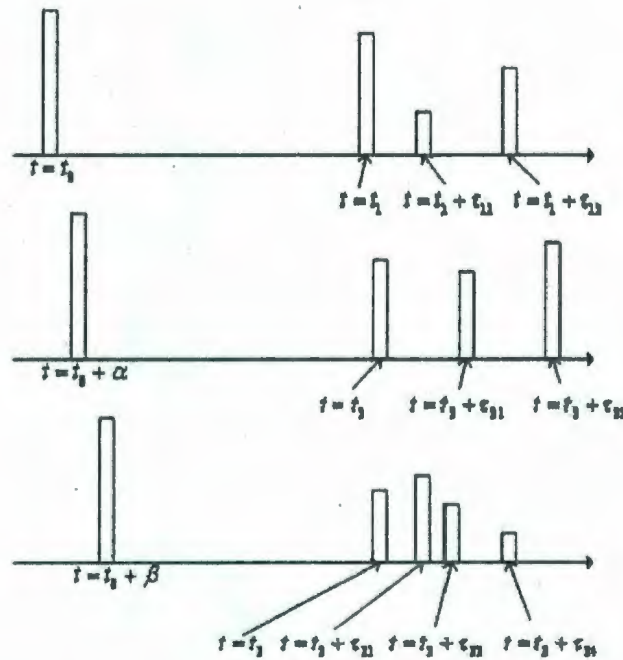


Figure 5-2: For a single narrow impulse, the time domain response of a channel is both time variant and dispersive.

The case where a line of sight exists in the communications channel, and the

overall signal is dominated by that component, leads to the definition of the Rice Factor, K ,

$$K = \frac{\text{Specular Power}}{\text{Scattered Power}}, \quad (5.7)$$

whereby the specular component of the received signal is the impulse received from the line of sight component, and the scattered signal is those that arrive at the receiver via alternate pathways. The Rice factor is simply the ratio of the two propagation mechanisms. In this case the response demonstrates various received multipath components with different amplitudes and delays when the channel is sounded at different times. Channel sounding is normally conducted with a single narrow impulse [82]. Characterization of the time domain attributes of the channel is often done using the mean excess delay (MXS) and the root mean excess delay. The mean excess delay is defined [85],

$$MXS = \bar{\tau} = \frac{\sum_k \alpha_k^2 \tau_k}{\sum_k \alpha_k^2}, \quad (5.8)$$

such that the mean excess delay is known as the first moment of the power delay spectrum. The root mean square (RMS) delay spread,

$$RMS = \sigma = \sqrt{\frac{\sum_k \alpha_k^2 \tau_k^2}{\sum_k \alpha_k^2} - \left(\frac{\sum_k \alpha_k^2 \tau_k}{\sum_k \alpha_k^2} \right)^2}, \quad (5.9)$$

is the square root of the second central moment of the delay profile. Here α_k corresponds to the signal magnitude occurring at time τ_k after the initial received signal, whereby τ_0 is the initial impulse of the received multipath signal, for all k multipaths between the transmitter and receiver.

5.6 Summary of Channel Modeling Concepts

This chapter has provided the fundamental aspects of characterizing a communications channel's performance in the frequency domain using the path loss equation and in the time domain, using the mean excess and root mean square delays. These models are well documented in the literature as they are utilized in every genre of wireless communications channel characterization. Collectively, these models provide the basis of the required information regarding the fast and slow fading effects of the communications channel, as well as the respective effects for impact on digital signalling protocols. Typically, these models are obtained through direct measurement and provide insight into the link budget contribution, such as transmit power and antenna gain, which are specified as part of the system design process. The data rates sustainable in the channel can be estimated based on the intersymbol interference as characterized by the respective mean excess and root mean square delay characteristics. In this research effort, evaluation of these parameters will be conducted through the proposed marine communications channel simulation methodology, whereby detailed knowledge of the random sea surface permits the establishment of generalized models suited to the marine communications channel that are functions of both frequency and observable sea surface height. The readily available details of the sea surface, which is innate to the FDTD methodology, is the distinct advantage when conducting overwater propagation analysis in the marine environment. This knowledge makes formulations of these communications channel performance parameters in conjunction with the physical attributes of the sea surface possible.

Chapter 6

Development of a Novel Marine Electromagnetic Propagation Analysis Tool

6.1 The History of EM Simulation

The study of electromagnetics (EM) has been a traditional area in science, mathematics and physics for many years. A number of classical academic problems can be found in undergraduate level texts on the subject [86]. In recent years with advancements in modern computing science, particularly with increased processing speed and available memory, a change in the approach to seeking solutions to Maxwell's equations has occurred. The field of computational electromagnetics is centered upon the use of novel numerical methods [87] to solve for EM fields, for a wide variety of geometries, particularly for which no analytical solution is easily attainable. The rational is easily understood. Rather than develop complex analytical expressions for EM solutions specific to a problem, the development of generalized recursive formulae can be used to obtain a numerical result for which an analytical solution is difficult, or even impossible, to obtain. A structure of interest is divided into discrete elements by

applying a finite mesh, whereby these formulae represent relations between elements of the structure. This approach is much more progressive than is the case with early methods of computer aided design, when computers had limited computational ability [17],[18]. This work will develop a novel EM simulator for the purpose of marine communications channel overwater propagation analysis. The finite difference - time domain method is used to produce transient solutions to Maxwell's equations for a known sea surface in which the sea surface is implemented as a perfectly conducting boundary condition in the EM problem [38].

For this study, a complete custom software solution is developed in Matlab without the use of any commercial products. The software approximates the communications channel by a 2-dimensional cross section rather than a 3-dimensional marine communications channel. The reason for this is the limited amount of computing resources available at the time of this study. In order to conduct a 3-dimensional study, approximately one thousand times the physical memory would be required of computing hardware. This is based on the fact that the 2-dimensional (x,y) cross section would have to be repeated with an approximate equal number of segments in the third dimension. Luckily, a 2-dimensional approximation provides a workable numerical approach to obtain the solution of a truly 3-dimensional problem [88]. This is common practice in the field of numerical analysis, whereby current methodologies of simulating 3-dimensional structures, such as printed transmission lines, were originally studied using 2-dimensional cross sections [72] as a reduced complexity approximation. The 3-dimensional solutions emerged later as increased computing resources were made available. The 3-dimensional simulation would yield a more realistic simulation result, as the multipath effect is a more complex mechanism in reality.

The concept of using direct solutions to Maxwell's equations for the purpose of propagation analysis is only possible with the recent advance in computing ability. This is particularly a result of the increased availability of computer memory [30]. The

original application of this approach for computational electromagnetics was primarily focused on planar circuits such as patch antennas, printed filters, and transmission line analysis [74],[89],[75]. Previous applications of this technique for channel modeling have been oriented toward room size channel simulation for the purpose of WLAN applications [32]. This work will develop a novel method for the simulation of marine communications channels, whereby the FDTD method is implemented and overwater propagation is modeled over a known sea surface. The aspect of being able to conduct marine communications channel propagation analysis provides an alternate approach to the deficiency of dealing with the unknown sea surface statistically, which has been the general method used during measurement studies. Using the proposed methodology, the innate availability of detailed knowledge regarding the attributes of the physical sea surface allows the establishment of direct relations between channel performance parameters in regard to both frequency and sea surface height.

One of the most common approaches to EM analysis is the Method of Moments (MoM) [76]. This technique, pioneered by R.F.Harrington, was the theoretical basis for the bulk of commercial EM solvers popular in the 1980s and 1990s. For this reason, some details of the operation of the MoM algorithm will be offered as they provide insight into the lack of development of numerical methods for channel simulation to date. The solutions for the MoM were based on dividing a structure by a finite grid, whereby the size of the elements were significantly less than the size of the structure, as well as a fraction of the size of a wavelength for the frequency of interest. These elements were then related to each other in the form of a mutual impedance matrix. Each element of the matrix for the MoM represents a mutual impedance between either itself or another element of the overall structure. A unique matrix was required for each frequency point of interest, and the solutions were obtained by inverting this matrix. Though very effective for planar circuits and compact structures, this method suffers from two deficiencies that quickly become apparent when using the MoM approach:

1. The matrix based method produces an N by N matrix for a structure divided into N elements. As the structure size increases, the more likely the efforts to obtain the solution will fail based on an ill-conditioned matrix due to numerical error.
2. With increasing matrix size, computing time to solve the solution for a single frequency point of interest increases proportional to the square of the number of discrete elements.

In short, the Method of Moments provided a fast means of obtaining a solution for a structure that is physically on the order of size of the wavelength for the frequency of interest. Furthermore, the solutions are obtained for a single frequency at a time, which lends this method very applicable to design optimization which tends to be very bandwidth limited in operation. Nonetheless, as physical size of the structure is increased, the method is more prone to error and computation time increases dramatically.

In the late 1990s, when low cost computing power became widely available on a desktop level, a new era in seeking numerical solutions to Maxwell's equations emerged [90],[91]. Other practical applications of computational electromagnetics surfaced, even in the field of electromagnetic compatibility, where the simulation of structures significantly larger than conventional RF circuits is commonly required [92]. High speed digital connectors were considered mixed signal components and also benefited from EM analysis [71]. High performance computers and sophisticated algorithms were being used for optimization of RF devices using repetitive and intelligent algorithms for refinement [93]. With an increased amount of available computer memory and computational power, the finite difference-time domain technique (FDTD) began to gain popularity in the commercial electromagnetic market space. Problems that were previously not feasible using state of the art computing hardware were suddenly workable on the desktop level. The FDTD method is based on a transient (time domain) solution of Maxwell's equations. Recursive solutions are used whereby

a pulse excitation was introduced into a transmission medium and then the electric and magnetic fields were solved in a "leap-frog" fashion over a series of discrete time steps [48]. Although the process of obtaining the solution seemed long in comparison to the Method of Moments, several advantages became immediately apparent:

1. The solution produced a broadband response based on the input signal. That is, numerous frequencies could be solved for simultaneously depending on the frequency content of the excitation pulse. Fourier analysis was used on the input and output transient signals from which convention scattering parameters could be calculated.
2. Numerically, it was possible to find solutions for extremely complex structures. The technique appeared more robust for structures on the same physical size of the wavelength of the frequency of interest with increasingly complex physical forms.
3. The computational effort required to solve a problem increased linearly, rather than exponentially as with the MoM, with the number of unknowns for analysis.

These factors offer a distinct pre-aptitude in using the FDTD algorithm for large size structure analysis, or as in this case, for channel propagation analysis.

This chapter will now detail the process of development of a novel methodology applying the FDTD technique for marine overwater propagation analysis. The key aspect of the proposed methodology is that with a known sea surface, marine propagation analysis can be studied and produce direct relations between channel response and sea surface height during post simulation analysis. This method is employed to augment the development of the theoretically-based marine geometrical theory of diffraction as previously formulated in this work, whereby this numerical analysis is used to produce a overwater propagation analysis complimentary to those conducted by direct channel measurements. The advantage of using the proposed method of simulation is that the models will be based upon propagation analysis where detailed

knowledge of the sea surface is available. The lack of knowledge of the sea surface over which propagation studies have been performed historically has been the largest challenge in understanding direct relations between channel performance parameters and physical attributes of the sea surface [38]. In this study, the modified Pierson-Moskowitz model is used for the random sea surface synthesis, which is specific to the north North Atlantic region, however any sea surface model may be used in the proposed methodology, depending on the specific region of interest.

Development of an EM simulator is a challenging and difficult process. Not only must the conceptual problem be developed and formulated, but it must be implemented in a practical fashion such that the simulation is effective, efficient and numerically accurate. The ability of this custom tool to accurately calculate diffraction will be proven by numerical simulation of the well known knife edge topology, for which analytical expressions can easily be evaluated and compared to the numerical results produced by the FDTD software. The theoretical formulations will be given in this work for the FDTD method as well as the process for developing a random sea surface, as both are fundamental to the implementation of this novel approach to marine communications channel propagation analysis. Some details of the implementation, such as the air-to-air boundary conditions [48],[30] and mathematical details regarding the random nature of the sea surface [79] are not detailed in the overview of this methodology, but readily available in the cited publications.

6.2 Formulation of the Finite Difference - Time Domain Problem

It would be unjust not to begin the process of the development of any electromagnetic simulation tool without first providing Maxwell's equations. From an electromagnetics perspective, in regard to the field of numerical analysis and computational electromagnetics [94], the primary objective is to find novel methods from which solutions

to Maxwell's equations can be obtained. This approach is primarily used for complex problems whereby analytic solutions are not easily attainable, or in some cases not attainable at all. In this work, we are seeking to perform electromagnetic analysis of the marine communications channel using the FDTD approach. This is a novel approach to marine communications channel simulation [1], and based on the difficulty in dealing with the problem analytically, it is an excellent opportunity to utilize computational electromagnetics to obtain understanding of overwater propagation effects. Maxwell's equations are thus defined as [86],

$$\nabla \times \vec{E} = -\frac{\partial \vec{B}}{\partial t} - \vec{M} \quad (6.1)$$

$$\nabla \times \vec{H} = \frac{\partial \vec{D}}{\partial t} + \vec{J} \quad (6.2)$$

$$\nabla \cdot \vec{H} = 0 \quad (6.3)$$

$$\nabla \cdot \vec{E} = \frac{\rho}{\epsilon}, \quad (6.4)$$

where

$$\vec{B} = \mu_o \vec{H} \quad (6.5)$$

and

$$\vec{D} = \epsilon_o \vec{E}. \quad (6.6)$$

The solutions in this case are obtained by transient means, whereby a finite difference approximation is formulated [30]. This is known as the central-difference approximation, and it is applied in a spatial and temporal sense to the above curl equations. For a one-dimensional problem, Maxwell's curl equations may be written as [48]:

$$\frac{E_x^{n+1/2}(k) - E_x^{n-1/2}(k)}{\Delta t} = -\frac{1}{\epsilon_o} \frac{H_y^n(k+1/2) - H_y^n(k-1/2)}{\Delta z} \quad (6.7)$$

$$\frac{H_y^{n+1}(k+1/2) - H_y^n(k+1/2)}{\Delta t} = -\frac{1}{\mu_o} \frac{E_x^{n+1/2}(k+1) - E_x^{n+1/2}(k)}{\Delta z} \quad (6.8)$$

In this form, n refers to the time step of the recursive formula. E_x and H_y are the electric and magnetic fields respectively. t refers to the time and ϵ_o and μ_o are the free space permittivity and permeability respectively. The terms in parenthesis, k , represent the spatial displacement. Thus for a practical simulation, whereby the transient response of a system that is of Z spatial dimension and the transient electric and magnetic fields are desired at time T , provided we designate the discrete element length to be Δx and the Δt , then the total physical length of the system is given

$$Z = \Delta x \cdot k \quad (6.9)$$

and the total transient length of the simulation is given by

$$T = \Delta t \cdot n. \quad (6.10)$$

It is interesting to note that the reference in the central difference approximation of Maxwell's equations references the physical location of the H fields to be located between the E fields. Functionally, the electric field for the entire grid structure is calculated at every location, followed by the magnetic field at every location. More explicitly, the formulations model each entity as interleaved with it's counterpart in both time and space. This is illustrated in Figure 6-1.

Once the concept of interleaving to produce a co-dependence of the electric and magnetic fields upon each other in both a time and space is established, it becomes necessary to rearrange the formulation to produce a recursive relationship between the two. For a one dimensional problem:

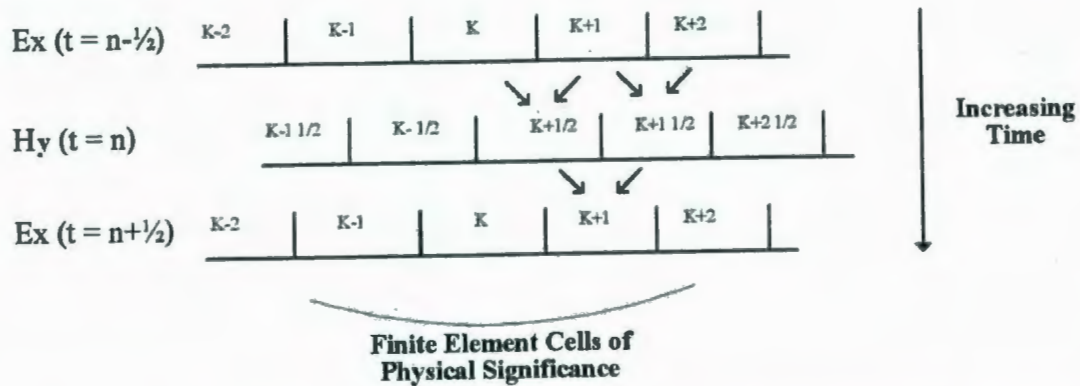


Figure 6-1: The "leapfrog" modeling approach to the finite difference technique, illustrating the E and H fields interleaved in both time and space.

$$\frac{\partial E_x}{\partial t} = \frac{1}{\sqrt{\epsilon_0 \mu_0}} \frac{\partial H_y}{\partial z} \quad (6.11)$$

$$\frac{\partial H_y}{\partial t} = -\frac{1}{\sqrt{\epsilon_0 \mu_0}} \frac{\partial E_x}{\partial z} \quad (6.12)$$

To produce a recursive solution, the E_x and H_y fields may be rewritten,

$$E_x^{n+1/2}(k) = E_x^{n-1/2}(k) + \frac{\Delta t}{\sqrt{\epsilon_0 \mu_0} \Delta x} [H_y^n(k+1/2) - H_y^n(k-1/2)] \quad (6.13)$$

$$H_y^{n+1}(k+1/2) = H_y^n(k+1/2) - \frac{\Delta t}{\sqrt{\epsilon_0 \mu_0} \Delta x} [E_x^{n+1/2}(k+1) - E_x^{n+1/2}(k)], \quad (6.14)$$

such that the current E_x and H_y field solutions at a finite interval in space, are dependent upon the previous field value at the same point in space, and the finite difference of the field counterparts of the previous $\frac{1}{2}$ time step at the adjacent interleaved points in space. The 3-dimensional problem is a more complex formulation. The extension of the "leapfrog" from one dimension to 3-dimensions leads to the Yee cell [48],[70].

The Yee cell is illustrated in 6-2.

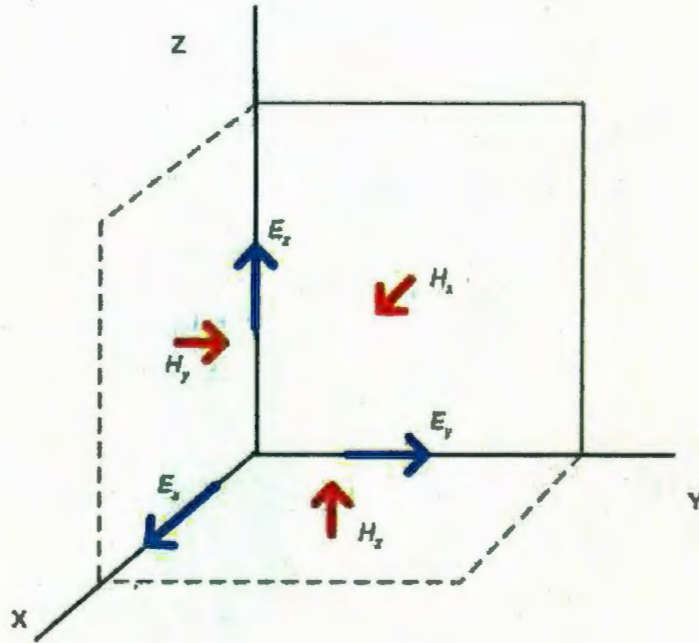


Figure 6-2: The 3-dimensional Yee cell illustrating the orientation of the \vec{E} and \vec{H} fields.

For the channel simulation of interest, a 2-dimensional cross section will be used. The 3-dimensional formulation as per the first derivation by Yee is of the form, [89]

$$\begin{aligned}
 E_x^{n+1}(i + \frac{1}{2}, j, k) &= \left(\frac{\epsilon - \sigma \Delta t / 2}{\epsilon + \sigma \Delta t / 2} \right) E_x^n(i + \frac{1}{2}, j, k) \\
 &+ \frac{\Delta t / \Delta y}{\epsilon + \sigma \Delta t / 2} \left[H_z^{n+1/2}(i + \frac{1}{2}, j + \frac{1}{2}, k) - H_z^{n+1/2}(i + \frac{1}{2}, j - \frac{1}{2}, k) \right] \\
 &- \frac{\Delta t / \Delta z}{\epsilon + \sigma \Delta t / 2} \left[H_y^{n+1/2}(i + \frac{1}{2}, j, k + \frac{1}{2}) - H_y^{n+1/2}(i + \frac{1}{2}, j, k - \frac{1}{2}) \right]
 \end{aligned} \tag{6.15}$$

$$\begin{aligned}
 E_y^{n+1}(i, j + \frac{1}{2}, k) &= \left(\frac{\epsilon - \sigma \Delta t / 2}{\epsilon + \sigma \Delta t / 2} \right) E_y^n(i, j + \frac{1}{2}, k) \\
 &+ \frac{\Delta t / \Delta z}{\epsilon + \sigma \Delta t / 2} \left[H_x^{n+1/2}(i, j + \frac{1}{2}, k + \frac{1}{2}) - H_x^{n+1/2}(i, j + \frac{1}{2}, k - \frac{1}{2}) \right] \\
 &- \frac{\Delta t / \Delta x}{\epsilon + \sigma \Delta t / 2} \left[H_z^{n+1/2}(i + \frac{1}{2}, j + \frac{1}{2}, k) - H_z^{n+1/2}(i - \frac{1}{2}, j + \frac{1}{2}, k) \right]
 \end{aligned} \tag{6.16}$$

$$\begin{aligned}
E_z^{n+1}(i, j, k + \frac{1}{2}) &= \left(\frac{\epsilon - \sigma \Delta t / 2}{\epsilon + \sigma \Delta t / 2} \right) E_z^n(i, j, k + \frac{1}{2}) \\
&+ \frac{\Delta t / \Delta x}{\epsilon + \sigma \Delta t / 2} \left[H_y^{n+1/2}(i + \frac{1}{2}, j, k + \frac{1}{2}) - H_y^{n+1/2}(i - \frac{1}{2}, j, k + \frac{1}{2}) \right] \\
&- \frac{\Delta t / \Delta y}{\epsilon + \sigma \Delta t / 2} \left[H_x^{n+1/2}(i, j + \frac{1}{2}, k + \frac{1}{2}) - H_x^{n+1/2}(i, j - \frac{1}{2}, k + \frac{1}{2}) \right]
\end{aligned} \tag{6.17}$$

$$\begin{aligned}
H_x^{n+1/2}(i, j + \frac{1}{2}, k + \frac{1}{2}) &= H_x^{n-1/2}(i, j + \frac{1}{2}, k + \frac{1}{2}) \\
&- \frac{\Delta t}{\mu \Delta y} \left[E_z^n(i, j, k + \frac{1}{2}) - E_z^n(i, j - 1, k + \frac{1}{2}) \right] \\
&+ \frac{\Delta t}{\mu \Delta z} \left[E_y^n(i, j + \frac{1}{2}, k) - E_y^n(i, j + \frac{1}{2}, k - 1) \right]
\end{aligned} \tag{6.18}$$

$$\begin{aligned}
H_y^{n+1/2}(i + \frac{1}{2}, j, k + \frac{1}{2}) &= H_y^{n-1/2}(i + \frac{1}{2}, j, k + \frac{1}{2}) \\
&- \frac{\Delta t}{\mu \Delta z} \left[E_x^n(i + \frac{1}{2}, j, k) - E_x^n(i + \frac{1}{2}, j, k - 1) \right] \\
&+ \frac{\Delta t}{\mu \Delta x} \left[E_z^n(i, j, k + \frac{1}{2}) - E_z^n(i - 1, j, k + \frac{1}{2}) \right]
\end{aligned} \tag{6.19}$$

$$\begin{aligned}
H_z^{n+1/2}(i + \frac{1}{2}, j + \frac{1}{2}, k) &= H_z^{n-1/2}(i + \frac{1}{2}, j + \frac{1}{2}, k) \\
&- \frac{\Delta t}{\mu \Delta x} \left[E_y^n(i, j + \frac{1}{2}, k) - E_y^n(i - 1, j + \frac{1}{2}, k) \right] \\
&+ \frac{\Delta t}{\mu \Delta y} \left[E_x^n(i + \frac{1}{2}, j, k) - E_x^n(i + \frac{1}{2}, j - 1, k) \right]
\end{aligned} \tag{6.20}$$

For the transverse magnetic TM mode of propagation,

$$E_x = E_y = H_z = 0 \tag{6.21}$$

the 3-dimensional formulation reduces to a simplified form

$$\begin{aligned}
E_z^{n+1}(i, j) &= \left(\frac{\epsilon - \sigma \Delta t / 2}{\epsilon + \sigma \Delta t / 2} \right) E_z^n(i, j) \\
&+ \frac{\Delta t / \Delta x}{\epsilon + \sigma \Delta t / 2} \left[H_y^{n+1/2}(i + \frac{1}{2}, j) - H_y^{n+1/2}(i - \frac{1}{2}, j) \right] \\
&- \frac{\Delta t / \Delta y}{\epsilon + \sigma \Delta t / 2} \left[H_x^{n+1/2}(i, j + \frac{1}{2}) - H_x^{n+1/2}(i, j - \frac{1}{2}) \right]
\end{aligned} \tag{6.22}$$

$$H_x^{n+1/2}(i, j + \frac{1}{2}) = H_x^{n-1/2}(i, j + \frac{1}{2}) - \frac{\Delta t}{\mu \Delta y} [E_z^n(i, j) - E_z^n(i, j - 1)] \tag{6.23}$$

$$H_y^{n+1/2}(i + \frac{1}{2}, j) = H_y^{n-1/2}(i + \frac{1}{2}, j) + \frac{\Delta t}{\mu \Delta x} [E_z^n(i, j) - E_z^n(i - 1, j)]. \quad (6.24)$$

Similarly, for the transverse electric TE mode of propagation,

$$H_x = H_y = E_z = 0 \quad (6.25)$$

$$E_x^{n+1}(i + \frac{1}{2}, j) = \left(\frac{\epsilon - \sigma \Delta t / 2}{\epsilon + \sigma \Delta t / 2} \right) E_x^n(i + \frac{1}{2}, j) + \frac{\Delta t / \Delta y}{\epsilon + \sigma \Delta t / 2} \left[H_z^{n+1/2}(i + \frac{1}{2}, j + \frac{1}{2}) - H_z^{n+1/2}(i + \frac{1}{2}, j - \frac{1}{2}) \right] \quad (6.26)$$

$$E_y^{n+1}(i, j + \frac{1}{2}) = \left(\frac{\epsilon - \sigma \Delta t / 2}{\epsilon + \sigma \Delta t / 2} \right) E_y^n(i, j + \frac{1}{2}) - \frac{\Delta t / \Delta x}{\epsilon + \sigma \Delta t / 2} \left[H_z^{n+1/2}(i + \frac{1}{2}, j + \frac{1}{2}) - H_z^{n+1/2}(i - \frac{1}{2}, j + \frac{1}{2}) \right] \quad (6.27)$$

$$H_x^{n+1/2}(i + \frac{1}{2}, j + \frac{1}{2}) = H_x^{n-1/2}(i + \frac{1}{2}, j + \frac{1}{2}) - \frac{\Delta t}{\mu \Delta x} [E_y^n(i, j + \frac{1}{2}) - E_y^n(i - 1, j + \frac{1}{2})] + \frac{\Delta t}{\mu \Delta y} [E_x^n(i + \frac{1}{2}, j) - E_x^n(i + \frac{1}{2}, j - 1)] \quad (6.28)$$

In free space, in which there are no conductors, propagation occurs in either the TE or TM and not the TEM mode. For this reason, and to demonstrate the proposed methodology of overwater propagation analysis, we will utilize the TM mode formulation for numerical simulations from this point forward. A similar analysis of the TE mode is possible using the same methodology, however such an analysis will not be conducted as part of this demonstration of the proposed methodology and subsequent numerical study.

6.3 Finite Elements of Space and Time

An electromagnetic wave in free space cannot go faster than the speed of light. This is a fundamental truth of modern physics. For this reason, the time step and the cell size

are closely related to FDTD simulation techniques in the sense that proper selection of both the cell size, Δx and Δy , and time step, Δt , is critical to ensure that the FDTD simulation is both numerically stable and accurate. It is a well studied problem in the field of computational electromagnetics that for accurate representation of a structure, it is commonly accepted that the cell segments should be allocated such that at least 10 [30] cells per wavelength of interest mesh the structure. Therefore, the upper frequency limit of interest provides the cell size in all dimensional directions such that in free space,

$$c = f\lambda \quad (6.29)$$

$$\Delta x \leq \frac{\lambda}{10} = \frac{c}{10 \cdot f}. \quad (6.30)$$

A similar situation exists in the y and z directions. Choosing a cell size that is larger than this limit may cause the transient solution of the FDTD algorithm to be non-convergent. The symptom of which is easily seen as the magnitude of the E and H fields will increase as they propagate through free space.

Choosing the time step value for the FDTD simulation is of equal importance to the choice of physical structure cell size. The time step has two effects for the channel simulation to be considered after the cell size has been specified:

1. The time step must satisfy the Courant Condition [49] such that the recursive formulations are convergent.
2. The individual time step in conjunction with the number of recursive iterations will dictate the overall length of the transient simulation, which must be maintained of sufficient duration such that the vast majority of energy has exited the communications channel model through free space boundaries.

Furthermore, as a practical application of the input pulse, if the excitation pulse

is based on a discrete number of time steps rather than a fixed duration, changing the time step will change the overall duration of the pulse, ultimately effecting the spectral content of the simulation. A smaller time step will result in an increasing amount of frequency bandwidth and conversely a longer time step results in a decreased amount of spectral content. Therefore, depending on what frequency bands are of interest, the excitation and the time step for the transient simulation must be chosen in conjunction with the cell sizes such that the impulse response for the relevant spectral content is obtained. A more detailed examination of the excitation waveform and subsequent spectral content will be given in the next section.

When selecting the cell size in one dimension, the time step must be less than the propagation time through the single spatial division. Assuming Δx , Δy and Δz are equal, the following time is required to propagate one cell distance,

$$\Delta t = \Delta x/c. \quad (6.31)$$

In two dimensions, rather than considering the width of the cell, we consider the diagonal distance. This then leads to the modified propagation time through the cell,

$$\Delta t = \frac{\Delta x}{\sqrt{2}c}. \quad (6.32)$$

Similarly, for the 3-dimensional case, the time required is not surprisingly given by,

$$\Delta t = \frac{\Delta x}{\sqrt{3}c}. \quad (6.33)$$

Thus, this leads to the Courant Condition [48], whereby for FDTD simulation of the time step should be chosen on the basis of numerical stability such that,

$$\Delta t \leq \frac{\Delta x}{\sqrt{nc}} \quad (6.34)$$

where Δx is the smallest cell size in all of the n -dimensional space.

Without proper selection of the cell size and subsequent time step, it is computationally costly to perform a sizeable simulation by numerical analysis and then obtain results that are either non-convergent or lack the relevant spectral content [30]. Numerical dispersion is also a concern when choosing the cell size for finite difference analysis [95]. The effects of the dispersion [30] are related to propagation through a square cell, and should be considered carefully when conducting transient simulation for propagation flight time calculations. The effect is particularly increased for structures requiring a larger number of cells for physical representation by the finite difference grid.

Once the the FDTD algorithm and excitation pulse are implemented, it is possible to conduct propagation studies inside a 2-dimensional cross section of a metal box. With no boundary conditions implemented, the FDTD algorithm naturally behaves as though the perimeter elements are a perfectly conducting surface. For studies in free space, boundary conditions must be applied to absorb the electromagnetic fields appropriately. The implementation of these boundary conditions is essential for numerical accuracy of the propagation analysis. A number of techniques can be employed. Either the perfectly matched layer (PML) [48] or the absorbing boundary condition (ABC) can be applied to suppress reflections from the perimeter of the 2-dimensional boundary [30], which emulates a free space boundary as would occur in an actual terrestrial communications channel on three sides. For the purpose of this work, a random sea surface is the boundary condition to be implemented on one side of the 2-dimensional cross section. The sea surface should be of realistic form for the geographical region of interest, and furthermore is approximated as a perfectly conducting surface. Synthesis and implementation of this surface is based on the modified Pierson-Moskowitz spectral models and it's implementation is a key component of this proposed methodology.

6.4 The Specifics of the north North Atlantic Ocean

The electromagnetic simulation engine that has been developed for simulation of over-water radio propagation analysis in a marine communications channel must contain a realistic sea surface implemented as a boundary condition during the FDTD analysis. For the purpose of this study, the modified Pierson-Moskowitz sea surface spectral model is used, as it pertains specifically to the north North Atlantic region [28]. The spectral functions, which were used in the development of the marine geometrical theory of diffraction previously given in this work for a single sea surface wave, are used once again for the boundary condition synthesis process. Instead of using a single wave, multiple waves are distributed at arbitrary locations along the 2-dimensional boundary to create a random sea surface [55]. With the well-known fact that higher sea heights and increased roughness increase fading in the communications channel [41],[42], to illustrate the significance of this work to the north North Atlantic region, we begin with an examination of regional sea state probabilities throughout the world.

The North Atlantic ocean is widely known to be one of the most extreme and harsh environments in the world [28]. The strength and power of the ocean plays no small part in obtaining this reputation. Thus, in order to generate a sea surface boundary condition for propagation analysis during various sea states, it becomes fundamental to understand the specific characteristics of the ocean surface for the region. Upon examination of the sea state probability of the North Atlantic ocean and the north North Atlantic ocean, it becomes immediately clear that the region is nearly twice as likely to have higher sea states compared to general conditions worldwide. This data is illustrated in table 6.1 [28].

With the increased probability of a higher sea state in the north North Atlantic region, knowing fading increases with increased sea surface height and roughness, it is of greater importance to evaluate these effects for any wireless marine communications channel application operating in the north North Atlantic. In this work, we focus on the effects of the sea surface during a shadowing condition, whereby the

Sea State	Description	Observed Wave Height (m)	% Probability		
			World	North Atlantic	North North Atlantic
0	Calm (Glassy)	0			
1	Calm (Rippled)	0-0.1	11.24	8.31	6.06
2	Smooth (Wavelets)	0.1-0.5			
3	Slight	0.5-1.25	31.69	28.2	21.57
4	Moderate	1.25-2.5	40.19	42.03	40.99
5	Rough	2.5-4.0	12.8	15.44	21.24
6	Very Rough	4.0-6.0	3.03	4.29	7.01
7	High	6.0-9.0	0.93	1.5	2.69
8	Very High	9.0-14.0	0.12	0.23	0.43
9	Phenomenal	>14.0	0.009	0.0016	0.0035

Table 6.1: The sea state/observed wave height probability by for the North Atlantic, the north North Atlantic compared to worldwide locations.

transmitter and receiver are not within line of sight of each other, and are obstructed by a sea surface wave. Implementation of a random sea surface as a boundary condition in the FDTD simulation engine requires some assumptions to be made about the sea surface to simplify the physical channel model and overwater radio propagation analysis thereof:

1. The sea surface is deemed to be a perfect conducting surface [26]. That is, there is no account of skin depth or loss due to imperfect reflection of the incident wave upon the boundary between the air and sea surface.
2. The communications channel is assumed to be in deep water, not shallow. The spectral models used are for fully developed deep sea conditions. Should a channel analysis in a different location be desired, the same process as outlined in this study can be used with the sea surface model respective to the specific conditions and geography.
3. There is no account for sea spray or higher order effects. That is, the general contour of the wave is used as the boundary condition only. This is a property of the Pierson-Moskowitz model. Breaking waves and subsequent effects that

this would have on the diffraction and scattering around the peaks of waves are excluded as a simplification in this effort.

4. The sea surface is assumed to be stationary throughout each electromagnetic simulation. Doppler effect is unrepresented in this numerical simulation, as the transmitter, receiver and sea surface remain in fixed positions for the duration of the propagation analysis, as does the sea surface boundary condition. The rate of velocities of the traveling sea surface waves and ocean going surface vessels are typical of moving objects in terrestrial communications channels, for which current mobile communications technology is already mitigating.

6.5 Generating A Random Sea Surface as a Physical Channel Model Component

Pierson and Moskowitz developed a wave spectral formulation for fully developed seas in the north North Atlantic ocean [96]. This spectrum was formulated as a function of wind speed that was measured at 19.4 m above the sea surface. Using classical sea surface theoretical techniques [79], this can be simplified such that sea surface spectral content is a function of observable wave height only for a fully developed sea, as is demonstrated previously in this work. The boundary condition synthesis segment for the proposed FDTD simulation method uses the development of the single sea surface wave as outlined for the marine geometrical theory of diffraction. Applying a Gaussian distribution process, multiple single waves are distributed randomly across a finite segment of length. The superposition of single sea surface waves results in a realistic random sea surface for a deep sea location [97]. This surface can then be implemented as a boundary condition in the FDTD propagation analysis, whereby the finite difference grid is a 2D cross section of a marine communications channel of known physical sea surface attributes. Such a sea surface is given in Figure 6-3.

Synthesis by this technique has been used for a variety of applications, including visual rendering of sea surfaces [55]. The DFT result of the spectral functions illustrates the displacement of a fixed surface location as waves travel past in time. Conversion to spatial displacement is accomplished using classical wave theory as outlined in Marine GTD formulation of this work.

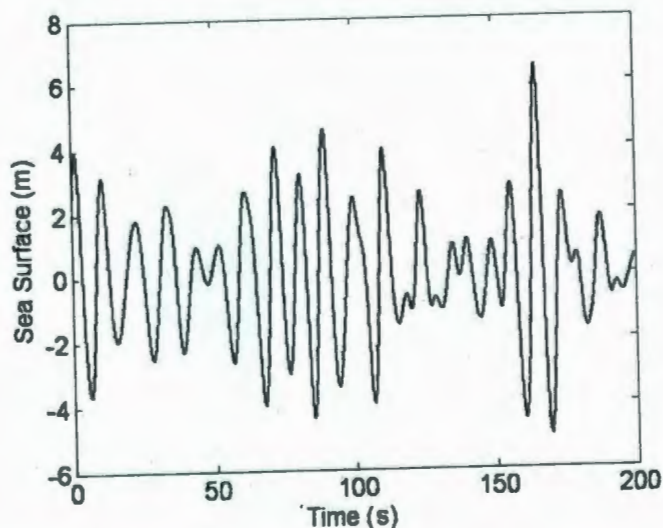


Figure 6-3: The stationary random Gaussian process has produced an arbitrary sea surface based on the modified Pierson-Moskowitz spectral functions as a function of time.

Note that by implementing this process, there is only the generation of the sea surface based on the superposition of individual sea surface waves at randomly generated offsets, and that there is no account for sea swell in the surface generation. Since the physical channel is generally deemed to be short with respect to the effects of swell, this composition method of the random sea surface is a reasonable short length approximation.

Using the spatial distribution of waves on the sea surface, the physical sea surface channel is then interpolated as elements in the 2D physical communications channel as mapped to the finite difference grid. The boundary condition is applied as a mask, and thus enforces the sea surface form as a perfect conducting surface during the

FDTD transient analysis at each discrete time step. A mask binary matrix used during simulation is shown in Figure 6-4.

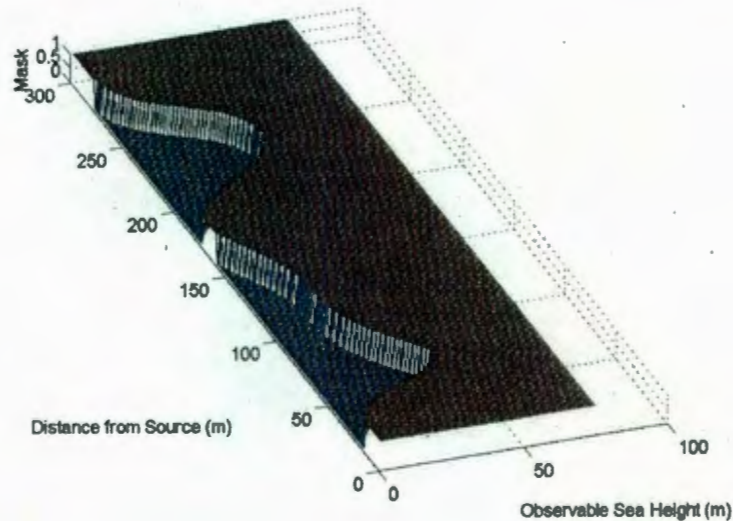


Figure 6-4: Sea surface boundary condition mask for the finite difference grid, implementing the sea surface boundary condition during the FDTD simulation.

Thus, with the FDTD simulation methodology and the modified Pierson-Moskowitz spectra model for the north North Atlantic region implemented as a boundary condition, a novel numerical approach to overwater radio propagation analysis for the marine communications channel is created. The details of the physical sea surface are retained and readily available during post simulation analysis. This methodology offers the opportunity to study relationships between communications channel performance parameters and both wave height and frequency [38]. Previously, with direct measurement methods, this would prove extremely difficult because of the difficulties with performing measurements of the sea surface at the precise instant of measurement [79]. Rather than knowing the specific details of the channel's physical state, a typically approximation is use of a floating platform located at either the transmitter or receiver [42]. This provides single point displacement recorded over the duration of the measurements and may not necessarily be reflective of the sea surface profile at the time of propagation measurement. Clearly, this common experimental method

would yield a less than accurate result of the sea surface profile at the instant of a path loss measurement, and due to the constant stochastic nature of the sea surface it may bear no resemblance to the profile whatsoever. Thus, the advantage of the proposed methodology in comparison to the use of a floating platform is the precise and detailed availability of the physical sea surface during transient electromagnetic simulation.

6.6 Shadowing Study Boundary Forcing Function

The study of shadowing requires that a physical obstruction be placed between a transmitter and receiver such that no line of sight exists. In this case, the most significant contributor to propagation between these locations is diffraction. In order to study the resulting effects in a controlled fashion, the positions of the transmitter and receiver must remain fixed as random sea surface waves are placed between them. In the innate form of the sea surface synthesis algorithm, depending on the random sea surface height, it is quite possible that the sea surface boundary may be created such that either the transmitter or receiver is located beneath the sea surface. Change of distance above the sea surface during wireless communications channel measurements has been a concern in previous measurement efforts [42]. To alleviate this occurrence, and control the sea surface such that a repeatable distance above the boundary is maintained, a forcing function is employed to ensure the sea surface height at the perimeter edges of the physical channel approach zero in proximity to the transmitter and receiver locations. The basis of this technique is an exponentially decaying weighting function to the sea surface as it approaches the left and right edges of the 2D finite difference grid. In other words, the proposed technique provides a smooth transition from a fully developed random sea surface to zero height in a smooth and simplistic fashion.

The formulation of the Boundary Forcing Function (BFF) is similar to that of the

Gaussian input pulse. It is first desirable to specify that the number of cells used for the rise of the weighting function, N_{rise} , to be 20% of the total number of cells used to represent the physical channel length. Furthermore, the number of cells used for the edge of the pulse, N_{Edge} , is set to be 30% of the total rise. Thus, the exponential decay located on both the left and right sides of the synthesized ocean surface may be expressed as,

$$BFF(x) = \exp\left(\frac{-1}{2} \cdot \frac{(N_{rise} - x)^2}{N_{Edge}}\right), \quad (6.35)$$

whereby the $BFF(x)$ takes the form as in 6-5 for a specified length of spatial cells.

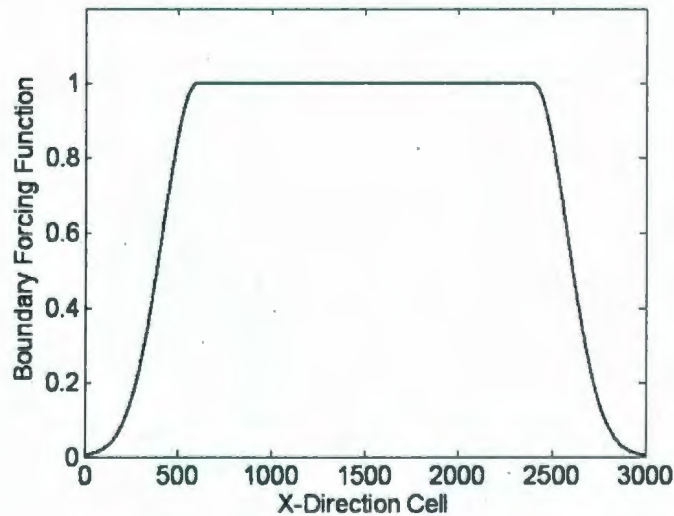


Figure 6-5: The proposed Boundary Forcing Function (BFF) used for shadowing study of ocean waves, forcing the outer limits of the sea surface to nil wave height in an exponentially decaying fashion.

The difference is clear when examining the sea surface boundary condition matrix mask as illustrated in Figure 6-4. Under all simulation conditions, using the BFF provides consistency in the random sea surface region in proximity to the transmitter and receiver locations. Propagation can be examined in a more controlled and consistent manner. This ensures the effects of the sea surface located between the transmitter

and receiver are the major environmental contributors to the scattering, as the height of the transmitter and receiver are held at constant levels above the ocean surface. Furthermore, this technique ensures that there are no abrupt corners and a consistent geometry in the near field of the source at the receiver locations. Random sea surfaces are illustrated before and after application of the forcing function in Figures 6-6 and 6-7 respectively. A smooth transition to zero height is observed on both the left and the right sides of the physical communications channel once the boundary forcing function is applied.

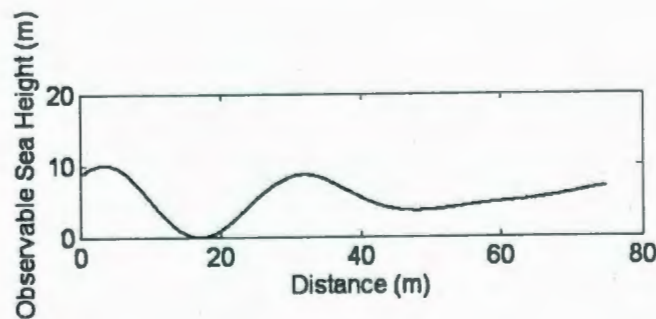


Figure 6-6: A sea surface boundary condition before application of the proposed boundary forcing function.

6.7 Input Pulse & Simulation Bandwidth

Virtually all RF and microwave devices are characterized by their frequency performance [86]. Few RF and microwave devices operate without significant change in performance even over narrow bandwidth, particularly in the VHF to microwave range and higher. Therefore, the accepted method of characterization of RF and microwave devices is generally by frequency response. Since the input pulse of the

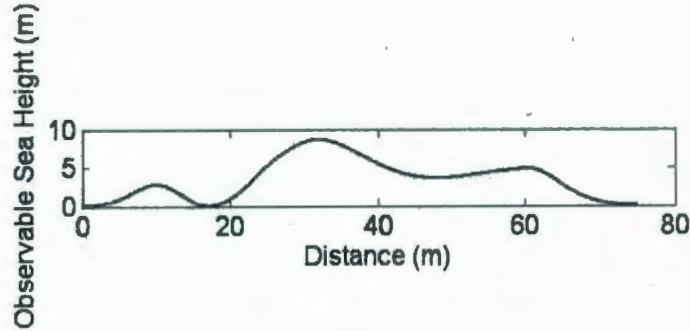


Figure 6-7: The same sea surface boundary condition after application of the proposed boundary forcing function.

FDTD simulation is transient in nature, the selection of input pulse for numerical simulation is of primary importance. If the excitation pulse does not contain the relevant spectral content, the desired frequency response characteristics cannot be determined during post transient analysis. The Gaussian pulse is a broadband pulse and provides spectral content that is more evenly distributed across the frequency spectrum than a trapezoidal pulse, which contains nulls in its spectral content function. For this reason, the Gaussian excitation, E , is commonly used for FDTD simulations,

$$E = E_o \exp \left[- \left(\frac{(n - n_o)}{n_{decay}} \right)^2 \right], \quad (6.36)$$

where n is time, n_o is the delay time before the pulse is introduced and n_{decay} designates the width. The shorter the width, the faster the pulse rises to peak amplitude E_o . With faster rise time comes higher spectral content. This concept is not only pertinent to the bandwidth of FDTD simulations, but also to high speed digital circuits [71]. To illustrate this concept further, if a Gaussian input pulse with a rise

time of approximately 1 ns is examined using Fourier analysis, it is determined that the spectral content of the pulse is significant to approximately 1 GHz. Graphical illustrations of the pulse and corresponding spectral content are illustrated in Figures 6-8 and 6-9 respectively. If the rise time is decreased, such that it occurs in approximately 300 ps, the pulse sharpens in the time domain. The corresponding transient excitation and spectral content of the faster pulse are illustrated in Figures 6-10 and 6-11 respectively.

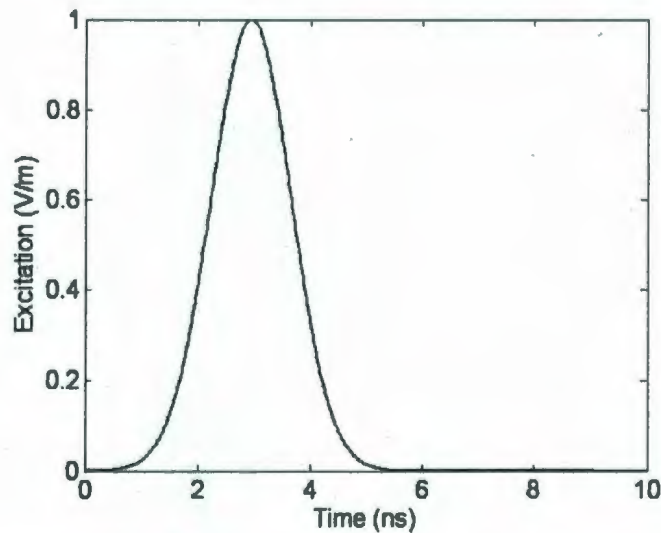


Figure 6-8: Transient illustration of a Gaussian pulse with approximately 1 ns rise time.

As a rule of thumb the bandwidth, BW , of the input pulse may be expressed as,
[72]

$$BW_{pulse} \approx \frac{1}{t_{rise}}. \quad (6.37)$$

where the rise time, t_{rise} , is the time required to rise from nil to full amplitude. Thus, to select the time step and input pulse to produce a simulation with the desired frequency content, the rising edge of the pulse is the primary consideration. Other pulses may be used to attain higher bandwidth for a similar rise, as is the case with

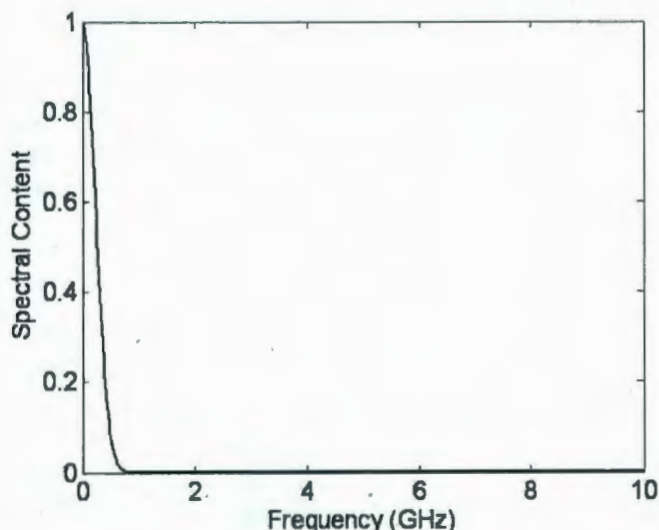


Figure 6-9: Normalized spectral content of a Gaussian pulse with approximately 1 ns rise time.

the trapezoidal waveform, but this excitation produces nulls in the magnitude of the spectral content, and this effect is undesirable. Because of the smoothness of the frequency content of the Gaussian pulse, it is selected as the input pulse used for this FDTD propagation analysis. A discrete Fourier transform is conducted on the Gaussian input pulse to determine the respective frequency content [78]. For this study, a Gaussian pulse is used such that spectral content is obtained between VHF and 3 GHz, as this band is the most relevant to current mobile communications systems.

6.8 EM Simulation Development Summary

This chapter has outlined the specific segments required for the development of a novel electromagnetic propagation analysis methodology suitable for study of over-water radio propagation in marine communications channels. The Finite Difference - Time Domain method, the synthesis of a realistic random sea surface and the implementation of the surface as a controlled boundary condition along with relevant

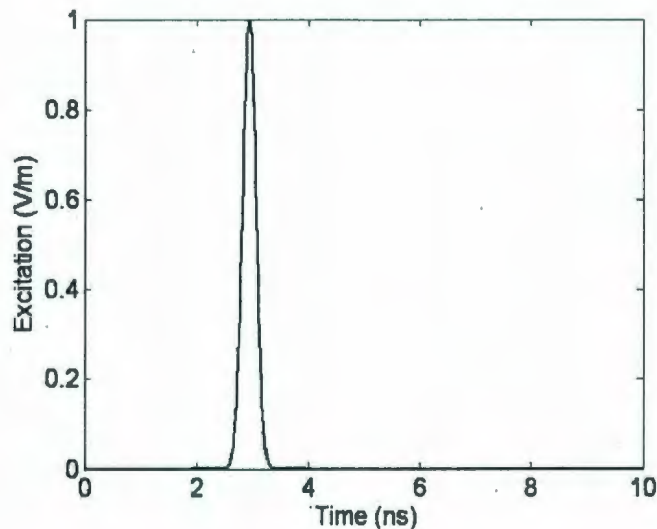


Figure 6-10: Transient illustration of a Gaussian pulse with approximately 300 ps rise time.

excitation pulse selection provides the needed components to conduct marine communications channel propagation analysis. This approach is distinctly advantageous, as the proposed method provides high accuracy propagation analysis obtained by direct solutions to Maxwell's equations, whereby detailed knowledge of the sea surface is retained and readily available. The aspect of conducting propagation studies for marine communications with a detailed knowledge of the sea surface has historically been a challenge in comprehending the effects of the sea surface and a limiting factor in measurement-based studies. The proposed numerical methodology provides a means to develop parameterized channel performance models as functions of both frequency and sea surface height, in a manner that overcomes the limitations and difficulties of previous measurement studies. The numerical accuracy and the ability of the FDTD simulation engine to perform diffraction analysis is evaluated by simulation of a knife edge topology, for which a well known analytical expression is available and easily compared to the numerical results obtained by the FDTD software. The issue of numerical accuracy and ability of the methodology to accurately calculate diffraction is addressed in the next section.

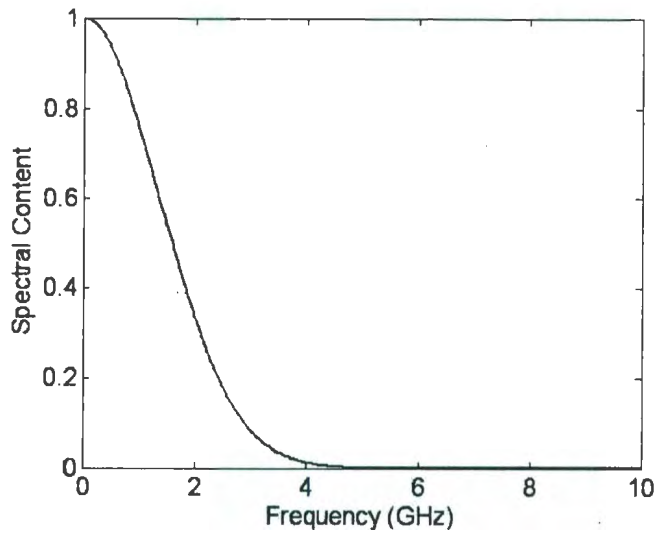


Figure 6-11: Normalized spectral content of a Gaussian pulse with approximately 300 ps rise time.

Chapter 7

Knife Edge Validation of FDTD Simulation Engine

7.1 Validation of the FDTD EM Simulation Tool by Analytic Knife Edge Diffraction and Free Space Propagation Analysis

Shadowing can be estimated by the use of the knife edge equation, whereby an obstructing body between a transmitter and receiver is approximated by a straight edge. This approximation is often used for channel features such as hills and buildings obstructing transmitter and receiver in a fixed terrestrial link. Application of the knife edge is usually done such that the highest point of the obstruction is replaced in the topology by a straight edge of equal height [98],[77]. The position above both transmitter and receiver locations is also included in the analytic expression as well as the lateral displacement from the base of the straight edge. This chapter will assess the ability of the implemented FDTD simulation tool to accurately calculate diffraction loss. A knife edge topology is simulated using the FDTD simulation engine, and

numerical results are obtained which are then compared to the analytical expression for the same physical channel topology. The knife edge is one of the best known diffraction approximations, and numerical agreement between the analytic and numerically obtained results will constitute the verification of the completely custom developed propagation analysis software. Free space propagation is also conducted to numerically determine the rate of propagation and path loss exponent as a secondary verification mechanism. This ensures that the simulator is capable of producing accurate diffraction, path loss exponent and transmission delay results when calculating propagation effects as a result of realistic profile of a sea surface during shadowing conditions.

7.2 Numerical Knife Edge Diffraction Analysis

Implementing a knife edge topology in the FDTD EM simulation tool provides a numerical result to a well-known analytical expression and commonly utilized physical approximation to determine shadowing effects from obstructions in terrestrial communications channels. The knife edge channel topology applied as an approximation to a terrestrial obstruction is illustrated in Figure 7-1.

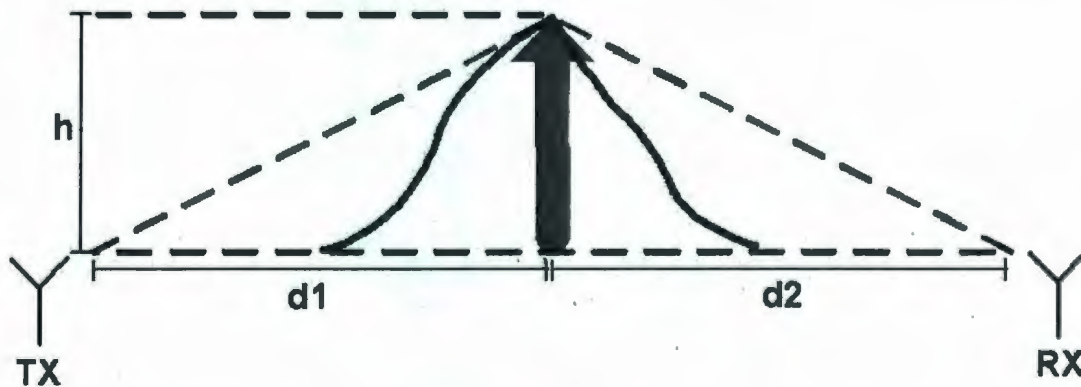


Figure 7-1: The knife edge topology

For the knife edge topology, the signal strength at the receiver due to diffraction

is [23],

$$E_{KE} = E_o \left(\frac{e^{-jk(d_1+d_2)}}{d_1+d_2} \right) \cdot \left(\frac{1+j}{2} \right) \cdot \int_u^\infty e^{-j\pi\tau^2/2} d\tau \quad (7.1)$$

where $u = h\sqrt{\frac{2(d_1+d_2)}{\lambda d_1 d_2}}$, such that k is the wave number, λ is the wavelength and d_1 , d_2 and h are dimensions as depicted in Figure 7-1. Clearly, E_{KE} is a function of wavelength, and thus multiple calculations are required for the same topology to obtain diffraction results within the relevant frequency band of interest.

Unfortunately, for the purposes of communications channel modeling, this widely accepted model does not account for the geometry of the actual obstruction [98]. These geometrical differences can have significant effect on the multipath propagation distance around the obstacle. The form of the geometry significantly affects performance parameters such as the delay spread of the channel. The knife edge does however provide a widely accepted benchmark upon which the validity of the FDTD simulation engine can be verified. A comparison is conducted between the numerical result of the knife edge FDTD simulation and the analytical result of the knife edge equation. The geometry of the overall structure is illustrated in 7-2 showing the knife edge protruding in the EM simulation boundary condition mask. The relevant physical parameters as they related to the Knife Edge diffraction formula are shown for clarity. The perfectly conducting body is implemented in the FDTD simulation in the same manner as the sea surface for overwater radio propagation analysis. The physical attributes as they pertain to the knife edge geometry are also depicted such as they are used for the evaluation of the analytical expression.

Three knife edge simulations are conducted for obstruction heights of 5.625 m, 7.967 m and 10.313 m. The same lateral size of the finite difference grid is used in the 2D channel cross section as is used for overwater propagation analysis. The results of each are compared to the knife edge expression and illustrated in Figures 7-3, 7-4 and 7-5 respectively.

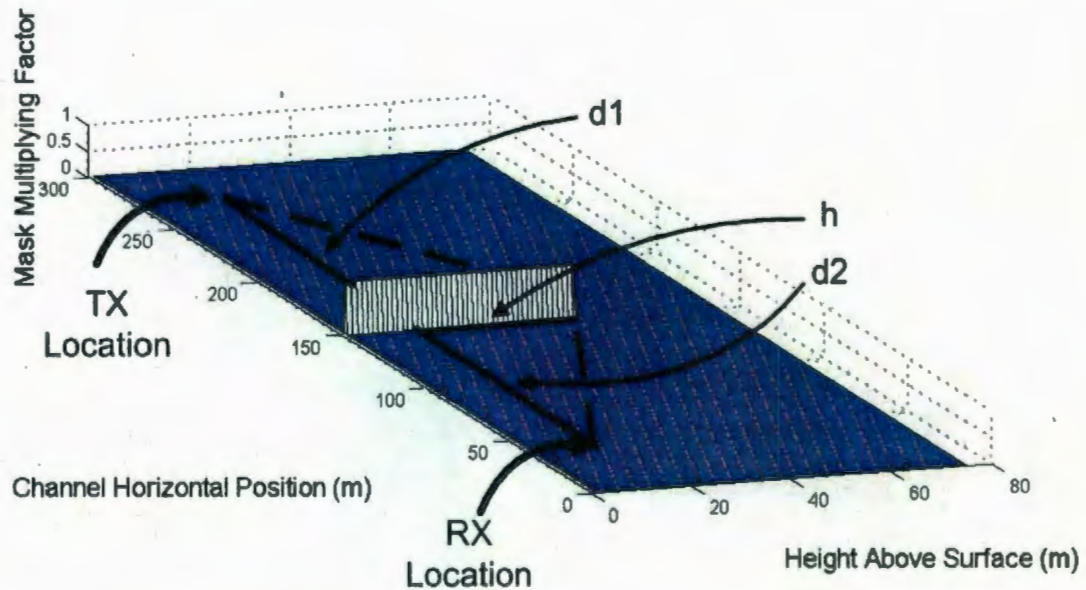


Figure 7-2: FDTD boundary condition knife edge mask. The knife edge topology is also illustrated for clarity.

It is important to remember that numerically, signal levels on the order of -60 and -80 dB loss are extremely small, and as the case with physically measured parameters using RF test hardware such as network analyzers, similar consideration should be given to numerical accuracy as is to measurement accuracy when considering the discrepancies between the numerical results and those obtained analytically for the knife edge topology. Overall, the agreement between the analytically obtained values and the numerically simulated results are excellent. The FDTD simulation software has demonstrated it's ability to calculate diffraction analysis for the knife edge geometry that correlate well with the analytical expression for knife edge diffraction.

7.3 Validation of the FDTD EM Simulation by Propagation in Free Space

The FDTD simulator is also validated by it's ability to calculate specific aspects

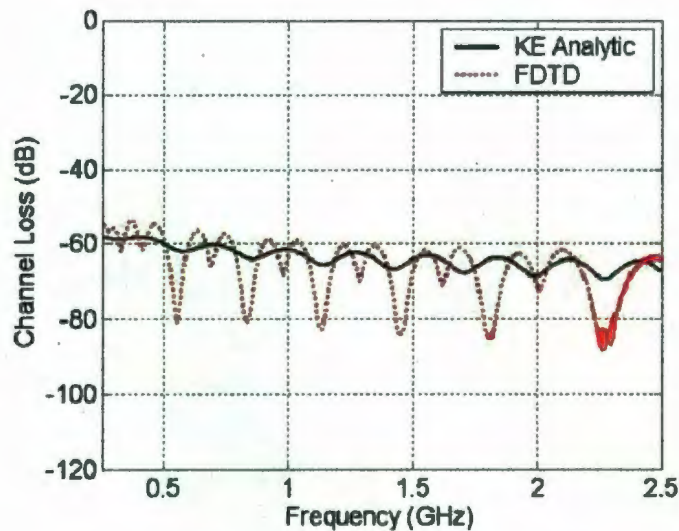


Figure 7-3: 5.625 m knife edge diffraction FDTD and analytic results.

of propagation in free space. That is, the simulator is configured such that there are absorbing boundary conditions on all four sides of the communication channel. A Gaussian excitation is used that is identical to that used for the overwater radio propagation analysis in the marine communications channel simulation segment. Numerical simulations are conducted to assess the following well known quantities:

1. The speed of light. The speed of light is a well-known constant. Based on the fixed distance between transmit and receive locations, it is possible through the examination of the flight time to calculate the rate of propagation obtained through the numerical implementation of the FDTD simulator.
2. The path loss exponent for various frequencies over the range of VHF to 3 GHz. The path loss exponent for all frequencies in free space, as outlined previously in this work is 2.

Visually the FDTD software developed in this work provides an excellent means to observe overwater radio propagation. Figure 7-6 shows the free space simulation at 20 % completion. Both the forward moving and reverse moving edge of the excitation

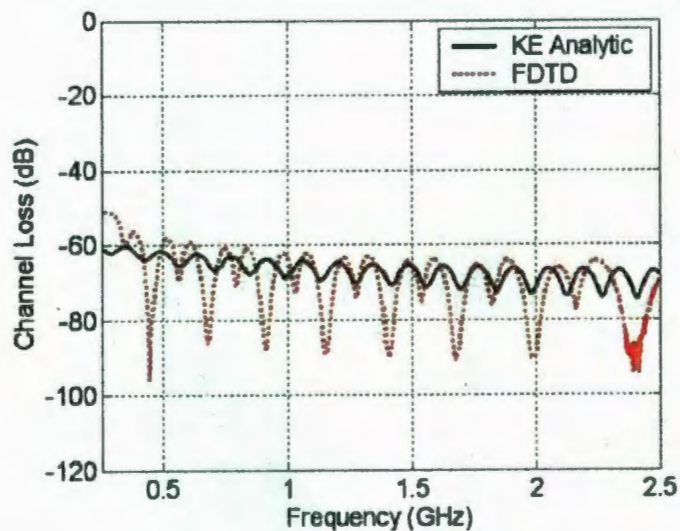


Figure 7-4: 7.967 m knife edge diffraction FDTD and analytic results.

pulse are visible. At 40 % complete, as in Figure 7-7, only the leading edge of the forward moving waveform remains. The reverse moving waveform has passed into the absorbing boundary. At 60 % complete, Figure 7-8 shows the leading edge of the forward moving waveform is approaching the absorbing boundary, and has decreased further in magnitude as it propagates through free space. Field magnitude is illustrated by the height above the horizontal plane, and shades of color differ between plots.

Even though the excitation is rapidly approaching the absorbing boundary with the simulation only slightly over 50 % complete, the remaining duration of the simulation is provided to allow multipath propagation signals that would be present with the implementation of a perfectly conducting sea surface boundary sufficient time to complete their respective pathway and for all significant energy to exit the finite difference grid. The transmitted and the received waveforms depict the flight time required to traverse the 2-dimensional communications channel cross section. The simulation is initiated with a Gaussian excitation, as in Figure 7-9. Figure 7-10 illustrates the numerical dispersion as propagation occurs over 68.75 m between the

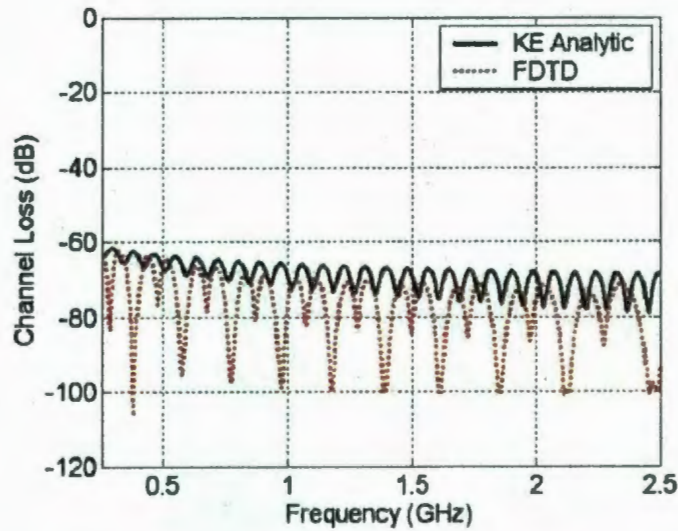


Figure 7-5: 10.313 m knife edge diffraction FDTD and analytic results.

transmitter and receiver locations. Numerical dispersion is a typical occurrence in FDTD implementations, and is known to become more severe with increasing physical size of the finite difference grid [30]. Figure 7-11 shows a closer examination of the received waveform of the free space propagation analysis.

As an effort to validate the implemented FDTD simulation tool, the numerically determined flight time based on the transmitted and received waveforms at the peak electric field values is,

$$234.5ns - 3.0ns = 231.5ns. \quad (7.2)$$

The total distance between the location of the input pulse and received pulse in the finite element channel is 68.75 m. Thus the speed of light as determined numerically,

$$\frac{68.75m}{229ns} = 3.002 \times 10^8 m/s \quad (7.3)$$

Numerically, this value obtained through EM simulation using the finite difference - time domain technique compared to the analytical value,

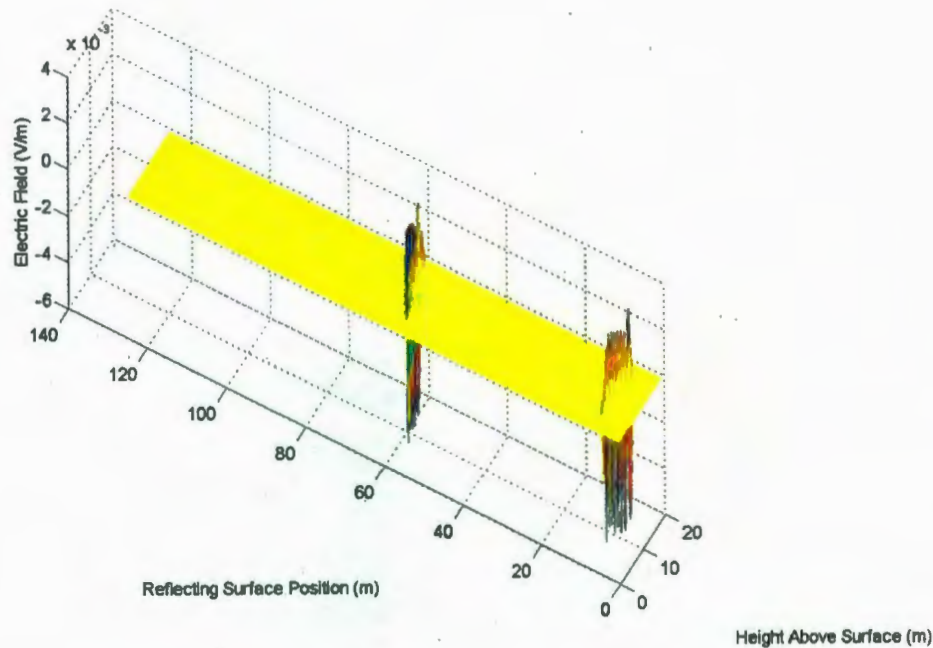


Figure 7-6: Free space FDTD simulation 20 % completed.

$$\frac{|3.002 \times 10^8 \text{ m/s} - 2.998 \times 10^8 \text{ m/s}|}{2.998 \times 10^8 \text{ m/s}} = 0.142\%. \quad (7.4)$$

Thus, the FDTD numerical simulation propagation rate differs from the analytical value by less than 0.2 %, giving a very supportive result regarding the ability of the tool to calculate the rate of propagation in free space. Clearly, distortion due to dispersion is a source of error in this calculation.

As a third benchmark for the FDTD tool, and furthermore as a verification of the post analysis ability of the software, the path loss exponents for several frequencies in the range of interest are determined. These include 2.492 GHz, 1.621 GHz and 162 MHz for the Globalstar (satellite communications), Iridium (satellite communications) and AIS (Automatic Identification System) systems respectively. Illustrations of the numerical results of transmission loss are given in Figures 7-12, 7-13, and 7-14 for propagation distances of 68.75 m respectively. These values are anticipated to be 2, as per the free space path loss exponent.

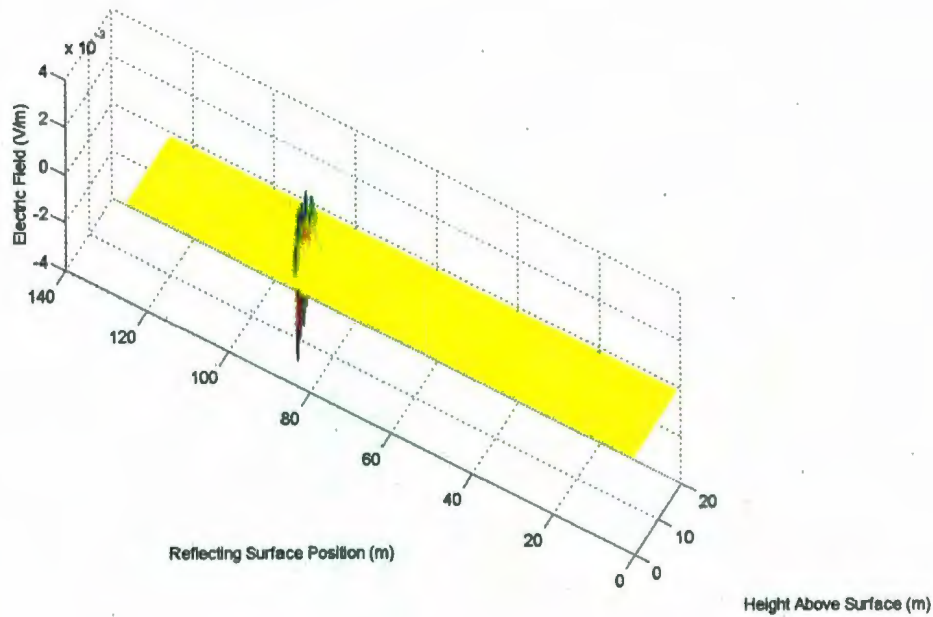


Figure 7-7: Free space FDTD simulation 40 % completed.

Interesting, the path loss experienced by the Iridium and Globalstar carrier frequencies is smooth as it decreases. This is not the case with the AIS path loss calculations. This is attributed to the number of grid elements allocated to the PML boundary. More specifically, the PML is becoming electrically short, and thus reflections at the lower frequencies are not being attenuated sufficiently during the transient analysis. Care must be taken to observe these signs of numerical error when using the FDTD for computational electromagnetic analysis.

Determining the path loss exponent, referred to as n , in the aforementioned formulation, linear regression analysis conducted on the free space propagation analysis is conducted in the same manner as is typically performed during measurement post analysis. Figures 7-15, 7-16, and 7-17 illustrate this for each of the Globalstar, Iridium and AIS relevant frequencies. The results are tabulated to summarize the free space evaluation of the FDTD propagation analysis software in Figure 7-18.

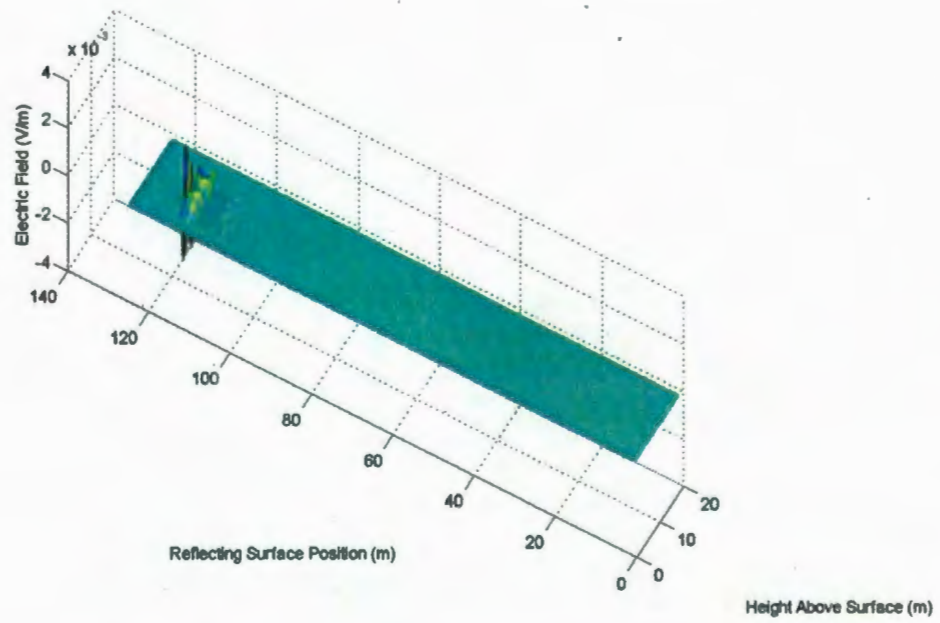


Figure 7-8: Free space FDTD simulation 60 % completed.

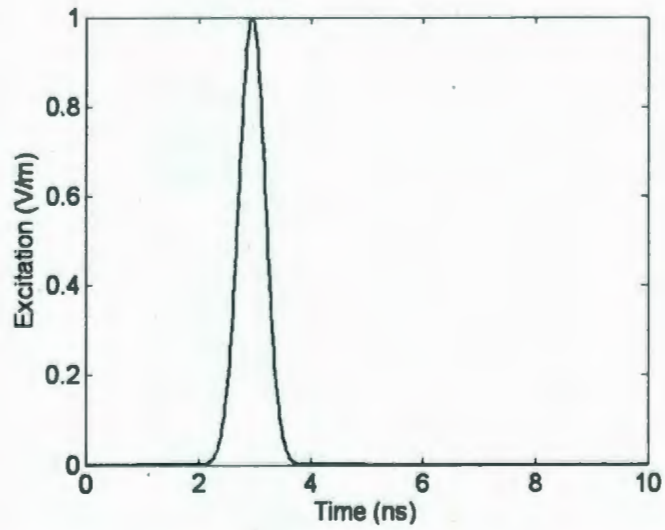


Figure 7-9: Free space FDTD Gaussian excitation pulse.

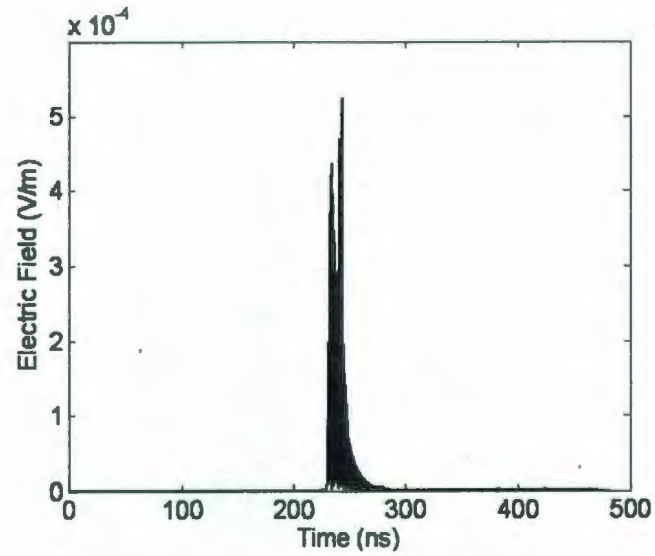


Figure 7-10: Free space FDTD received pulse.

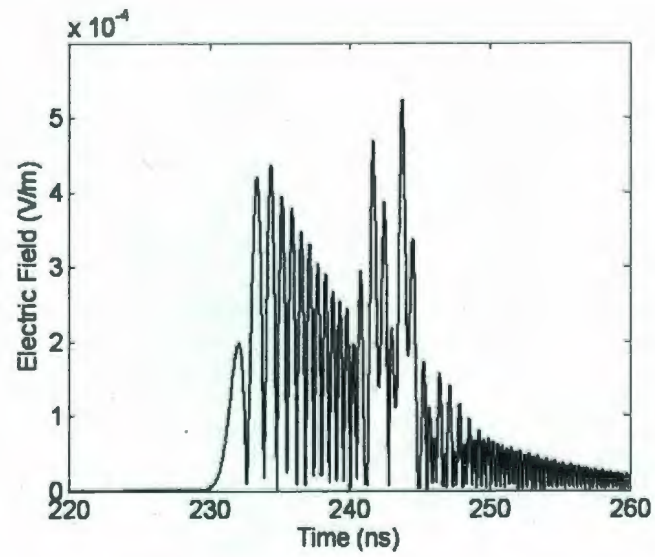


Figure 7-11: Free space FDTD received pulse.

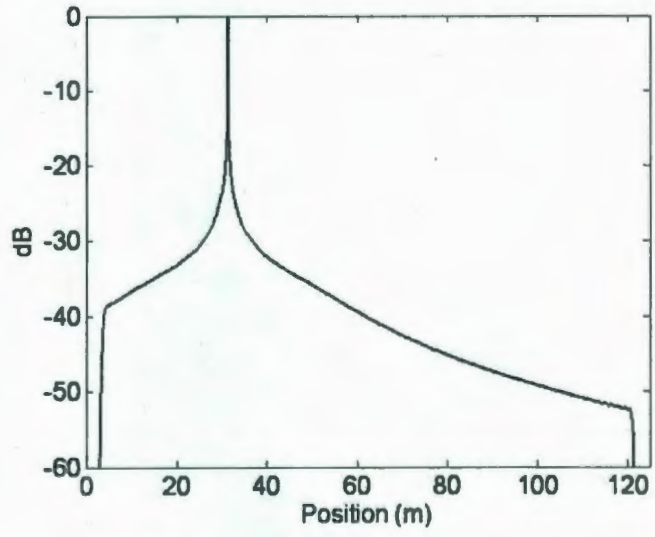


Figure 7-12: Globalstar (2.492 GHz) transmission loss through free space.

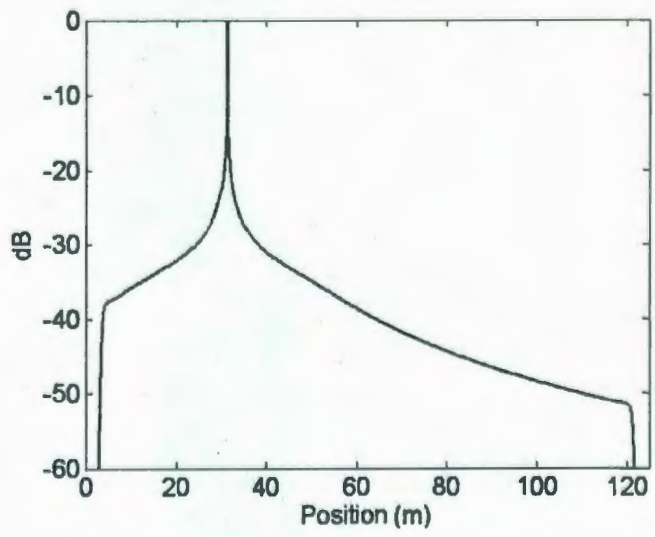


Figure 7-13: Iridium (1.621 GHz) transmission loss through free space.

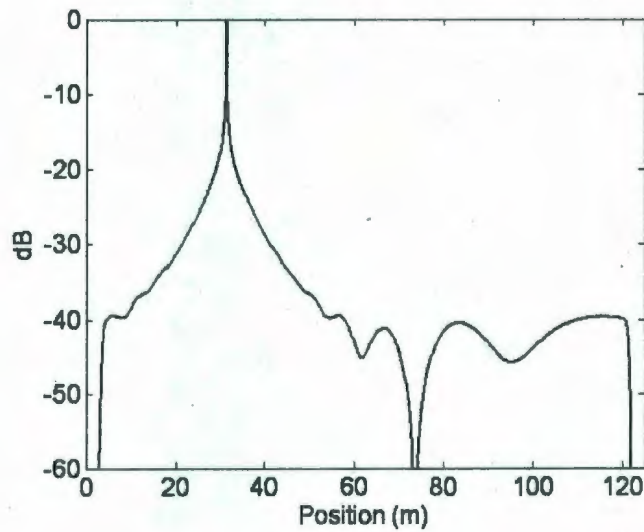


Figure 7-14: AIS (162 MHz) transmission loss through free space.

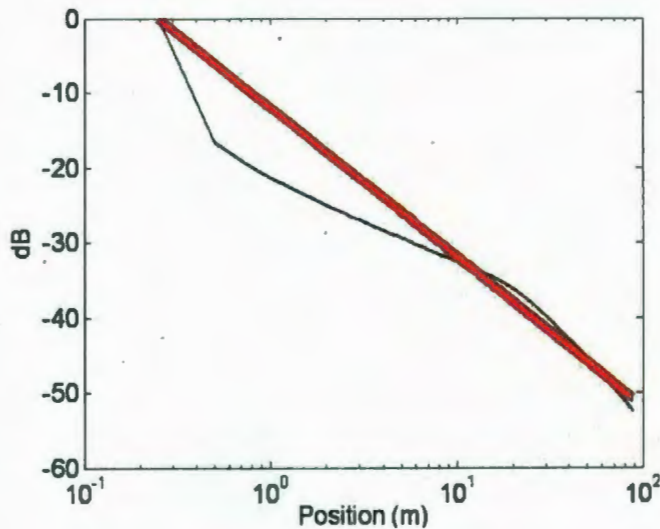


Figure 7-15: Linear regression analysis of Globalstar (2.492 GHz) transmission loss through free space.

The numerical results obtained for the path loss exponent of the Globalstar and Iridium satellite provider carrier frequencies are excellent, with low standard deviations in free space. These slight deviations due to numerical error are for the most part insignificant. Most interestingly is the result obtained for the AIS carrier frequency, as shown in Figure 7-14, for which the loss curve is not smooth in comparison to those obtained for the higher carrier frequencies. AIS operates at 162 MHz, which is far lower than the 2.492 GHz and 1.621 GHz of the Globalstar and Iridium providers. Subsequently, the wavelength of for AIS is much longer. The discrepancy is due to the short electrical length of the absorbing boundary condition at the perimeter of the finite difference grid for AIS. That is, the number of cells of the absorbing boundary condition is somewhat low compared to the electrical length at higher frequencies, which is demonstrated by the smooth curves of Figures 7-12 and 7-13. The linear regression analysis compensated for this fact, still calculating an accurate path loss exponent, with the symptom of an increase observed in the standard deviation. This practical consideration demonstrates the trade off between increased physical

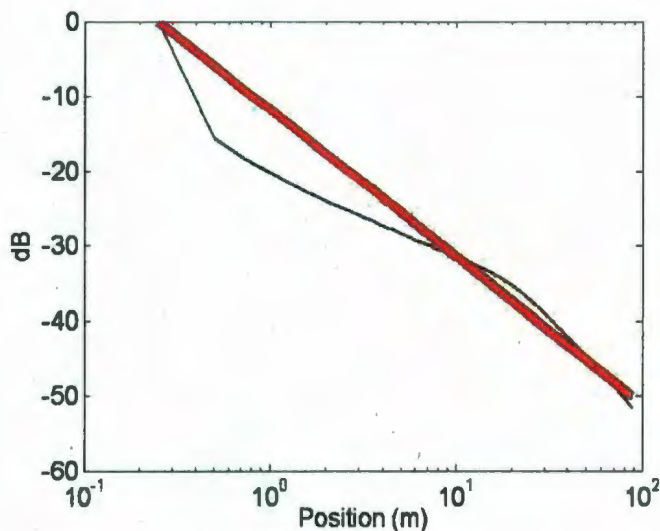


Figure 7-16: Linear regression analysis of Iridium (1.621 GHz) transmission loss through free space.

channel size and necessary absorbing boundary conditions to emulate open free space boundaries at the perimeter of the channel and how boundary condition errors can contribute to the discrepancy of numerical results. Careful consideration to this aspect should be given when using the proposed methodology for channel propagation analysis, or any other FDTD application. Boundary condition limitations are an overall difficulty when using the FDTD method, and results should be interpreted accordingly.

7.4 Knife Edge and Free Space Validation Summary

This segment has demonstrated the ability of the FDTD simulation tool to accurately calculate parameters relevant to this numerical study. Diffraction loss, the most important parameter is determined for the well known knife edge geometry. Numerical results from the FDTD software are directly compared to the analytical for a com-

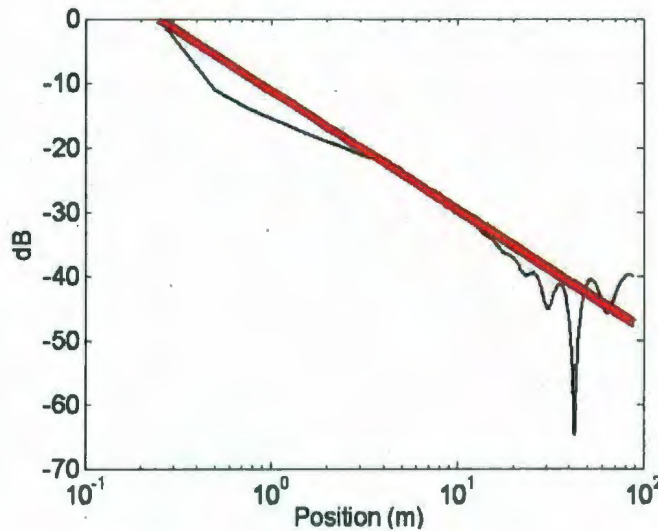


Figure 7-17: Linear regression analysis of AIS (162 MHz) transmission loss through free space.

	Frequency (GHz)	PL Exponent	Std Dev
Globalstar	2.4920	1.9900	1.8943
Iridium	1.6210	1.9600	1.8108
AIS	0.1620	1.8500	4.8026

Figure 7-18: Free space path loss exponent linear regression analysis summary.

mon channel topology, verifying the ability of the software to be used for diffraction analysis. Also, the rate of propagation in free space is determined to be accurate within 0.2 %, and the path loss exponents for several pertinent carrier frequencies are numerically determined to be very close to the analytical value of 2. These numerical benchmarks of analytical relationships and free space propagation attributes prove the accuracy and validity of the FDTD simulator and results obtained for propagation and diffraction analysis over a well-known geometry. This accuracy will be the same for any boundary condition such as a realistic random sea surface. For diffraction analysis, excellent overall agreement is observed between the numerical result and the FDTD EM simulation. Higher frequency discrepancies near the 2.5 GHz range can be attributed to the low spectral content in the excitation signal and low number

of grid elements per wavelength, and lower frequency discrepancies are due to the the short electrical length of the absorbing boundary as demonstrated during the free space propagation analysis. As with any FDTD simulation, boundary condition errors contribute through the non-ideal absorption of signals at the boundary locations causing reflections back into the finite difference grid during transient analysis. These reflections are inappropriate, and their minimization is continual effort in the application of the FDTD method for computational electromagnetics. This is particularly relevant for the lower frequencies of interest, whereby severe propagation loss levels are experienced with the knife edge diffraction analysis and the 162 MHz AIS carrier frequency during free space propagation analysis, as the inappropriate reflections from the boundary approach and the actual received signal levels approach the same order of magnitude. Boundary condition implementation and excitation pulse spectral content are two prime sources of error for this and any other FDTD implementations. Overall, excellent agreement is observed between the analytical functions for diffraction loss and the free space propagation attributes when compared with the numerically evaluated FDTD EM simulation results. The results in this section prove the ability of the FDTD method and the implemented numerical analysis software to accurately determine diffraction loss, path loss exponent and transmission delays for the knife edge topology, and subsequently any other realistic surface implemented as a boundary condition in the propagation analysis tool.

Chapter 8

FDTD Marine Communications Channel Propagation Analysis and Modeling Results

8.1 Overview

The field of computational electromagnetics is centered upon using recursive formulations and numerical techniques to find solutions to Maxwell's equations to problems for which analytical study is difficult, or even impossible. This work is focused on developing a novel methodology for the study of overwater propagation for a realistic sea surface. Because of the random nature of the sea, analytic development is extremely difficult if not impossible, making the subject an excellent topic for use of numerical methods. The numerical approach is in stark contrast to the proposed marine geometrical theory of diffraction, whereby a practical model is developed for marine communications sea surface shadowing as an extension of the theoretical geometrical theory of diffraction. The Marine GTD model does however rely on the approximation that only the profile of a single sea surface wave is predominant in the diffraction loss experienced during sea surface shadowing conditions. In sacrificing accuracy, this

method is comparable to other such estimation techniques, including the knife edge approximation. Accuracy is sacrificed for ease and efficiency. The numerical approach and methodology offers a solution to this deficiency, at the cost of computational effort. While the Marine GTD provides a rapid mechanism for diffraction analysis requiring minimal computational effort, the numerical approach is quite extensive as it uses electromagnetic analysis to obtain transient solutions directly from Maxwell's equations. A single FDTD simulation on a dual core 2.5 GHz desktop computer with 4 GB of memory at this point in time requires approximately 8 hours to complete a single propagation analysis, whereas an Marine GTD calculation can be performed in microseconds.

The FDTD work is done using a 2D approximation of what is actually a 3D problem. The cross section approach of the physical channel is a commonly used approximation for conducting electromagnetic analysis. There are a number of reasons for this. First, a 2D approximation can be utilized as a means to reduce computational time. Second, a numerical problem that requires resources beyond the capability of current computing technology is often first analyzed using a 2D approximation such that the problem can be studied. In this case, the propagation analysis given requires the full amount of available computer memory. For the same 2D finite difference grid to be extended into the third dimension with equal cells per wavelength would require approximately one thousand times the memory of the standard desktop computer. Though slight differences would be anticipated when simulating the complete 3D problem, the overall general behavior observed in the 2D problem are typically the same. For both these reasons, pursuing a numerical solution as a 2D problem has been a long standing practice in the field of computational electromagnetics. For this reason, due to the size and novelty of the proposed methodology, the same approach will be used for the FDTD implementation of the overwater radio propagation analysis.

The FDTD overwater propagation simulation and modeling segment of this re-

search effort may be divided into two components:

- Sea surface shadowing study and propagation analysis for path loss evaluation and frequency domain model development.
- Sea surface shadowing transient analysis and model development.

The sea surface shadowing study and post simulation analysis is focused about conducting VHF to 3 GHz propagation analysis. The objective is to develop parameterized models using the proposed methodology [1] to develop channel performance models that establish a relationship between performance and observable sea surface height over the frequency band of interest. The implementation is centered around the fact that the random sea surface boundary condition used during the transient analysis retains detailed knowledge about the physical attributes of the sea surface. The parametrization refers specifically to model development based on this retained surface knowledge, such that model synthesis can be performed on a post simulation data population to characterize path loss, standard deviation, mean excess delay and root mean square delay such that the models are suitable for usage in the link budget analysis during the system specification and design phase of a marine communications system. Though this effort was supported by Unmanned Aerial Vehicle applications for airborne maritime surveillance, the methodology is suitable for any marine communications application. Establishment of these relations has not previously been accomplished in measurement studies, and the proposed technique offers much improved understanding of the marine communications channel [1].

The second segment is the measurement of a fixed communications channel link at an inshore location. The results of the deep sea simulation effort will offer a clear relationship of increase in the standard deviation of the random contribution term to the path loss equation with increased sea surface height. Though the modified Pierson-Moskowitz models as used during the deep sea study do not provide insight into sea surfaces at an inshore location, the result is evaluated from a qualitative

perspective where the fading is measured over a fixed link channel whereby two peaks are separated by a moving body of water under two distinctly different observable sea surface heights. This is an attempt to verify the generalized result as obtained through the numerical study and should not be interpreted as a completed validation of the simulated results.

8.2 Sea Surface Shadowing Propagation Analysis for Path Loss Evaluation and Frequency Domain Model Development

Sea surface waves often create physical features that obstruct the view of two ocean surface locations. In wireless communications channels, this effect is known as shadowing. Diffraction occurs around the peaks of the individual waves as signals propagate from transmitter to receiver. As diffraction is often cited as a higher order effect during marine communications channel measurement, this effort will quantify the effects using the numerical methods. A simulation population set is created whereby distinct random sea surfaces of various observable sea surface heights over which FDTD propagation studies are conducted. From the collective results, unique and novel models are developed taking full advantage of the known physical attributes of the sea surface. The fact that this methodology provides detailed knowledge of the sea surface and the subsequent propagation analysis of that physical channel allows formulation of unique path loss, standard deviation, mean excess delay and root mean square delay models that are functions of both observable sea surface height and frequency simultaneously. The topology of the general physical communications channel is given in Figure 8-1.

The analysis begins by establishing a random sea surface using the Pierson-Moskowitz spectral models to create a realistic sea surface of known height. The

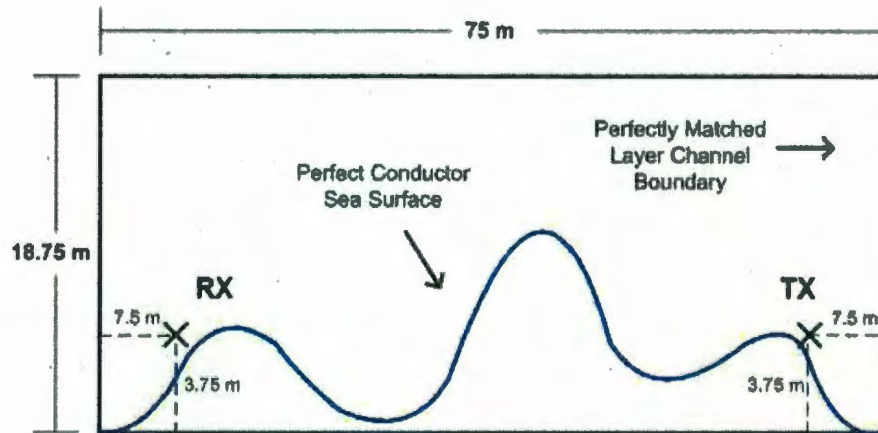


Figure 8-1: Sea surface shadowing condition communications channel topology.

excitation pulse is key to the transient simulation and must contain sufficient spectral content to evaluate the relevant frequencies of interest when calculating transmission loss. Figure 8-2 illustrates such a Gaussian pulse used for excitation at a discrete point in the finite difference grid. This pulse has a rise time of approximately 1 ns.

To illustrate the spectral content of the excitation pulse, DFT is numerically conducted on the transient signal to obtain the frequency domain content for the numerical simulation. The concern in this analysis is to ensure the simulation has adequate bandwidth to characterize the required frequencies of interest, mainly VHF to 3 GHz. The DFT results are given in Figure 8-3. The spectral content of the Gaussian excitation can be seen to contain relevant spectral content to at least 2.5 GHz.

By similar using of DFT, the spectral content of a single sea surface wave as specified by significant wave height and evaluated from the Pierson-Moskowitz model, and illustrated in Figure 8-4, is then used to synthesize the transient displacement of a single wave. The resulting transient displacement is given in Figure 8-5.

Once the single sea surface wave is obtained, it gives the displacement of a single sea surface point over time as the wave travels past. Using the same classical wave theory to map the transient function to a spatial distribution, as previously outlined

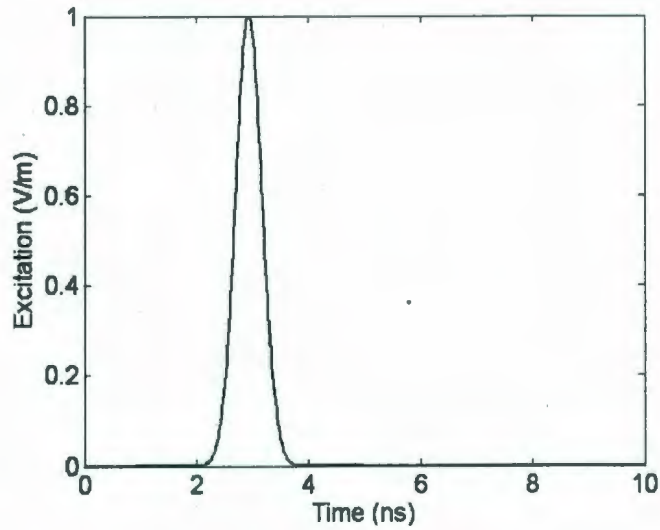


Figure 8-2: Gaussian excitation pulse for the FDTD shadowing study.

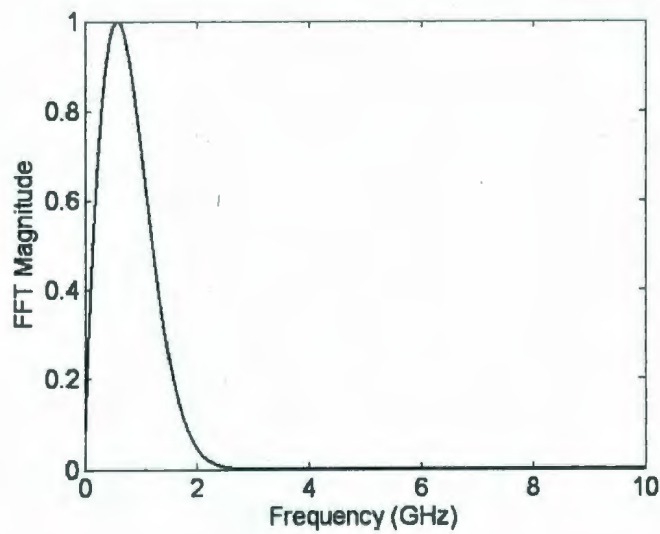


Figure 8-3: Spectral content of the Gaussian excitation pulse.

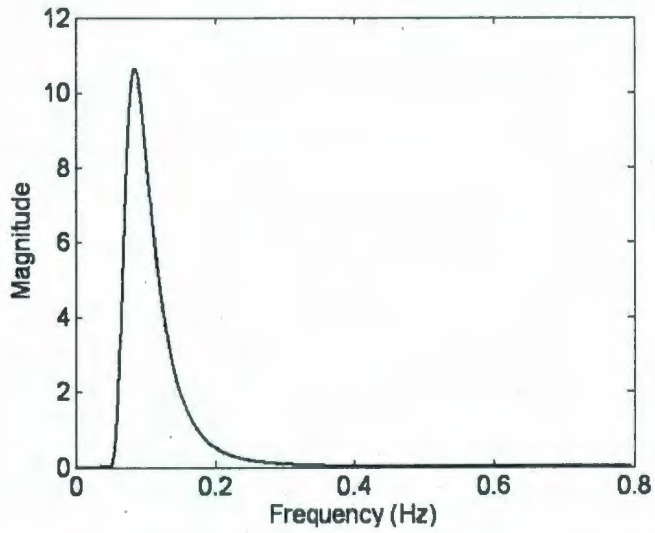


Figure 8-4: Pierson Moskowitz spectral content for a single wave of a specified significant sea surface height.

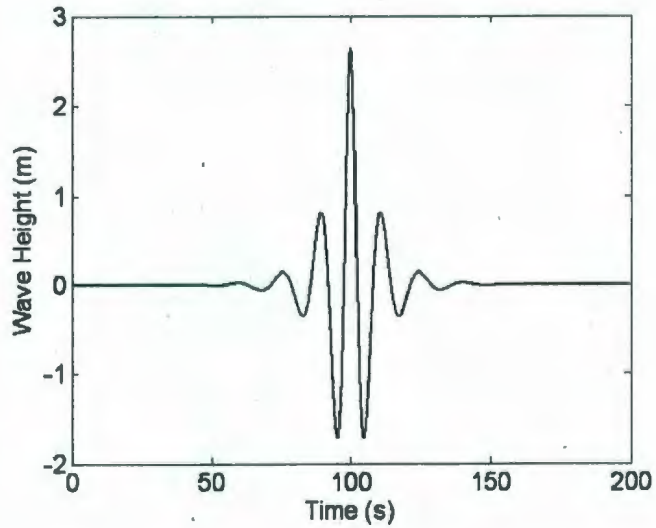


Figure 8-5: Single sea surface wave obtained through DFT of Pierson Moskowitz spectral functions.

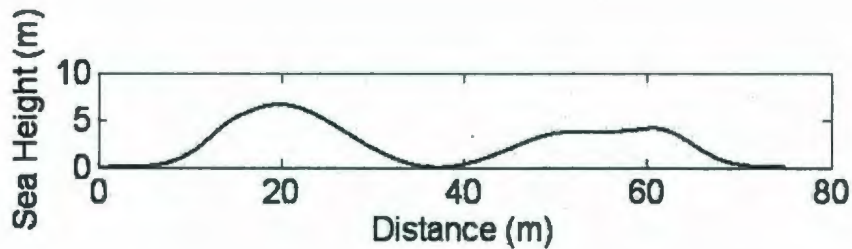


Figure 8-6: Sea surface subsection implemented as a boundary condition during propagation analysis.

for the Marine GTD, multiple waves can be superposed over a length of distance to create a realistic random sea surface. The sea surface is interpolated to the same size elements as established for the finite difference grid of the FDTD simulation. This is illustrated in Figure 8-6. A subsection of that sea surface, the same size as the physical communications channel, is then implemented as a boundary condition for the FDTD simulation with the BFF applied. The boundary condition assumes that the sea surface is perfectly conducting, and thus is implemented in the same manner as that of a perfectly conducting metal.

Clearly, upon visual inspection of the sea surface as synthesized using the random distribution of single sea surface waves the features of the actual sea surface can differ significantly from the envelope of the single wave. This aspect accentuates the difference in the approximation of a single wave during diffraction analysis, as outlined in the Marine GTD, and the form of the realistic sea surface as produced by the PM method. The fact that these features are not easily addressed analytically leads this problem to evaluation of overwater propagation by numerical methods.

Propagation analysis for a random sea surface is then conducted after the boundary condition is implemented in the finite difference grid. The E field transient response at the RX cell is recorded as the excitation pulse is injected at the TX cell. Examination of the transient response for each unique sea surface illustrates how multipath and diffraction effect the transient response during marine communications.

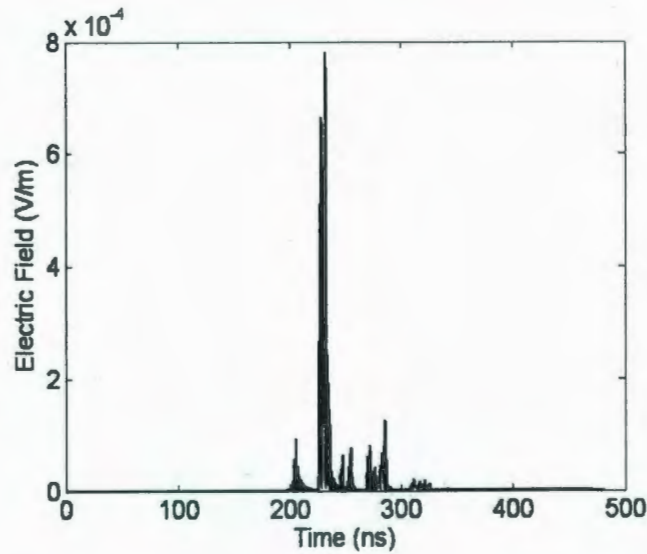


Figure 8-7: Transient response at the RX location for a random sea surface simulation.

Three such results, each from a unique sea surface, are illustrated in Figures 8-7, 8-8 and 8-9. Of course the transient responses for each random sea surface are obtained from direct solutions to Maxwell's equations. Thus, these results include all aspects of electromagnetic propagation. Some models, such as ray tracing, though fast and effective for analysis, do not include higher order effects in their direct application. Using of the FDTD simulation approach, there is no ambiguity in what is obtained. All higher order effects are provided when Maxwell's equations are directly solved.

Visually, propagation can be observed easily using the FDTD method. Propagation around sea surfaces and diffraction is readily available for inspection. Figures 8-10, 8-11 and 8-12 depict the propagation of the incident pulse as it moves through the finite difference grid, and is effected by the random sea surface boundary and ultimately exits the grid leaving smaller magnitude multipath components.

Once propagation analysis is complete, system transfer functions are determined based on DFT analysis of the input and output transient signals for each frequency of interest [86]. Some of the key communications systems carrier frequencies are used for post simulation analysis. They include:

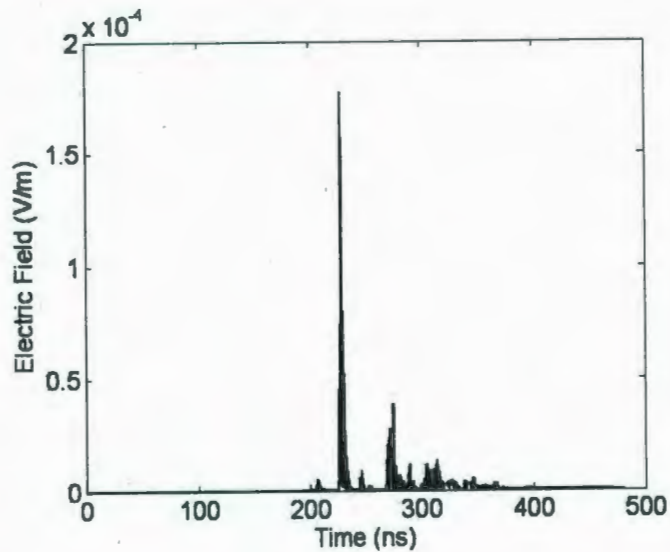


Figure 8-8: Transient response at the RX location for a random sea surface simulation.

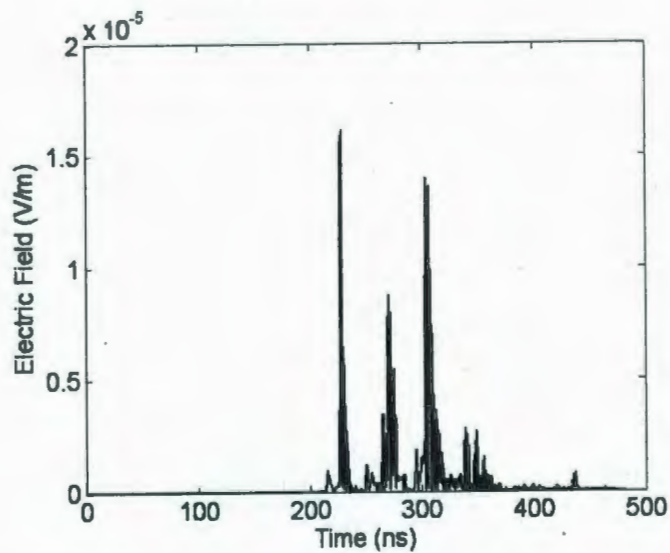


Figure 8-9: Transient response at the RX location for a random sea surface simulation.

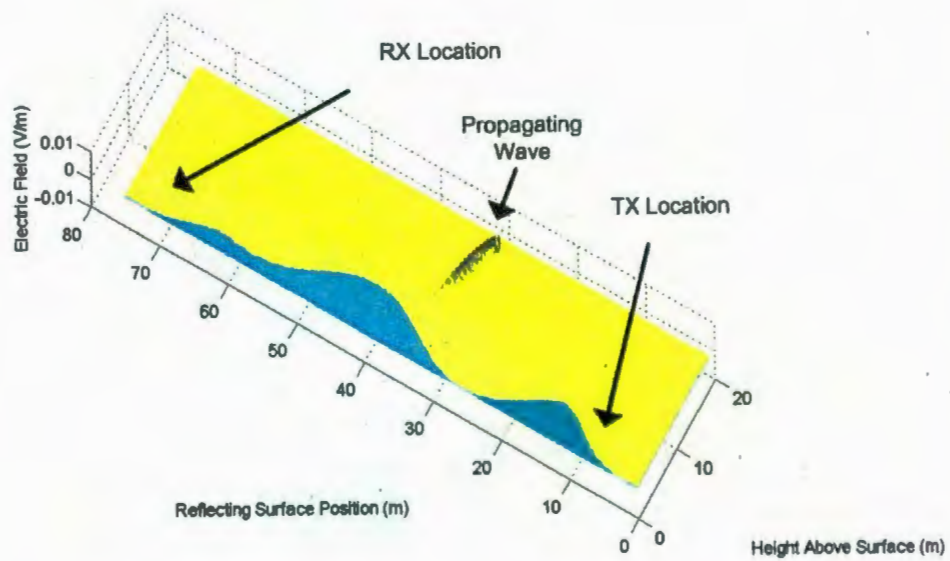


Figure 8-10: E_z field at 20 % completed simulation.

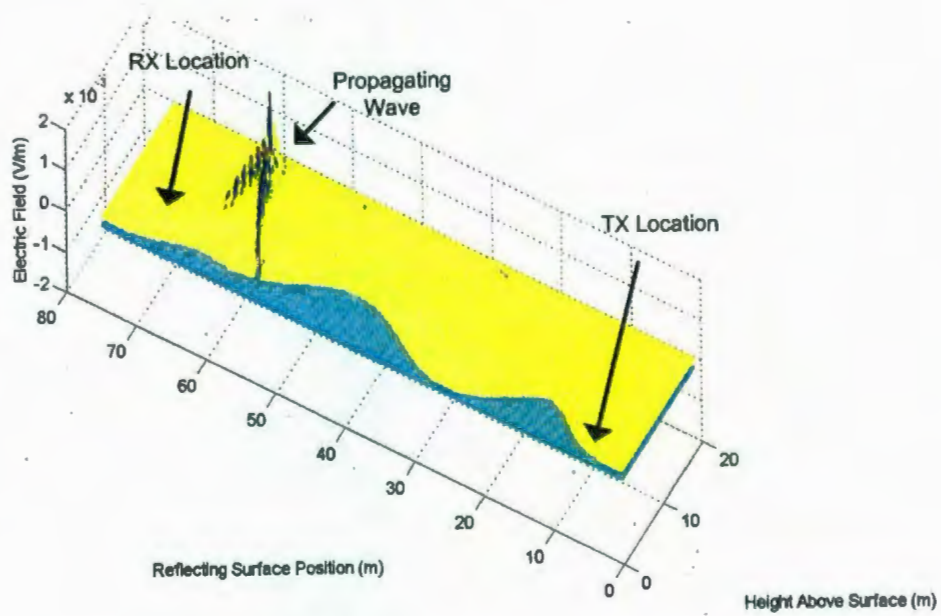


Figure 8-11: E_z field at 40 % completed simulation.

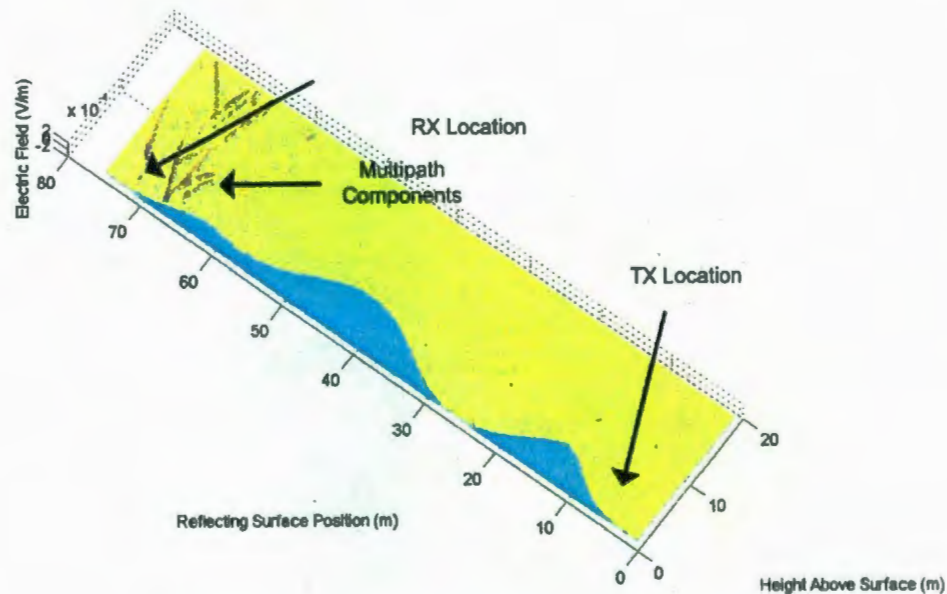


Figure 8-12: E_z field at 60 % completed simulation.

- 162 MHz – the AIS (Automatic Identification System) communications channels.
- 433 MHz – a public band for wireless communications.
- 913 MHz – a public band for wireless communications.
- 1.621 GHz – the Iridium satellite TX/RX carrier frequency, as well as the Globalstar satellite TX channel.
- 1.800 GHz – PCS communications channel.
- 2.492 GHz – the Globalstar RX communications channel, Ethernet.
- 3.000 GHz – the top end of the spectral content for the input pulse.

These frequencies are chosen because they are of specific interest for generalized communications. Any frequency can be chosen using this methodology. Since the technique is wide band in nature, it is possible to determine system transfer functions

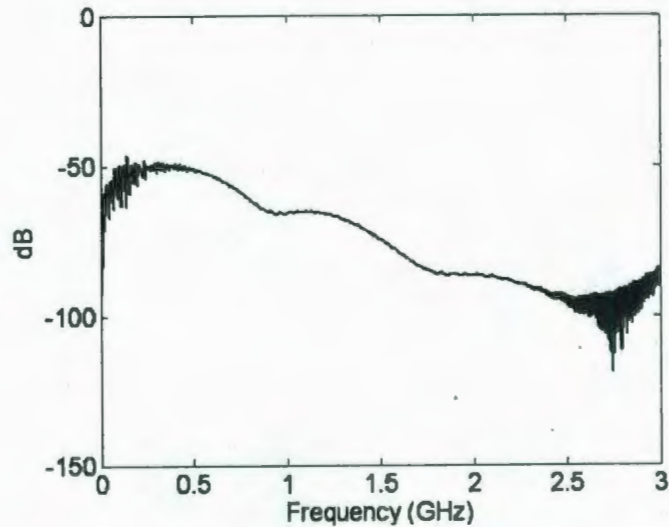


Figure 8-13: System transfer function between a TX and an RX location over a random sea surface showing attenuation from VHF to 3 GHz.

for the entire band of interest. Figures 8-13 and 8-14 illustrate two unique frequency responses for propagation over random sea surfaces.

Figures 8-13 and 8-14 illustrate some significant items worth mentioning in the post simulation analysis. Both system transfer functions are unique in nature. Both generally increase in attenuation as frequency increases, however the nulls of Figure 8-14 illustrate how fading effects based on the specific geometry and subsequent multipath can adversely effect a communications channel. Also, it is worth noting the indicators of numerical stability. In both system transfer functions, the lower and higher frequency bands are beginning to demonstrate erratic behavior. This is due to the numerical accuracy limits of the FDTD approach. At the upper spectrum, the spectral content of the pulse was somewhat limited above 2.5 GHz. At less than 500 MHz, after several investigations, it is concluded that the physical length of the absorbing boundary condition becomes electrically short, inducing reflections back into the grid that are erroneous. In dealing with numerical analysis and the implementation thereof, it is important to understand the effects of solving problems through

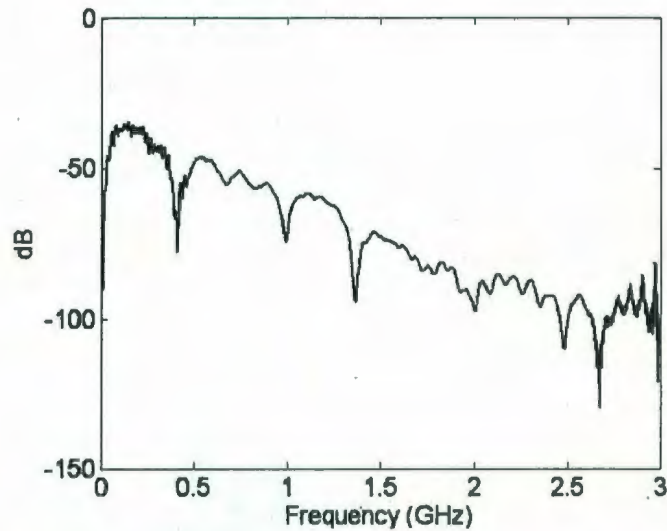


Figure 8-14: System transfer function between a TX and an RX location over a random sea surface showing attenuation from VHF to 3 GHz.

these means, and to be aware of indicators when solutions should be interpreted accordingly.

Now that the system transfer functions are determined, it is possible to examine the path loss as a function of distance between TX and RX locations for each frequency of interest. The path loss experienced along a straight line between transmitter and receiver for the 433 MHz, 1.6 GHz and 2.5 GHz carrier frequencies are illustrated in Figures 8-15, 8-16 and 8-17 respectively. It is interesting to note that the locations where no attenuation is depicted are actually points located inside the sea surface boundary condition. Also, the shadowing effects due to the individual peaks is observable directly following these regions, as loss plummets quickly. For the three cited carrier frequencies, it is observed that path loss becomes more severe as both frequency and distance increase. This is of course an anticipated result.

The objective of this work is to determined parameters of the path loss equation. This requires evaluation of the path loss exponent and standard deviation due to fast fading in the channel. For this purpose, we optimize the path loss exponent function

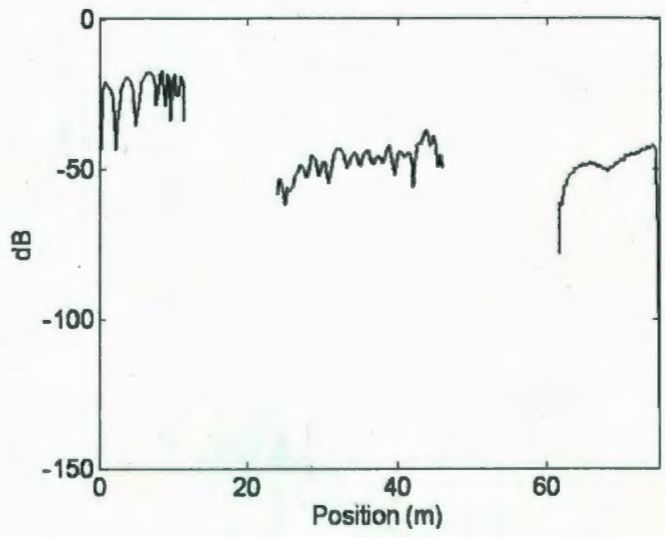


Figure 8-15: Path Loss between TX and RX locations for 433 MHz.

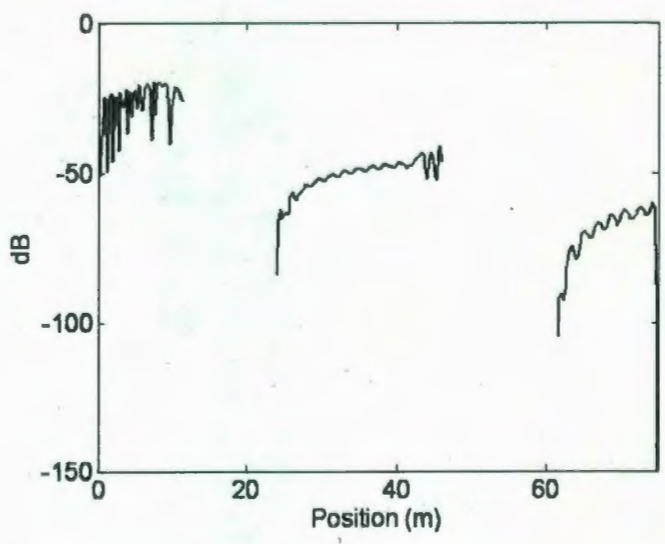


Figure 8-16: Path Loss between TX and RX locations for 1.621 GHz.

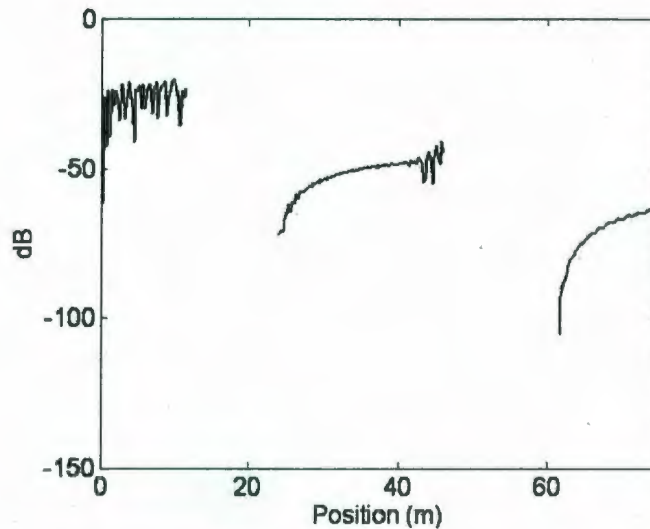


Figure 8-17: Path Loss between TX and RX locations for 2.492 GHz.

to fit the path loss experienced in the specific channel over the distance simulated. Once the path loss exponent is determined, the standard deviation of the fit is also calculated. This is not done at a single point, but rather optimized over a region to ensure that the path loss and standard deviation are reflective of the average system transfer functions as a whole, and not to a localized null. Illustration of this small region over which optimization occurs is provided in Figures 8-18 and 8-19. Completing the same analysis for the frequencies of interest, it becomes apparent that by using the detail of the known maximum observable sea surface height in the marine communications channel leads to a relationship between both loss exponent and standard deviation for the observable sea surface height.

The path loss exponent linear regression analysis for the specified relevant frequencies of interest are illustrated in Figures 8-20 to 8-26.

A summary of the path loss exponent vs. observable wave height regression analysis is given in Figure 8-27. k is the standard error, LB and UB are the lower and upper bounds, and R and R^2 are given as a measure of the goodness of fit. 95 % confidence bounds are illustrated in each regression analysis for loss exponent versus

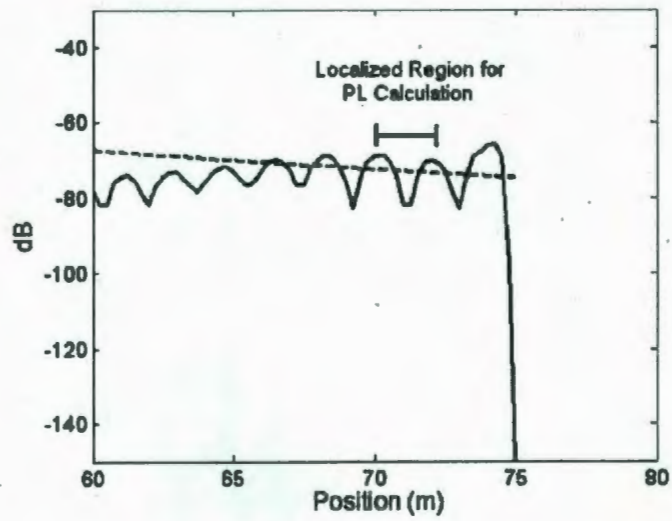


Figure 8-18: A localized region of optimization used for determining the path loss exponent and standard deviation.

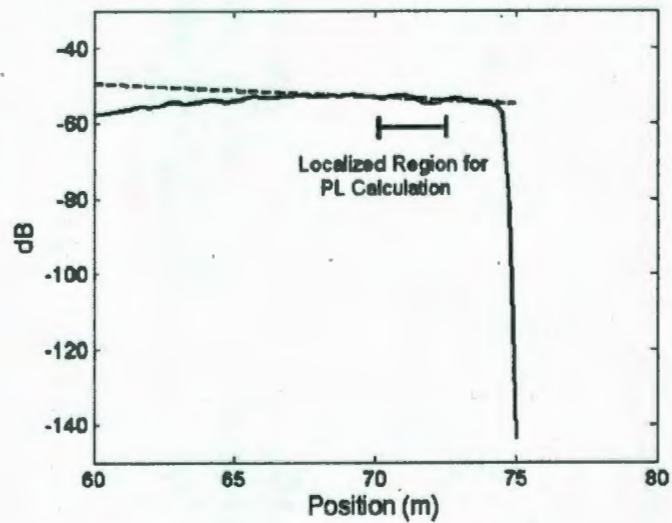


Figure 8-19: A localized region of optimization used for determining the path loss exponent and standard deviation.

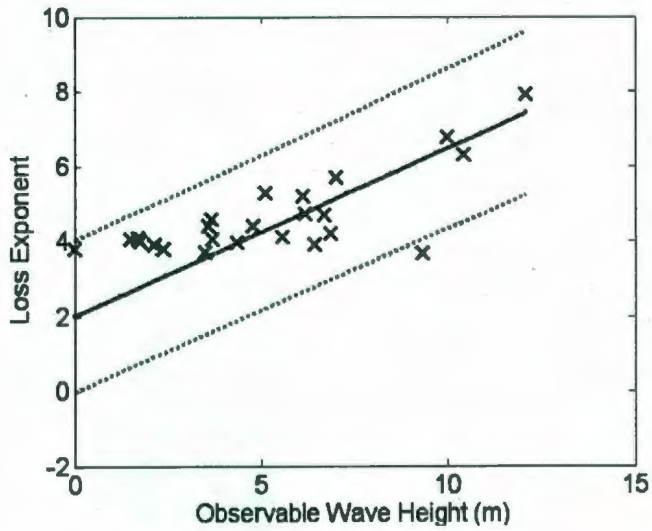


Figure 8-20: Path Loss Exponent vs. Observable Wave Height for 162 MHz with 95% confidence bounds.

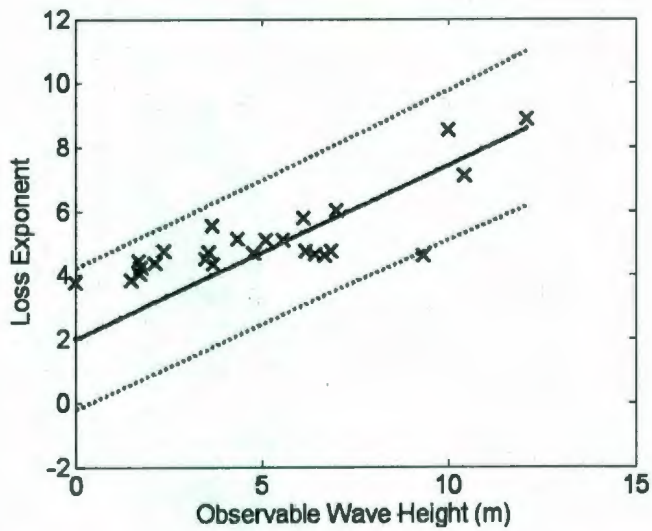


Figure 8-21: Path Loss Exponent vs. Observable Wave Height for 433 MHz with 95% confidence bounds.

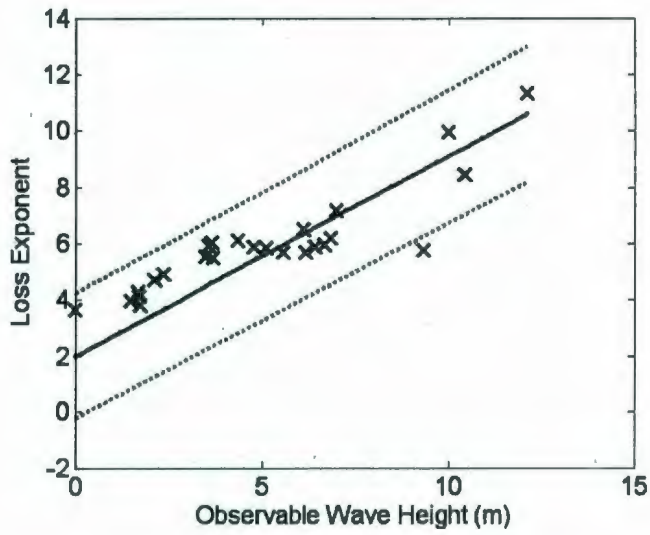


Figure 8-22: Path Loss Exponent vs. Observable Wave Height for 913 MHz with 95% confidence bounds.

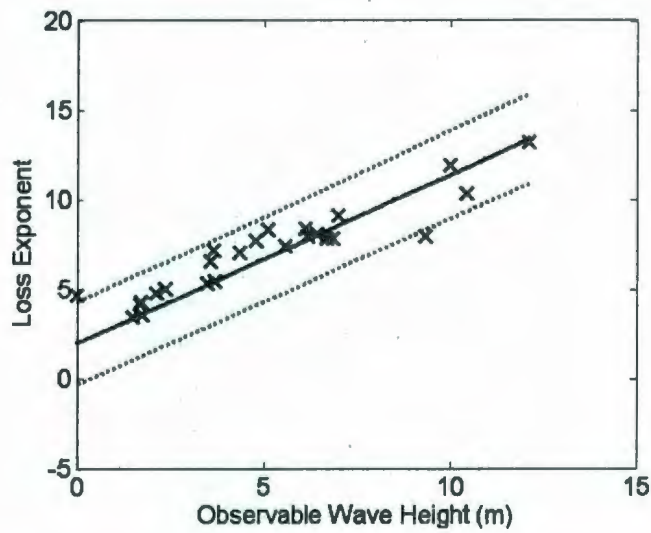


Figure 8-23: Path Loss Exponent vs. Observable Wave Height for 1.62 GHz with 95% confidence bounds.

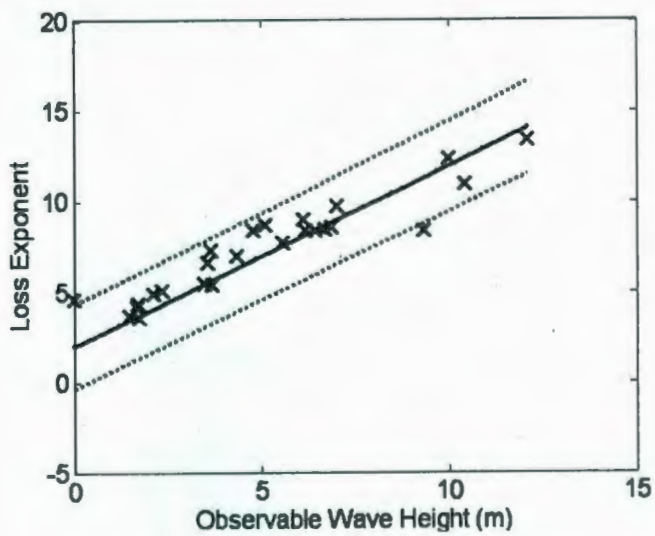


Figure 8-24: Path Loss Exponent vs. Observable Wave Height for 1.8 GHz with 95% confidence bounds.

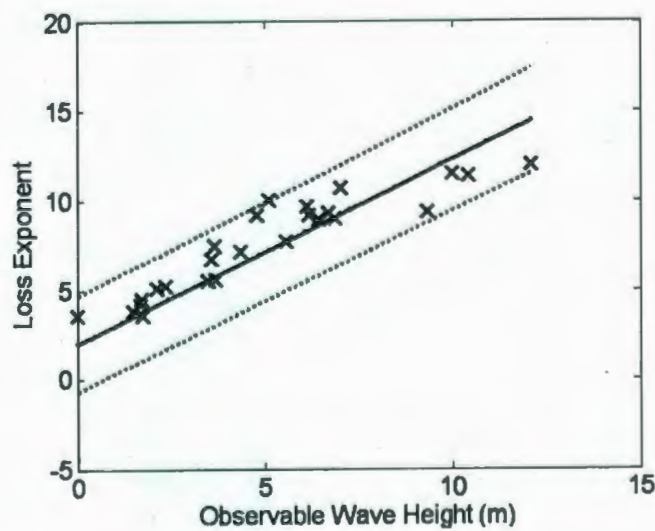


Figure 8-25: Path Loss Exponent vs. Observable Wave Height for 2.5 GHz with 95% confidence bounds.

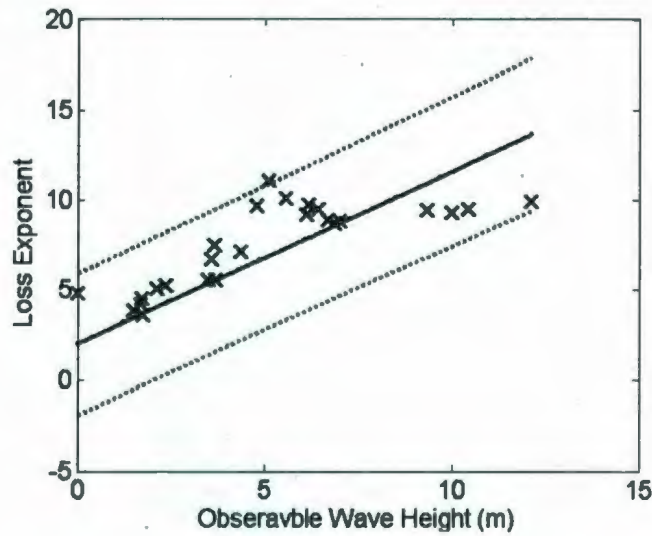


Figure 8-26: Path Loss Exponent vs. Observable Wave Height for 3.0 GHz with 95% confidence bounds.

Freq (GHz)	Slope (LE/m)	LB	UB	k	R ²	R
0.162	0.4465	0.3778	0.5152	0.0687	0.1341	0.3662
0.433	0.5433	0.4679	0.6186	0.0754	0.3035	0.5509
0.913	0.7094	0.6336	0.7852	0.0758	0.6287	0.7929
1.61	0.9409	0.8623	1.019	0.0786	0.7911	0.8894
1.8	0.995	0.9151	1.075	0.0799	0.8087	0.8993
2.492	1.029	0.9376	1.12	0.0914	0.7603	0.8720
3	0.9595	0.8265	1.093	0.1330	0.3469	0.5890

Figure 8-27: Loss exponent linear regression analysis summary.

observable wave height.

During the regression analysis, the intercept of these relations is required to be 2. This will prove advantageous when subsequent analysis is conducted in regard to frequency. 2 is an appropriate approximation, as at nil observable sea surface height the path loss exponent reduces to the same value as is used for free space path loss. If we further then consider these newly obtained values of loss exponent per meter (LE/m) in conjunction with the frequency of interest for each, examining the loss exponent slope/m and frequency provides a secondary relationship. The collective slopes versus frequency are depicted in Figure 8-28, whereby the relationship between path loss exponent per meter of observable sea surface height and frequency can be

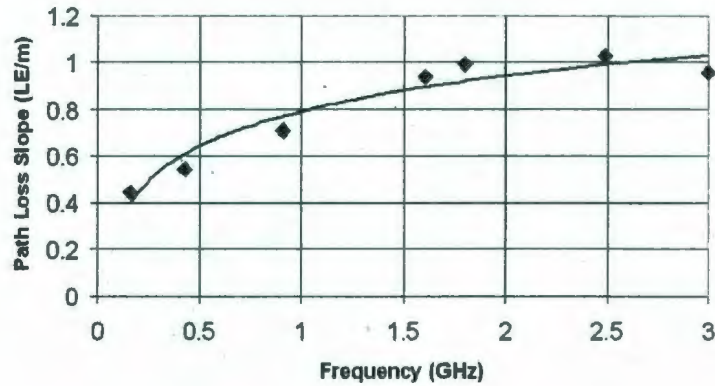


Figure 8-28: Path Loss Exponent per Wave Height (LE/m) vs. Frequency (GHz).

modeled as a logarithmic function.

For both the path loss exponent and standard deviations, the regression analysis provides results in the form of,

$$f(x) = p1 * x + p2. \quad (8.1)$$

The linear regression analysis results for the path loss exponent/m versus the log of the respective frequencies, illustrated in Figure 8-29, for which the previous analysis are numerically determined, where k is the standard error that may be used to evaluate statistical confidence levels for the coefficients. The lower and upper bounds, LB and UB respectively, are given for a 95% statistical confidence level. The k value may be utilized to evaluate other confidence level bounds if so desired. The coefficient of determination, R^2 , was determined to be 0.9245 and the multiple correlation coefficient was evaluated to be 0.9615. This indicates an extremely strong relationship between the path loss exponent/m and the \log_{10} of frequency.

The linear regression analysis of LE/m vs. frequency suggests that a generalized path loss model can be written for the marine communications channel during sea surface shadowing conditions in the north North Atlantic region in the form,

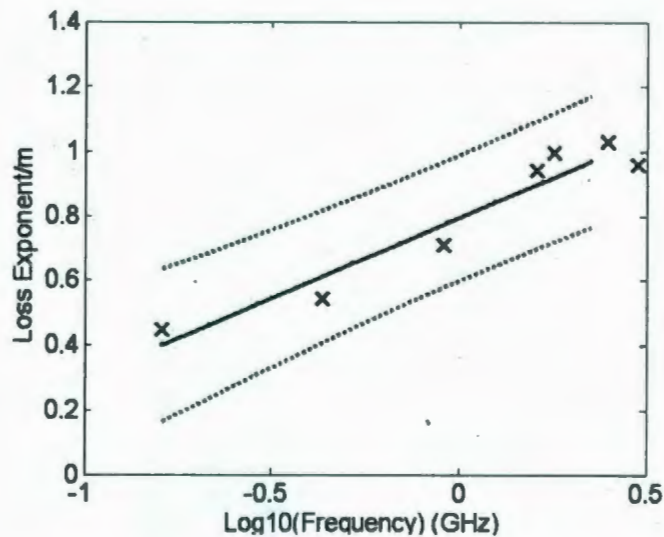


Figure 8-29: Path Loss Exponent per Wave Height (LE/m) vs. Log10(Frequency) (GHz) with 95% confidence bounds.

$$PL(h, f) = PL(d_o) + 10 * [(0.498 \log_{10}(f) + 0.793) * h + 2] \log_{10}(d) + X_f \quad (8.2)$$

where $PL(d_o)$ is the path loss at 1 m, h is the observable wave height of the sea surface in meters, f is the frequency of interest in gigahertz, and the contribution of X_f , is the random value given with standard deviation $\sigma(h)$. In order to account for the random factor contribution to the path loss model, the standard deviation is considered in a similar manner to the analysis of the path loss exponent versus observable sea surface height. The results are given in Figures 8-30 to 8-36.

A summary of the standard deviation vs. observable wave height regression analysis is given in Figure 8-37. k is the standard error, LB and UB are the lower and upper bounds, and R and R² are given as a measure of the goodness of fit. In the case of the standard deviation, the intercept of the regression analysis is required to be 0. Having a common intercept for the standard deviation is advantageous for subsequent analysis, and is a reasonable assumption as it is commonly known that with

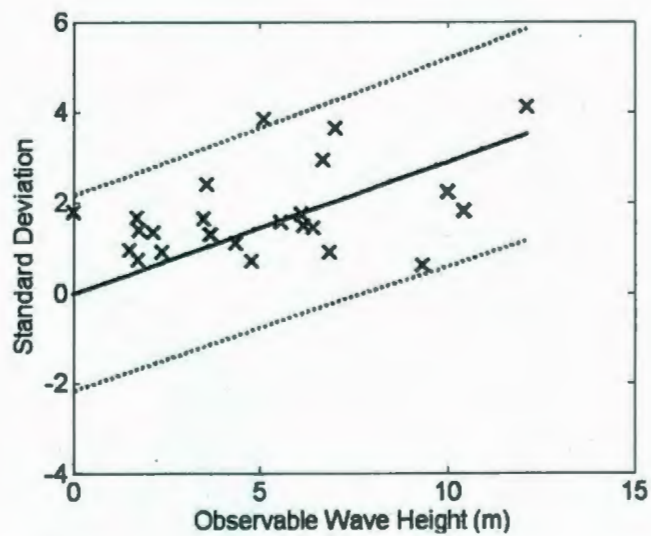


Figure 8-30: Standard Deviation vs. Observable Wave Height for 162 MHz with 95% confidence bounds.

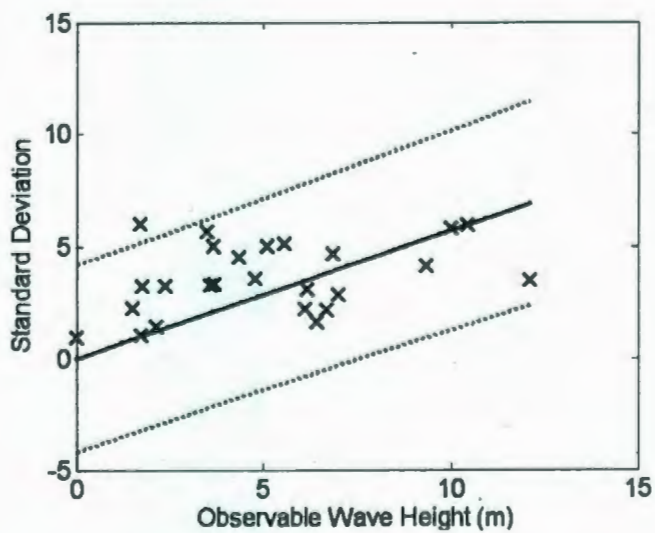


Figure 8-31: Standard Deviation vs. Observable Wave Height for 433 MHz with 95% confidence bounds.

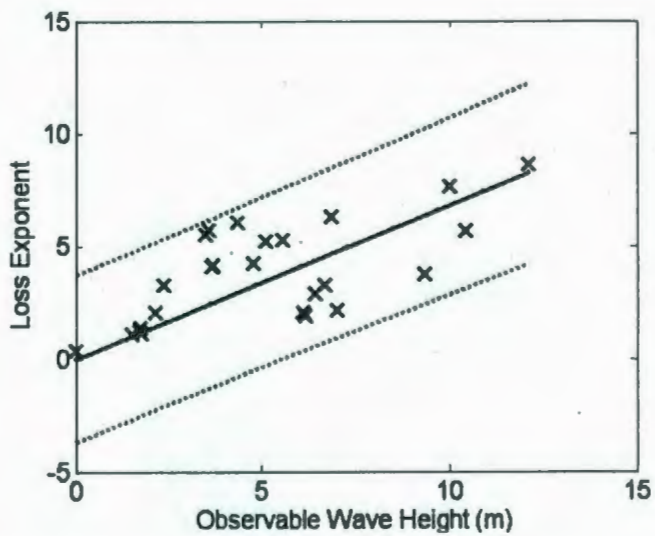


Figure 8-32: Standard Deviation vs. Observable Wave Height for 913 MHz with 95% confidence bounds.

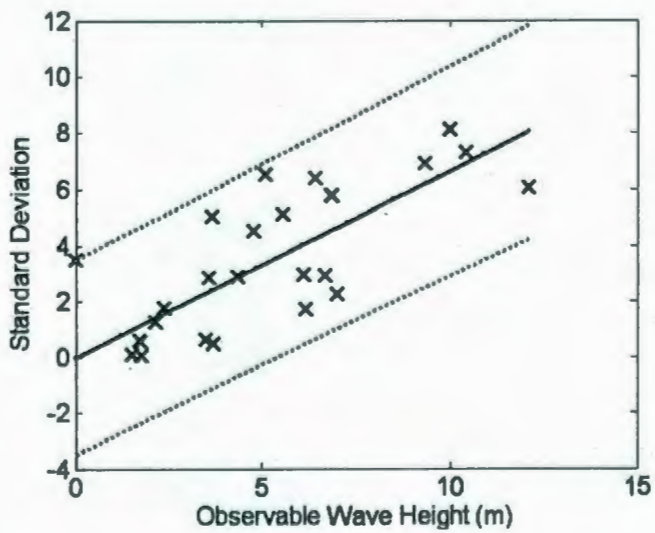


Figure 8-33: Standard Deviation vs. Observable Wave Height for 1.62 GHz with 95% confidence bounds.

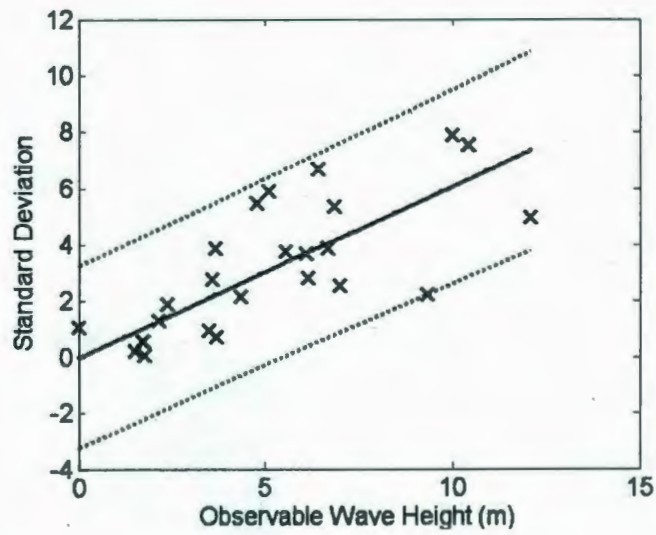


Figure 8-34: Standard Deviation vs. Observable Wave Height for 1.8 GHz with 95% confidence bounds.

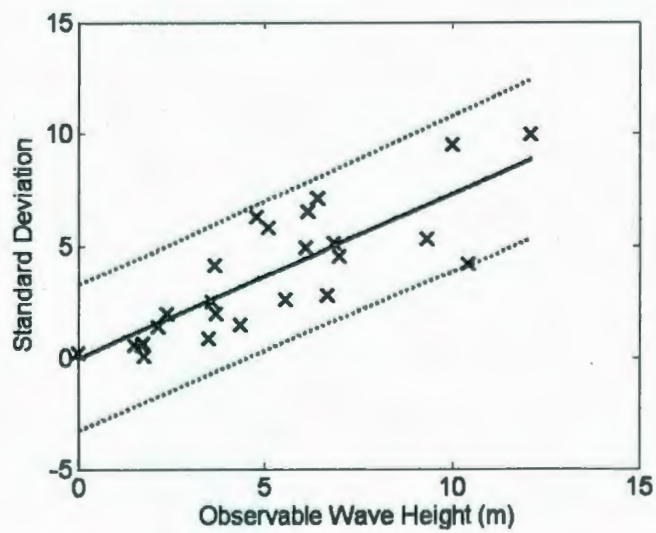


Figure 8-35: Standard Deviation vs. Observable Wave Height for 2.5 GHz with 95% confidence bounds.

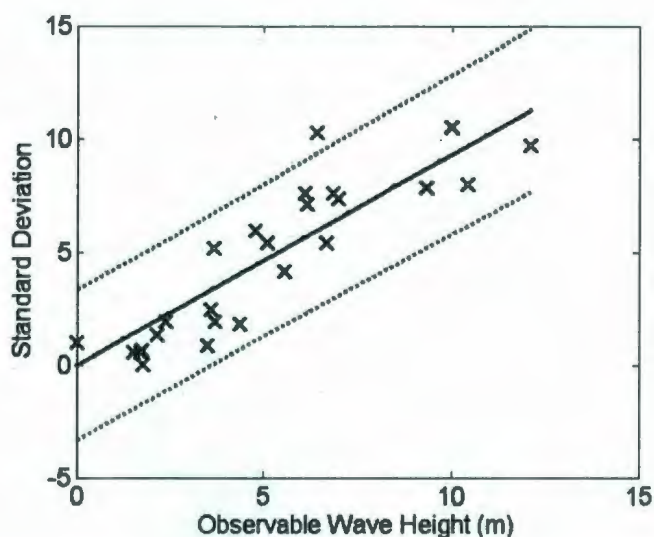


Figure 8-36: Standard Deviation vs. Observable Wave Height for 3.0 GHz with 95% confidence bounds.

Freq (GHz)	Std Dev	LB	UB	k	R ²	R
0.162	0.2893	0.2161	0.3626	0.0732	0.1943	0.4408
0.433	0.5713	0.4292	0.7136	0.1421	0.6984	0.8357
0.913	0.6064	0.496	0.7166	0.1104	0.5430	0.7369
1.61	0.6636	0.5445	0.7827	0.1191	0.5468	0.7395
1.8	0.6806	0.5549	0.8065	0.1257	0.3324	0.5765
2.492	0.7318	0.6208	0.8428	0.1110	0.6872	0.8290
3	0.9318	0.8192	1.045	0.1126	0.7811	0.8838

Figure 8-37: Standard deviation linear regression analysis summary.

increasing sea surface height, standard deviation is anticipated to increase. Thus, with no sea surface height, 0 standard deviation is a reasonable generality.

A summary of the raw data upon which this analysis was conducted is given for the reader in Figure 8-38. For various randomly generated sea surfaces, the results include loss exponent, standard deviation, as well as transient delay profiles for 10 dB, 15 dB and 20 dB. Mean excess delay, root mean square delay and the Rice factor all also given, for all frequencies of stated interest. The Rice factor in this case is defined with respect to the first impulse from the diffracted signal, rather than the line of sight component and the multipath components.

When examining the standard deviation experienced per meter of observable sea

Max Waveh	AIS LE	AIS STD	IRIDIUM LE	IRIDIUM STD	GS LE	GS STD	433 LE	433 STD	1800 LE	1800 STD	913 LE	913 STD	3000 LE	3000 STD	10dB DP	15dB DP	20dB DP	MXS D (ns)	RMS D (ns)	K
6.685	4.710	2.949	7.840	2.935	9.330	2.612	4.63	2.1677	8.45	3.6688	5.97	3.278	8.9	5.4512		77.929	102.825	230.749	8.822	2.115
6.118	5.190	1.761	8.400	2.999	9.890	4.961	5.78	2.2279	9.01	3.6693	6.52	2.0969	9.21	7.6155	55.922	69.974	115.671	234.408	16.288	1.253
9.329	3.670	0.632	8.010	6.905	9.360	5.333	4.63	4.1543	8.43	2.2467	5.78	3.7723	9.43	7.8479	57.099	57.718	104.563	231.829	9.429	3.132
10.445	6.310	1.837	10.360	7.306	11.390	4.239	7.11	5.9554	10.95	7.5472	8.44	5.6986	9.5	7.9975	122.330	210.512	211.690	277.482	36.422	0.276
10.008	6.770	2.234	11.960	8.119	11.510	9.531	8.55	5.8475	12.36	7.9092	9.97	7.6939	9.31	10.5494	122.094	203.765	241.713	305.187	19.501	0.088
7.007	5.690	3.655	9.170	2.298	10.700	4.546	6.01	2.8617	9.78	2.5488	7.15	2.1986	8.81	7.3781	51.578	95.960	131.316	232.740	14.422	1.586
6.875	4.200	0.924	7.850	5.773	9.050	5.139	4.76	4.73	8.60	5.35	6.20	6.32	8.71	7.64		57.452	93.868	231.183	7.989	3.640
6.425	3.920	1.455	8.080	6.415	8.970	7.163	4.65	1.86	8.39	6.70	5.89	2.92	9.50	10.31		56.274	103.061	231.542	7.350	4.014
6.170	4.720	1.514	7.990	1.760	9.220	6.546	4.75	3.10	8.44	2.85	5.69	1.92	9.73	7.15	55.478	57.158	86.738	230.531	7.488	3.332
5.560	4.110	1.586	7.460	5.140	7.720	2.622	5.10	5.16	7.77	3.78	5.67	5.29	10.14	4.15	80.758	81.995	121.298	232.702	9.627	1.971
12.113	7.900	4.110	13.190	6.051	12.010	9.967	8.88	3.50	13.42	4.97	11.39	8.63	9.92	9.73	51.913	100.026	202.026	309.405	12.652	0.345
5.118	5.280	3.850	8.340	6.518	10.040	5.832	5.09	5.06	8.70	5.91	5.86	5.24	11.09	5.46	49.085	89.685	140.567	236.308	19.524	0.946
4.789	4.400	0.723	7.740	4.553	9.200	6.318	4.7	3.6057	8.42	5.4657	5.9	4.2657	9.66	5.9947	55.685	57.305	88.418	230.744	8.860	2.371
3.502	3.710	1.664	5.350	0.666	5.540	0.848	4.54	5.6798	5.47	0.9592	5.54	5.5548	5.53	0.6747	80.993	87.593	103.591	229.624	14.892	1.000
3.690	4.070	1.328	5.470	0.481	5.590	1.994	4.34	3.3282	5.43	0.7439	5.5	4.1514	5.57	1.914	50.411	87.063	95.401	223.702	16.347	0.997
3.675	4.590	1.328	7.220	5.043	7.480	4.169	5.55	5.0652	7.33	3.8711	6.03	4.1336	7.51	5.2086	30.907	97.551	147.137	230.619	8.631	2.529
4.349	3.980	1.122	7.050	2.917	7.170	1.481	5.12	4.5737	7.03	2.179	6.13	6.0705	7.14	1.8249	67.647	78.283	118.352	230.734	7.265	2.631
3.577	4.420	2.400	6.590	2.878	6.750	2.500	4.72	3.3037	6.65	2.7964	5.93	5.7387	6.72	2.4531	68.972	109.219	145.428	230.185	10.017	1.737
1.504	4.060	0.981	3.490	0.112	3.860	0.567	3.83	2.27	3.75	0.22	3.98	1.11	3.82	0.55	34.648	40.777	85.442	209.459	7.950	4.832
1.783	3.990	1.422	3.610	0.051	3.610	0.069	4.24	3.25	3.59	0.05	3.81	1.14	3.59	0.06	41.985	82.820	84.617	211.105	9.206	4.122
2.156	3.910	1.370	4.850	1.280	5.110	1.367	4.38	1.47	4.93	1.30	4.70	2.10	5.09	1.37	70.298	123.302	139.064	217.420	14.068	2.902
1.740	4.030	0.762	4.310	0.557	4.530	0.674	4.05	1.08	4.38	0.59	4.13	1.38	4.51	0.66	41.101	106.361	121.387	214.535	12.884	2.761
1.717	4.080	1.677	4.210	0.599	4.230	0.558	4.44	6.02	4.20	0.57	4.28	1.27	4.22	0.55	41.808	82.849	111.664	214.763	12.805	2.887
2.375	3.800	0.922	5.060	1.799	5.260	1.972	4.76	3.26	5.13	1.90	4.91	3.32	5.24	1.95	38.154	82.555	140.272	223.874	13.778	1.916
0.007	3.800	1.796	4.700	3.522	3.620	0.232	3.76	0.9462	4.67	1.0623	3.65	0.3631	4.82	1.0316	39.451	49.115	86.355	207.380	6.601	4.055

Figure 8-38: Shadowing study data set obtained through FDTD simulation for various randomly generated sea surfaces.

surface height in regard to the carrier frequency, as illustrated in Figure 8-39, a secondary relationship materializes allowing us to relate the standard deviation to both observable wave height and frequency simultaneously, as was the relationship with the path loss exponent.

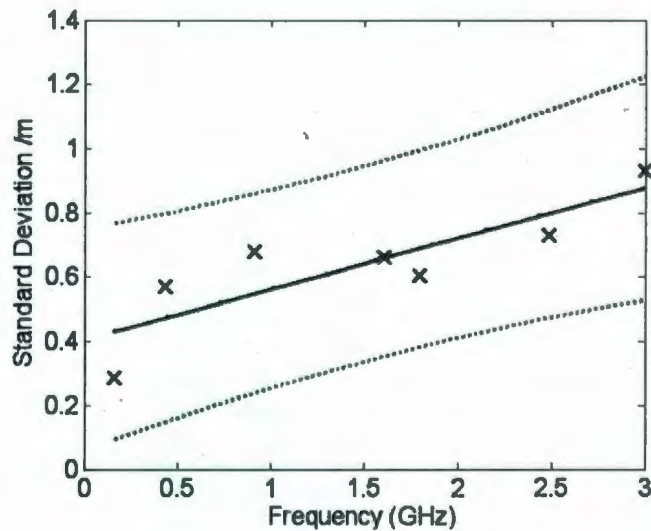


Figure 8-39: Standard Deviation per Wave Height (LE/m) vs. Frequency (GHz).

The coefficient of determination, R^2 , was determined to be 0.602 and the multiple correlation coefficient was evaluated to be 0.776. Though the statistical analysis is not as strong for the standard deviation as a function of frequency in comparison to the path loss exponent, where a firm relationship is clear. Thus the proposed generalized model for the standard deviation, σ_f , as a function of frequency is,

$$\sigma_f = [0.157f + 0.405] * h, \quad (8.3)$$

where f again is in gigahertz and the observable sea height, h , is in meters. This model thus provides insight into the random contribution of X_f when considering the path loss model for a sea surface shadowing condition.

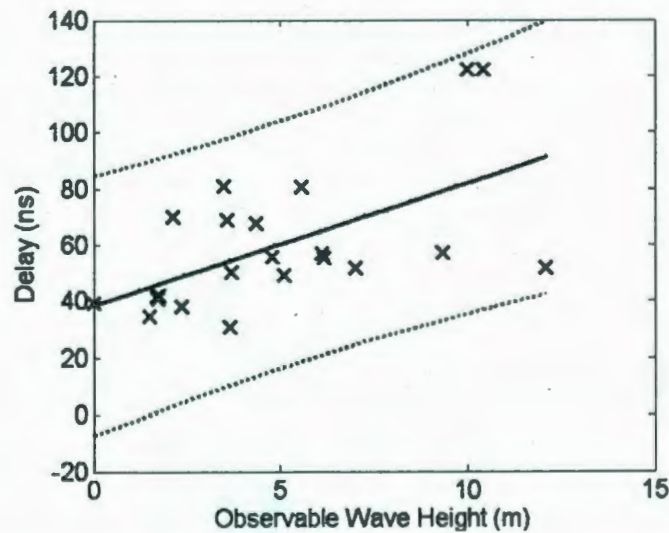


Figure 8-40: 10 dB Delay Profile versus Observable Wave Height and corresponding data fit along with 95% statistical confidence bounds.

8.3 Sea Surface Shadowing Transient Analysis & Model Development

Using the transient response generated directly by the FDTD electromagnetic channel simulation, it is possible to evaluate the delay profiles and transient characteristics of the communications channel based on the immediate output of the marine propagation simulations. As with the previous loss exponent evaluation, the data is then investigated with regard to the observable wave height. Figures 8-40 to 8-42 illustrate the 10 dB, 15 dB and 20 dB transient delay profiles for the FDTD sea surface shadowing population data set.

The linear regression analysis for 10 dB, 15 dB and 20 dB delay profiles are determined based on the same form as used for the path loss exponent and standard deviation. The collective results are illustrated in Figure 8-43. Thus, for a 10 dB delay profile for a 60 m TX to RX separation, the generalized model based on the linear regression analysis may be written as,

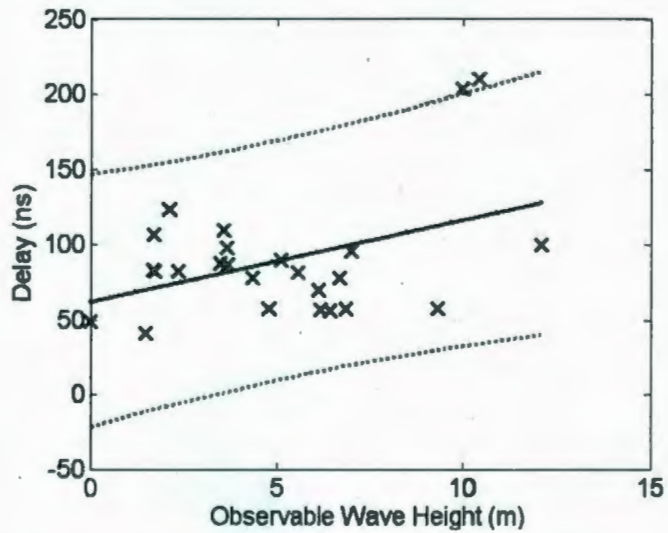


Figure 8-41: 15 dB Delay Profile versus Observable Wave Height and corresponding data fit along with 95% statistical confidence bounds.

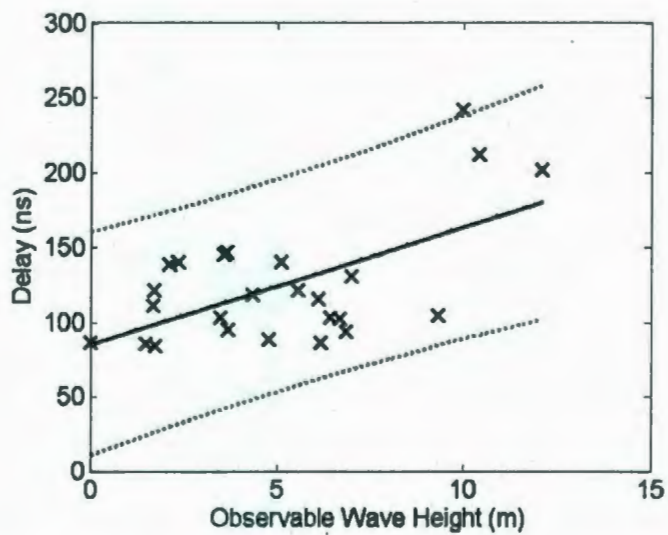


Figure 8-42: 20 dB Delay Profile versus Observable Wave Height and corresponding data fit along with 95% statistical confidence bounds.

	Coefficient	Result	LB	UB	k	R ²	R
10dB	p1	3.97	1.25	6.70	1.36	0.28	0.53
	p2	38.24	22.12	54.35	8.06		
15dB	Coefficient	Result	LB	UB	k	R ²	R
	p1	5.42	0.27	10.57	2.58	0.17	0.41
	p2	62.26	31.80	92.71	15.23		
20dB	Coefficient	Result	LB	UB	k	R ²	R
	p1	7.81	3.23	12.39	2.29	0.35	0.59
	p2	85.31	58.23	112.40	13.54		

Figure 8-43: Linear Regression Analysis for delay profiles at 10 dB, 15 dB and 20 dB. The standard error, k , is given for a 95% statistical confidence level with respective lower and upper bounds.

$$Delay_{10dB}(ns) = 3.97 * h + 38.24 \quad (8.4)$$

Similarly, for the 15 dB and 20 dB delay profiles,

$$Delay_{15dB}(ns) = 5.42 * h + 62.26 \quad (8.5)$$

and

$$Delay_{20dB}(ns) = 7.81 * h + 85.31, \quad (8.6)$$

where the standard error can be applied to each coefficient as illustrated previously. Clearly, based on the statistical analysis, the quality of the function fit to the delay profile is lower than that observed in the regression analysis of the path loss exponent and the standard deviation. The linear regression analysis exhibits a moderate correlation at best. Consideration to this fact should be given when using these proposed models for channel characterization. To model the mean excess delay and the root mean square delay, linear regression analysis is once again conducted on the transient response at the RX location for the simulation population. The regression analysis for each is given in Figures 8-44 and 8-45 respectively. 95% confidence bounds for each are also included.

The transient performance models must be considered with respect to the 60 m

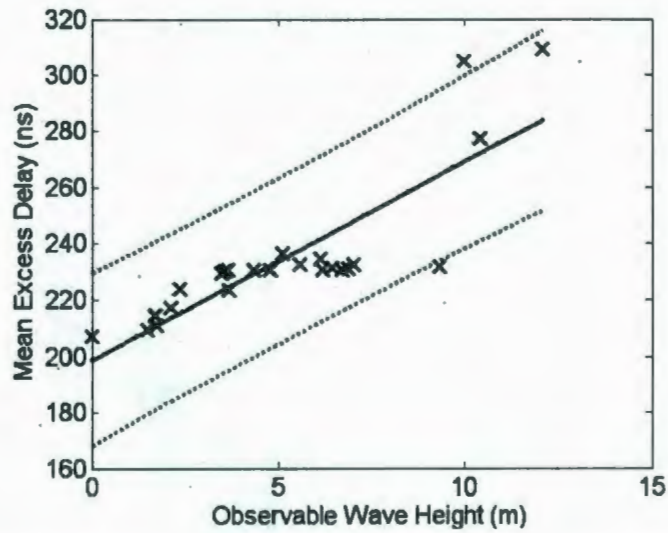


Figure 8-44: Mean Excess Delay versus Observable Wave Height and corresponding linear regression analysis. The standard error for a 95% statistical confidence level is given with respective lower and upper bounds.

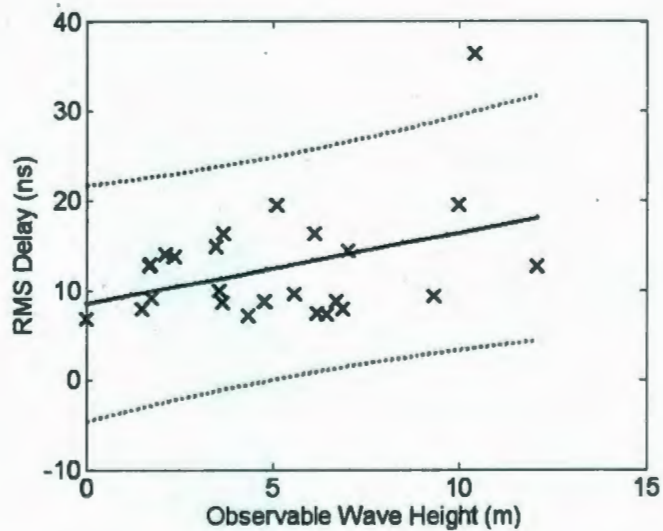


Figure 8-45: Root Mean Square delay versus Observable Wave Height and corresponding linear regression analysis. The standard error for a 95% statistical confidence level is given with respective lower and upper bounds.

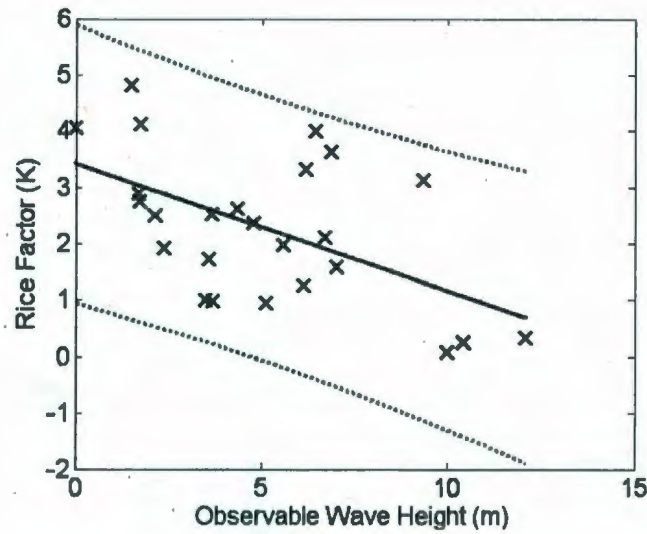


Figure 8-46: K factor versus sea height, and corresponding data fit function. The 95% lower and upper bounds are given.

TX-RX separation communications channel from which they were derived. Therefore, the mean excess delay may be modeled as a function of observable wave height may be expressed in nanoseconds as,

$$MXD(L, h) = \frac{L}{60} (7.02h + 198.70). \quad (8.7)$$

Similarly the root mean square delay model based on the post simulation linear regression analysis is of the form,

$$RMS(L, h) = \frac{L}{60} (0.78h + 8.54). \quad (8.8)$$

In both cases the length of the channel of interest is represented by L , and given in metres. The height of the sea surface is denoted in meters by h . Levels of statistical confidence may be adjusted using the respective standard error as provided in the linear regression analysis using the standard error, k .

The ratio of the initial diffracted received power to the multipath received power

MXS	Coefficient	Result	LB	UB	k	R ²	R
	p1	7.019	5.133	8.905	1.886		
	p2	198.7	187.6	209.9	11.1		
RMS	Coefficient	Result	LB	UB	k	R ²	R
	p1	0.7849	-0.0171	1.587	0.802		
	p2	8.542	3.8	13.28	4.742		
K	Coefficient	Result	LB	UB	k	R ²	R
	p1	-0.2248	-0.3765	-0.07315	0.1517		
	p2	3.421	2.524	4.318	0.897		

Figure 8-47: Linear regression analysis summary for the mean excess, root mean square and Rice factor.

was calculated based on the transient response for the fixed channel length of 60 m. Numerical results are given in 8-46. A trend was observed as the sea surface height was varied. For the shadowing case, K is considered as the ratio of the first received impulse to the subsequent multipath contributions occurring after the initial impulse. Interestingly, it is observed that this ratio decreases as sea surface height increases. Linear regression analysis of the FDTD simulated data was performed. For the channels analyzed in this study, and by the described definition of K , the post simulation analysis produces a model,

$$K(h) = -0.225h + 3.421 \quad (8.9)$$

where h is the observable sea surface height in metres. A summary of the regression analysis for the mean excess, root mean square and diffracted Rice factor analysis is give in Figure 8-47.

These models, obtained using the FDTD method for overwater radio propagation analysis during sea surface shadowing conditions offer a unique insight into the effects of diffraction due to realistic sea surfaces. Using this novel numerical approach to study a problem that is difficult to address by analytic means, if possible at all, has produced parameterized models of path loss exponent and standard deviation as functions of both frequency and observable wave height. The mean excess delay,

delay profiles and the Rice factor are characterized based on the observable wave height only. In using this proposed methodology, the readily available detail of the sea surface over which propagation occurs makes this study and subsequent model synthesis possible. Although these channel performance models are based on the modified Pierson-Moskowitz spectral model for the north North Atlantic region, the methodology could be used in conjunction with sea surface models for other regions of interest. The development of this approach to overwater radio propagation analysis and marine communications channel simulation during sea surface shadowing conditions has produced novel channel performance models that are functions of both frequency and observable sea height. Conveniently, these models can be used for link budget analysis during the system design process to quantify the effects of the sea surface for a variety of marine applications.

8.4 Inshore Measurement Outline

Obtaining deep sea measurements of wireless communications channel performance is a difficult task. In this work it is not feasible to conduct a complete validation of the sea surface shadowing models, particularly in combination with obtaining details of the sea surface such that it is a known entity at the time of propagation analysis can be directly compared to FDTD simulation results. This is due primarily to the inaccessibility of the deep sea location, particularly during high sea states. Furthermore, to perform a flight test using a UAV is currently restricted by Transport Canada. Rather, a near shore measurement procedure is conducted to assess the general numerical result obtained during the FDTD analysis that the standard deviation contribution to the path loss equation increases as observable wave height increases. Though the specific diffraction and scattering mechanism is different than that of deep sea locations due to different spectral content of the sea surface, this generalized principle is anticipated to maintain for either propagation environment.



Figure 8-48: The gorge over which the transmitter (left peak) and receiver (right peak) are positioned for measurements.

The site chosen for the inshore measurements is an inlet near Cape Spear, Newfoundland, Canada. Though this effort does not directly verify the validity of the sea surface shadowing channel performance models developed previously in this work, an experimental study can examine one of the key generalized claims obtained during numerical analysis in a qualitative fashion.

The location of experiment is chosen to be an inlet upon which a fixed communications link is established over a body of sea water. Figures 8-48 and 8-49 show the actual measurement site. Power is measured over a random sea surface of variable height. The physical separation of the TX and RX locations was measured using a laser distance finder to be 41.5 meters. This is advantageous in some aspects, as the height of both the transmitter and receiver remain fixed, alleviating a common problem experienced in conducting measurements using floating platforms at sea. Unlike the FDTD simulation agenda for shadowing, the two antennas are located in line of sight condition. Two high gain Yagi antennas are used at fixed locations above the communications channel for both the transmitter and receiver. One such antenna is shown in Figure 8-50.



Figure 8-49: A second perspective of the transmitter location above the communications channel.



Figure 8-50: The high gain RX Yagi antenna is fixed pointed at the transmitter location. The TX antenna is identical, located at the other side of the inlet.

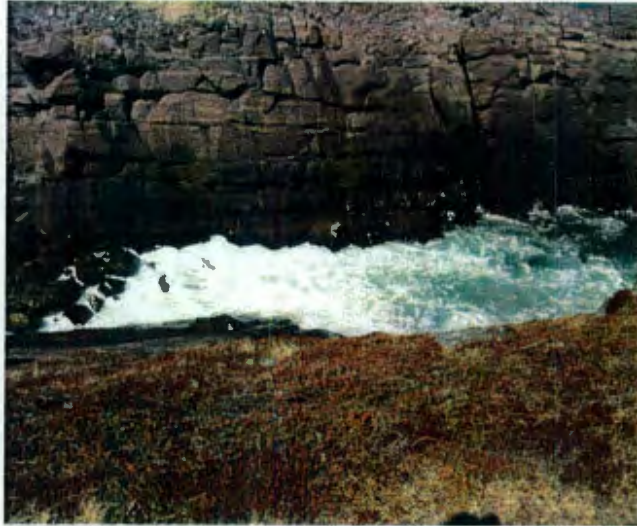


Figure 8-51: An instantaneous random sea surface.

Measurements of received power were taken over the random sea surface located at the bottom of the inlet. Several images were taken to illustrate the dynamics of the sea surface as a reflecting body in the channel under which the measurements were conducted. Figures 8-51 to 8-53 show the changing sea surface.

Measured data was collected using a Spectrum Analyzer, model HP 8560E. The transmit signal was generated using an RF signal generator, model HP 8657A, at a power level of +13 dBm. Measurements were collected over a two day period. At the time of each measurement set, the received power was recorded at equal time sampling intervals. Wind speed was recorded, as it is the basis for the Pierson-Moskowitz spectral model in the deep sea location, however, the wind speed was extremely random between 0 and 10 knots over the entire measurement period. Unlike the fully developed deep sea models, the random sea surface seemed to be a function of tidal effects at the time of day, rather than the wind. Measurements were conducted for two distinct sea surface conditions. First, for an observable sea surface of approximately 0.3 m and second, for an approximate 1 m sea surface. The wave height was estimated based on the physical displacement of the sea surface upon a the solid rock side of the gorge structures located in the basin of the channel. Based on historical experience



Figure 8-52: An second instantaneous random sea surface.



Figure 8-53: An third instantaneous random sea surface.

at the location, these wave heights were a relatively calm circumstance for the area.

The high gain antennas used were intended for cellular applications, operating ideally between 800 - 900 MHz. The spectrum analyzer was suitable for 1 MHz to 3 GHz measurements, however, the RF source could only operate up to 990 MHz. As radiation patterns generally change for antennas as a function of frequency, particularly high gain antennas, the limited bandwidth range of 600 MHz to 990 MHz was chosen for this experiment to avoid radical changes in radiation pattern. Moreover, the antennas were used in the approximate frequency range for which they were intended.

The calibration of the channel measurements was based upon a land based measurement of the received power for the two high gain antennas separated by a distance of 1 m. This configuration is illustrated in Figure 8-54. During the land based calibration process, the standard deviation for the received power was evaluated at all frequencies between 600 and 990 MHz. Thus, as the ground surface between the antennas remained constant and flat during the calibration measurements, it is reasonable to assume that this will also be the case as the observable sea surface height approaches zero. The standard deviation of the system unaffected by the sea surface can then be removed from the measurements after experimental results over the inlet are completed. The land calibration measurements are given in Figure 8-55.

Obtaining the measured standard deviation is the main objective of interest in this experiment during sea surface conditions of different significant sea surface heights. The FDTD simulation for the fully developed deep sea surface predicted that the standard deviation of the path loss equation would increase as a function of observable sea height. To assess this, the average power and subsequent standard deviation for the frequencies over both the 0.3 m and 1.0 m wave heights is measured. The raw data collected over the fixed link channel are given in Figure 8-56. The adjusted standard deviation results, removing the standard deviation innate to the system are given in Figure 8-57. These results are also plotted in Figure 8-58, providing data for



Figure 8-54: The 1 meter land based measurement used for standard calibration procedure of the path loss measurement.

Frequency MHz	Land Calibration		
	AVG mW	STD mW	% AVG
600	0.00182	0	0.00
750	0.033113	0	0.00
900	0.032854	0.000773	2.35
913	0.032587	0.000734	2.25
925	0.023734	0.000472	1.99
950	0.002752	0.00017	6.17
975	5.13E-05	2.53E-06	4.94
990	2.04E-05	6.64E-07	3.25

Figure 8-55: Measured power and standard deviation of land calibration.

Frequency MHz	0.3 m Observable Wave Height			1.0 m Observable Wave Height		
	AVG mW	STD mW	% AVG	AVG mW	STD mW	% AVG
600	2.74E-06	1.06E-07	3.85	2.94E-06	1.69E-07	5.75
750	9.34E-05	4.56E-06	4.88	7.29E-05	8.62E-06	11.83
900	7.64E-05	3.54E-06	4.63	4.74E-05	3.18E-06	6.70
913	4.71E-05	1.63E-06	3.46	3.59E-05	2.08E-06	5.81
925	5.28E-05	1.56E-06	2.95	3.26E-05	1.26E-06	3.87
950	4.98E-06	3.66E-07	7.35	2.37E-06	1.43E-07	6.03
975	1.29E-07	1.1E-08	8.48	5.43E-08	4.93E-09	9.09
990	2.94E-08	3.06E-09	10.41	5.48E-09	8.53E-10	15.56

Figure 8-56: Measured Power and standard deviation of the fixed inlet link for 0.3 m and 1.0 m observable wave heights.

Frequency	0.3 m	1.0 m
MHz	% AVG	% AVG
600	3.85	5.75
750	4.88	11.83
900	2.28	4.35
913	1.21	3.56
925	0.96	1.88
950	1.18	-0.14
975	3.53	4.14
990	7.16	12.30

Figure 8-57: Standard deviation increase for the fixed inlet link at 0.3 m and 1.0 m observable wave heights calibration adjusted.

all three measurement sets, as well as the calibration adjusted standard deviations for 0.3 m and 1.0 m observable wave heights in Figure 8-59.

Once the data has been collected, the standard deviation is calculated in mW and converted to percentile of the average measured power. The raw data is then adjusted to remove the calibration standard deviation to eliminate any effects of the measurement hardware. The adjusted results are given in Figure 8-59. Factors of error in this process should certainly include the possibility of RF energy being measured originating for equipment other than the RF source. Clearly, examining the measured results, the standard deviation has increased between the 0.3 m observable wave height and the 1.0 m observable wave height for all but one frequency. The standard deviation for the 1.0 m wave was measured up to 12% whereas the maximum measured value for the 0.3 m observable wave height was only 7%. Thus, although the sea surface at the shoreline and respective measurements are anticipated to be significantly different than those that would be obtained in a fully developed deep sea location, the measured data supports the basic result obtained by FDTD marine communications channel simulation that an increase in observable wave height for a random sea surface will produce an increase in the standard deviation of the received power between a transmitter and receiver propagating over a body of sea water.

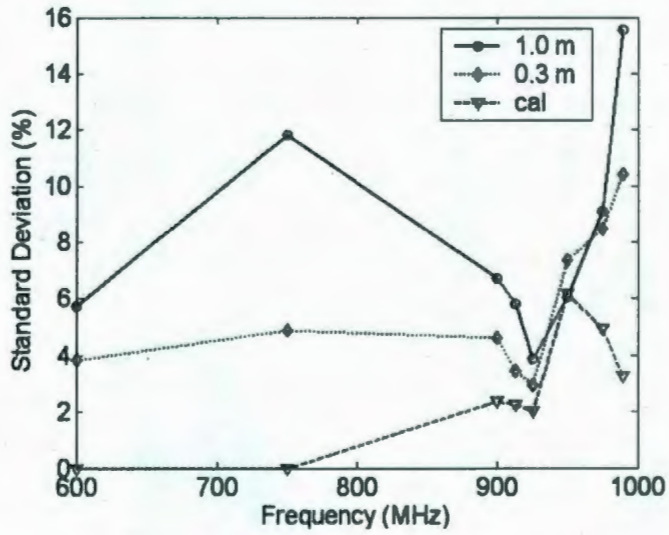


Figure 8-58: The raw standard deviation for the .3 m, 1 m observable wave heights compared to the standard deviation observed during the land based calibration process.

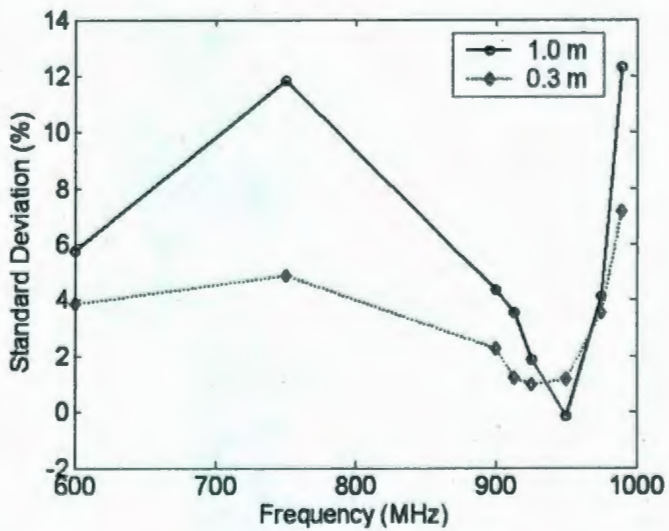


Figure 8-59: The standard deviation increase for the .3 m and 1 m observable wave heights adjusted by calibration results.

Chapter 9

Conclusion

This research effort has introduced new techniques in evaluating communication channel propagation effects during sea surface shadowing conditions in the marine environment. Two distinctly different modeling methodologies were developed to support system design for the marine communications channel. First, the marine geometrical theory of diffraction was developed as an extension of the geometrical theory of diffraction. Through the Marine GTD, diffraction analysis can be estimated requiring only knowledge of the sea surface height and the TX and RX location in proximity to a wave peak. Second, a marine communications channel modeling methodology was developed and implemented using the finite difference - time domain method. This method uses a highly accurate transient approach to obtain direct solutions to Maxwell's equations to evaluate propagation over a random sea surface. The random sea surface is synthesized using the Pierson-Moskowitz spectral model. The numerical analysis method has produced novel parameterized channel performance models that can be used to quantify the effects of the sea surface on wireless communications as functions of sea surface height and frequency. This has not previously been possible. The objective of this research effort has been to study the effects of the sea surface on the marine communications channel, namely path loss during shadowing conditions, contribution of fading to the path loss equation, and to quantify the effects such that

they can be represented accurately in the link budget component of the system design process. By development of the Marine GTD, a fast convenient procedure is devised to estimate diffraction loss based on the single highest peak of a sea surface. Though based on the geometrical theory of diffraction, which has proved very accurate for terrain features on land, the methodology is still an approximation of a more complex sea surface profile. Such an approach is characteristic of models such as the knife edge that approximate physical features by simpler geometries. In contrast, the numerical methodology developed in this work is centered around propagation analysis using the FDTD method. This approach offers a more accurate depiction of both the sea surface and the electromagnetic propagation effects. That is, the overwater radio propagation analysis is conducted by highly accurate electromagnetic simulation providing analysis of all propagation phenomena, and furthermore, the sea surface is comprised of many superposed waves that more accurately reflects the sea surface. The numerical methodology has made a general study possible for the north North Atlantic region, and the advantage of retaining the details of the sea surface has made synthesis of performance models that relate propagation effects directly to observable sea surface height possible. All software developed in this research was developed in Matlab. Both the FDTD software and the numerical analysis conducted to synthesize the relevant parameters of the Marine GTD used no commercially or privately available products. The Marine GTD and numerical methods proved effective in comparison to the widely accepted knife edge diffraction model, which was used as a benchmark to judge the validity and ensure the accuracy of the Marine GTD and the FDTD based numerical methodology to calculate diffraction loss.

The marine geometrical theory of diffraction has been formulated to quickly estimate diffraction effects from a single sea surface wave as an extension of the geometrical theory of diffraction. This methodology offers a pragmatic solution for the system designer to obtain insight into the diffraction effects of the sea surface for waves up to 25 m in height. The profile of the obstructing wave is based on the Pierson-Moskowitz

spectral model. Solutions are readily available from the analytic form for a known channel topology. The Marine GTD can be used in the same manner as the well known knife edge diffraction model, with the added benefit of the increased accuracy in typical of diffraction calculations using the geometrical theory of diffraction. The Marine GTD methodology was developed by synthesizing parameters pertinent to the GTD specifically for the sea surface such that it retains closer physical form to the obstructing wave. It is suitable for estimation of diffraction effects in the link budget analysis segment of the system design process. Although this formulation is based on the modified Pierson-Moskowitz spectral functions for the north North Atlantic, the methodology presented in this work can be used to develop similar models for any other region, provided the pertinent spectral model is available. The formulation of this model was generated by parameterizing all aspects as functions of observable sea surface height, and thus use of the Marine GTD requires no knowledge of the physical shape of the sea surface. Compared to the knife edge diffraction calculations for a common topology, the Marine GTD gave comparable diffraction results where discrepancies were typical for terrestrial measurement studies comparing the GTD and knife edge models.

The second methodology developed in this work for marine communications channel modeling is a numerical approach that uses the finite difference - time domain method. This methodology was implemented in Matlab, such that marine propagation analysis was possible through transient electromagnetic analysis methods without the use of any commercial software. All segments were developed specifically for this effort. The combination of the three independent components including the PM sea surface synthesis, FDTD electromagnetic simulation implementation, and the path loss equation characterization algorithm have been combined to produce a novel methodology for the purpose of transient propagation analysis of the the marine communications channel. Overwater propagation is simulated numerically by obtaining direct solutions to Maxwell's equations recursively. As a key advantage, the method-

ology retains detailed knowledge of the sea surface over which propagation occurs, overcoming the key difficulty when conducting measurement based studies. The sea surface is implemented as a perfect conducting boundary during propagation analysis in the FDTD engine. For sea surface shadowing conditions, novel parameterized channel performance models based on both frequency and observable wave height have been developed in a manner that has not previously been possible. Models developed as a result of this effort include the path loss exponent, the standard deviation of the random contribution to the path loss equation. Transient models obtained by this study include the mean excess delay, the root mean square delay, delay profiles by dB, and the Rice factor which are parameterized as functions of observable wave height. These models are compact, convenient, require no detailed knowledge of the sea surface and are intended to quantify effects of the marine communications channel during the link budget calculations of the general wireless communications system design process.

The validity of the FDTD implementation is assessed through diffraction analysis upon an ideal knife edge structure. Numerical results obtained through simulation from the FDTD implementation are compared to the analytic solution given by the knife edge equation. Free space propagation is also used as a benchmark, as the FDTD tool is also supported by accurate calculations of the path loss exponent and speed of light calculations in free space. The numerical results proved to be in very good agreement with the analytical knife edge equation, as well as the free space path loss exponent and determination of the speed of light. A brief measurement agenda was also conducted at an inshore location to confirm the generalized result that standard deviation of the random contribution in the path loss equation increases with observable wave height. Though the measurement effort cannot verify the parameterized channel performance models developed for deep sea locations with fully developed seas, the measurement agenda does support the qualitative claim that standard deviation does increase with observable wave height. The difficulties that were observed

in the numerical analysis and implementation of the FDTD simulation tool included boundary condition errors and the limitation of the physical size of the channel by available computer memory. The boundary condition errors experienced in this work are typical of all FDTD implementations, and can be decreased by increasing the cells allocated to the absorbing perimeter of the finite difference grid. The 2D cross section approach to channel simulation is limited by available physical memory at this time of modern computing hardware. 3D simulations prefaced by 2D work, as has been the progression of most previous computational electromagnetics approaches, will be possible in the future.

Overall, the objective for which this research was undertaken has been achieved. The goal of development of new methodologies for studying marine communications channel effects has produced novel theoretically-based and numerical methods to quantify sea surface shadowing effects on channel performance in both the time and frequency domain. Practical channel performance models that are parameterized in regard to both frequency and sea surface height provide a means to quantify channel effects of the sea surface, and are well suited for use in link budget calculations. It is the author's hope that these results find their way to the system level designer, and that the novel models produced during this research provide insight in the system design process such that wireless communications links developed for the purpose of general maritime traffic and life saving devices are ultimately designed with increased robustness and reliability such that they have benefited from this research endeavor.

Bibliography

- [1] I. Timmins and S. O'Young, "Marine communications channel modeling using the fdtd method," *IEEE Transactions on Vehicular Technology*, vol. 58, no. 6, pp. 2626-2637, 2009.
- [2] G. Wigley and J. M., "A low cost, high performance reconfigurable computing based unmanned aerial vehicle," *IEEE Aerospace Conference 2006*, pp. 1-13, 2006.
- [3] R. Bennett, "Satellite relay for unmanned air vehicle data," *IEEE Proceedings of Military Communications Conference*, vol. 3, pp. 1146-1150, 1992.
- [4] J. Evans, "Satellite systems for personal communications," *Proceedings of the IEEE*, vol. 86, pp. 1325-1341, July 1998.
- [5] C. Yoo and I. Ahn, "Low cost gps/ins sensor fusion system for uav navigation," *IEEE Proceedings of Digital Avionics Systems Conference*, vol. 2, pp. 8.A.1-1-8.A.1-9, 2003.
- [6] I. Timmins, "Communications channel modeling in the maritime environment using the finite difference - time domain method," *UVS Canada Conference*, pp. 77-81, 2007.
- [7] A. Ayyagari, J. Harrang, and S. Ray, "Airborne information and reconnaissance network," *IEEE Proceedings of Military Communications*, vol. 1, pp. 230-234, 1996.

- [8] A. Ryan, M. Zennaro, A. Howell, R. Sengupta, and J. Hedrick, "An overview of emerging results in cooperative uav control," *43rd IEEE Conference on Decision and Control December 2004*, pp. 602-607, 2004.
- [9] K. Crowe and R. Raines, "A model to describe the distribution of transmission path elevation angles to the iridium and globalstar satellite systems," *IEEE Communications Letters*, vol. 3, pp. 242-244, August 1999.
- [10] H. Keller, H. Salzwedel, G. Schorcht, and V. Zerbe, "Comparison of the probability of visibility of the most important currently projected mobile satellite systems," *IEEE Vehicular Technology Conference*, vol. 1, pp. 238-241, 1997.
- [11] R. Lewis and I. Timmins, "A predictive algorithm for enhanced situational awareness," *UVS Canada Conference*, 2004.
- [12] I. Timmins, D. Stikeleather, W. Everette, S. Vaden, S. Seo, L. Burtseva, and J. Yanik, "Telecommunication connectivity system," *United States Patent 7,690,921*, April 2010.
- [13] I. Timmins, D. Stikeleather, W. Everette, S. Vaden, S. Seo, L. Burtseva, and J. Yanik, "Telecommunications connectivity system and associated patch panel mounting system," *United States Patent 7,448,875*, November 2008.
- [14] I. Timmins, M. Leins, S. Hayes, and R. Bassman, "Information handling system including a bus in which impedance discontinuities associated with multiple expansion connectors are reduced," *United States Patent 6,868,467*, March 2005.
- [15] I. Timmins, M. Leins, S. Hayes, and R. Bassman, "Method and system for reducing aggregate impedance discontinuity between expansion connectors," *United States Patent 6,978,333*, December 2005.

- [16] I. Timmins and K.-L. Wu, "An efficient and systematic approach to model extraction for passive microwave circuits," *IEEE Transactions on Microwave Theory and Technique*, vol. 48, no. 9, pp. 1565–1573, 2000.
- [17] K. Gupta, R. Garg, and R. Chadra, *Computer Aided Design of Microwave Circuits*. Artech House, Norwood MA, 1981.
- [18] M. Medley Jr., *Microwave and RF Circuits: Analysis Synthesis and Design*. Artech House, Norwood MA, 1993.
- [19] M. Hata and T. Nagatsu, "Mobile location using signal strength measurements in cellular systems," *IEEE Transactions on Vehicular Technology*, vol. 29, pp. 245–251, 1980.
- [20] M. Feuerstein, K. Blackard, T. Rappaport, S. Seidel, and H. Xia, "Path loss, delay spread, and outage models as functions of antenna height for microcellular system design," *IEEE Transactions on Vehicular Technology*, vol. 43, pp. 487–498, August 1994.
- [21] V. Erceg, L. Greenstein, S. Parkoff, A. Gupta, B. Kulic, A. Julius, and R. Jastrzab, "An empirically-based path loss model for wireless channels in suburban environments," *IEEE Journal on Selected Areas in Communications*, vol. 17, pp. 1205–1211, July 1999.
- [22] S. Ohmori, A. Irimata, H. Morikawa, Y. Kondo, K. and Hase, and S. Miura, "Characteristics of sea reflection fading in maritime satellite communications," *IEEE Transactions on Antennas and Propagation*, vol. AP-33, pp. 838–845, August 1985.
- [23] M. Yacoub, *Foundations of Mobile Radio Engineering*. CRC Press, Boca Raton, FL., 1993.

- [24] B. Sklar, "Rayleigh fading channels in mobile digital communications part i: Characterization," *IEEE Communications Magazine*, July 1997.
- [25] I. Timmins, "Cellular distribution system using structured cabling improves in-building cell service," *Bicsi News*, vol. 30, no. 9, pp. 24–27, 2009.
- [26] G. Durgin and T. Rappaport, "Theory of multipath shape factors for small-scale fading wireless channels," *IEEE Transactions on Antennas and Propagation*, vol. 48, pp. 682–693, May 2000.
- [27] Y. Ogawa, M. Ohmiya, and K. Itoh., "A shipborne fading reduction antenna system for maritime satellite communications," *IEEE Transactions on Antennas and Propagation*, vol. AP-32, pp. 724–725, July 1984.
- [28] T. Fossen, *Guidance and Control of Ocean Vehicles*. John Wiley and Sons, New York, New York, 1995.
- [29] K. Chamberlin and R. Luebbers, "An evaluation of longly-ricc and gtd propagation models," *IEEE Trans. Ant. Prop.*, vol. AP-30, no. 6, pp. 1093 – 1098, 1982.
- [30] A. Taflove and A. Hagness, *Computational Electrodynamics: The Finite-Difference Time-Domain Method: 2nd Edition*. Artech House, Norwood MA, 2000.
- [31] R. Mognia, I. Bahl, and P. Bhartia, *RF and Microwave Coupled-Line Circuits*. Artech House, Norwood MA, 1999.
- [32] R. Sato and H. Shirai, "Simplified analysis for indoor propagation of a wlan channel," *IEEE Topical Conference on Wireless Communication Technology*, pp. 248–249, 2003.

- [33] B. Urgan and J. Johnson, "Time statistics of propagation over the ocean surface: A numerical study," *IEEE Trans on Geoscience and Remote Sensing*, vol. 38, pp. 1626-1634, July 2000.
- [34] W. Mohr, "Wideband propagation measurements of mobile radio channels in mountainous areas in the 1800 mhz frequency range," *IEEE Vehicular Technology Conference*, pp. 49-52, 1993.
- [35] P. Pugh, R. Bultitude, and P. Vigernon, "Path loss measurements with low antennas for segmented wideband communications at vhf," in *IEEE Military Communications Conference*, pp. 1-5, September 2006.
- [36] K. Yonezawa, T. Maeyama, H. Iwai, and H. Harada, "Path loss measurements in 5 ghz macro cellular systems and consideration of extending existing path loss prediction methods," *IEEE Wireless Communications and Networking Conference*, vol. 1, pp. 279-283, 2004.
- [37] X. Zhao, L. Razoumov, and L. Greenstein, "Path loss estimation algorithms and results for rf sensor networks," *IEEE Vehicular Technology Conference*, vol. 4, pp. 4593-4596, 2007.
- [38] Y. Karasawa and T. Shiokawa, "Characteristics of l-band multipath fading due to sea surface reflection," *IEEE Transactions on Antennas and Propagation*, vol. AP-32, pp. 618-623, June 1984.
- [39] A. Mondloch, "Overwater propagation of millimeter waves," *IEEE Ants and Prop*, vol. AP-17, pp. 82-85, January 1969.
- [40] T. Inoue and T. Akiyama, "Propagation characteristics on line-of-sight over-sea paths in japan," *IEEE Ants and Prop*, vol. AP-22, pp. 557-565, July 1974.

- [41] C. Beard and I. Katz, "The dependence of microwave radio signal spectra on ocean surface roughness," *IRE Transactions on Antennas and Propagation*, vol. 5, no. 2, pp. 183 – 191, 1957.
- [42] C. Beard and I. Katz, "Coherent and incoherent scattering of microwaves from the ocean," *IRE Transactions on Antennas and Propagation*, vol. 9, no. 5, pp. 470 – 483, 1961.
- [43] A. Lagrone, A. Straiton, and H. Smith, "Synthesis of radio signals on overwater paths," *IRE Transactions on Antennas and Propagation*, vol. 3, pp. 48 – 52, April 1955.
- [44] T. Rappaport, S. Seidel, and R. Singh, "900-mhz multipath propagation measurements for u.s. digital cellular radiotelephone," *IEEE Transactions on Vehicular Technology*, vol. 39, pp. 132-139, May 1990.
- [45] K. Blackard, M. Feuerstein, T. Rappaport, and S. Seidel, "Path loss and delay spread models as functions of antenna height for microcellular system design," *IEEE Conference on Vehicular Technology*, vol. 1, pp. 333-337, 1992.
- [46] S. Seidel, T. Rappaport, S. Jain, and R. Singh, "Path loss, scattering, and multipath delay in four european cities for digital cellular and microcellular radiotelephone," *IEEE Transactions on Vehicular Technology*, vol. 40, pp. 721-730, November 1991.
- [47] B. Sklar, "Rayleigh fading channels in mobile digital communications part ii: Mitigation," in *IEEE Communications Magazine*, September 1997.
- [48] D. M. Sullivan, *Electromagnetic Simulation Using the FD-TD Method*. IEEE Press, NY, 2000.

- [49] B. Urgan and J. Johnson, "Numerical simulations of propagation over a time varying ocean surface," *IEEE Proceedings of Antennas and Propagation Society International Symposium*, vol. 1, pp. 80-83, May 1998.
- [50] S. Ohmori and S. Miura, "A fading reduction method for maritime satellite communications," *IEEE Transactions on Antennas and Propagation*, vol. AP-31, pp. 184-187, January 1983.
- [51] E. Ebuchi, H. Kawamura, and Y. Toba, "Physical processes of microwave backscattering from laboratory wind-generated wave surface," *IEEE Geosensing and Remote Sensing Symposium*, vol. 2, pp. 773-775, 1993.
- [52] A. Colliander, P. Yla-Oijala, and J. Pullianen, "Electromagnetic scattering from ocean surface using single integral equation and adaptive integral method," *IEEE Proceedings of Geoscience and Remote Sensing Symposium*, pp. 413-416, 2004.
- [53] D. Barrick, "First-order theory and analysis of mf/hf/vhf scatter from the sea," *IEEE Transactions on Antennas and Propagation*, vol. AP-20, pp. 1-10, January 1972.
- [54] D. Green and E. Gill, "Extracting wind parameters from high frequency ground wave backscatter," *IEEE Antennas and Propagation International Symposium*, pp. 696-699, 2005.
- [55] H. He, H. Liu, F. Zeng, and G. Yang, "A way to real-time ocean wave simulation," *IEEE Proceedings of International Conference on Computer Graphics, Imaging and Vision*, pp. 409-415, 2005.
- [56] N. Blaunstein and Y. Ben-Shimol, "Prediction of frequency dependence of path loss and link-budget design for various terrestrial communications links," *IEEE Transactions on Antennas and Propagation*, vol. 52, pp. 2719-2729, October 2004.

- [57] R. Kouyoumjian and P. Pathak, "A uniform geometrical theory of diffraction for an edge in a perfectly conducting surface," *Proceedings of the IEEE*, vol. 62, no. 11, pp. 1448 – 1461, 1974.
- [58] J. Keller, "Geometrical theory of diffraction," *J. Opt. Soc. Amer.*, vol. 52, pp. 116– 130, 1962.
- [59] J. Keller, "The geometric optics theory of diffraction," *McGill Symposium Microwave Optics A.F. Cambridge Research Center, Rep. TR-59-118*, pp. 207 – 210, 1959.
- [60] B. W. Pathak, P.H. and R. Marhefka, "A uniform gtd analysis of the diffraction of electromagnetic waves by a smooth convex surface," *IEEE Trans. Ant. Prop.*, vol. AP-28, no. 5, pp. 631 – 642, 1980.
- [61] R. Luebbers, "Propagation prediction for hilly terrain using gtd wedge diffraction," *IEEE Trans. Ant. Prop.*, vol. AP-32, no. 9, pp. 951 – 955, 1984.
- [62] H. Mokhtari and P. Lazaridis, "Comparative study of lateral profile knife-edge diffraction and ray tracing technique using gtd in urban environment," *IEEE Transactions on Vehicular Technology.*, vol. 48, no. 1, pp. 255–261, 1999.
- [63] J. Cashman, "Comments on a uniform geometrical theory of diffraction for an edge in a perfectly conducting surface," *IEEE Ants and Prop*, vol. AP-25, no. 3, pp. 477 – 451, 1977.
- [64] H. Mokhtari and P. Lazaridis, "Comparative study of lateral profile knife-edge diffraction and ray tracing technique using gtd in urban environment," *IEEE Veh. Tech.*, vol. 48, no. 1, pp. 255 – 261, 1999.
- [65] J. Rodriguez, J. Molina-Garca-Pardo, and L. Juan-Llcer, "An improved solution expressed in terms of utd coefficients for multiple-building diffraction of plane waves," *IEEE Ant. Prop. Letters*, vol. 4, pp. 16 – 19, 2005.

- [66] P. Husser, "A uniform gtd treatment of surface diffraction impedance and coated cylinders," *IEEE Ants and Prop*, vol. AP-46, no. 7, pp. 998-1008, 1998.
- [67] R. Luebbers, "A heuristic utd slope diffraction coefficient for rough lossy wedges," *IEEE Ants and Prop*, vol. AP-37, no. 2, pp. 206-211, 1989.
- [68] D. N. Rouviere, J.-F. and P. Combes, "Diffraction by lossy dielectric wedges using both heuristic utd formulations and fdtd," *IEEE Ants and Prop*, vol. AP-47, no. 11, pp. 1702 - 1708, 1999.
- [69] N. Zhu and F. Landstorfer, "Numerical study of diffraction and slope-diffraction at anisotropic impedance wedges by the method of parabolic equation: Space waves," *IEEE Ants and Prop*, vol. AP-45, no. 5, pp. 822 - 828, 1997.
- [70] K. Yee, "Numerical solution of initial boundary value problems involving maxwell's equations in isotropic media," *IEEE Transactions on Antennas and Propagation*, vol. AP-14, pp. 302-307, May 1966.
- [71] H. Johnson and M. Graham, *High-Speed Digital Design - A Handbook of Black Magic*. Prentice Hall, Upper Saddle River, NJ, 1993.
- [72] S. Hall, G. Hall, and J. McCall, *High-Speed Digital System Design - A Handbook of Interconnect Theory and Design Practices*. John Wiley and Sons, NY, 2000.
- [73] C. Balanis, *Antenna Theory Analysis and Design 2nd Edition*. John Wiley and Sons, New York, NY., 1997.
- [74] K. Carver and J. Mink, "Microstrip antenna technology," *IEEE Transactions on Antennas and Propagation*, vol. AP-29, pp. 2-24, January 1981.
- [75] R. Mailloux, *Phased Antenna Array Handbook, 2nd Edition*. Artech House, Norwood MA, 2005.

- [76] R. Harrington, *Field Computation by Moment Methods*. McMillan, New York, NY, 1968.
- [77] R. Luebbers, "Finite conductivity uniform gtd versus knife edge diffraction in prediction of propagation path loss," *IEEE Trans. Ant. Prop.*, vol. AP-32, no. 1, pp. 70 – 76, 1984.
- [78] W. Press, S. Teukolsky, W. Vetterling, and B. Flannery, *Numerical Recipes in FORTRAN, 2nd Edition*. Cambridge University Press, New York, NY., 1992.
- [79] B. Kinsman, *Wind Waves: Their Generation and Propagation on the Ocean Surface*. Dover Publishing Inc., Mineola, NY, 1965.
- [80] G. Stuber, *Principles of Mobile Communication, 2nd Edition*. Kluwer Academic Publishers, Norwell, MA, 2001.
- [81] W. Blair and M. Brandt-Pearce, "On the probability distribution of monopulse measurements in the presence of sea-surface induced multipath," in *29th South-eastern Symposium on System Theory (SSST '97)*, pp. 445–449, September 1997.
- [82] D. Lacroix, C. Despins, G. Delisle, and V. Spiegel, "Impulse response measurements in the uhf and shf bands for outdoor microcellular quasi-static environments," *IEEE Global Telecommunications Conference*, vol. 3, pp. 1584–1588, 1997.
- [83] W. Elliot, "Results of a vhf propagation study," *IEEE Transactions on Antennas and Propagation*, vol. 29, pp. 808–811, September 1981.
- [84] J. Anderson, T. Rappaport, and S. Yoshia, "Propagation measurements and models for wireless communications channels," *IEEE Communications Magazine*, pp. 42–49, January 1995.

- [85] T. Rappaport, S. Seidel, and K. Takamizawa, "Statistical channel impulse response models for factory and open plan building radio communication system design," *IRE Transactions on Communications*, vol. 39, pp. 794 – 807, May 1991.
- [86] D. Pozar, *Microwave Engineering*. Addison Wesley, Reading MA, 1993.
- [87] A. Taflove and K. Umashankar, "The finite-difference time-domain method for numerical modeling of electromagnetic scattering," *IEEE Transactions on Magnetics*, vol. 25, pp. 3086–3091, July 1989.
- [88] J. Carpentier, S. Gellida, D. Gloria, G. Morin, and H. Jaouen, "Comparison between s-parameter measurements and 2d electromagnetic simulations for microstrip transmission lines on bimos process," *Proceedings of the International Conference Microelectronic Test Structures*, pp. 235 – 240, 2000.
- [89] R. Garg, P. Bhartia, I. Bahl, and A. Ittipiboon, *Microstrip Antenna Design Handbook*. Artech House, Norwood MA, 2000.
- [90] K. Umanshankar and A. Taflove, "A novel method to analyze electromagnetic scattering of complex objects," *IEEE Transactions on Electromagnetic Compatibility*, vol. 23, pp. 377–382, 1981.
- [91] A. Taflove and M. Brodwin, "Numerical solution of steady state electromagnetic scattering problems using the time-dependent maxwell's equations," *IEEE Transactions on Microwave Theory and Techniques*, vol. 23, pp. 623–730, 1975.
- [92] C. Paul, *An Introduction to Electromagnetic Compatibility*. John Wiley and Sons, NY, 1992.
- [93] N. Herscovici, M. Osorio, and C. Peixeiro, "Miniaturization of rectangular microstrip patches using genetic algorithms," *IEEE Antennas and Wireless Propagation Letters*, vol. 1, pp. 94–97, 2002.

- [94] C. Steele, *Numerical Computation of Electric and Magnetic Fields: 2nd Edition*. Chapman and Hall, NY, 1997.
- [95] J. Schneider and C. Wagner, "FDTD dispersion revisited: Faster-than-light propagation," *IEEE Microwave and Guided Wave Letters*, vol. 9, pp. 54-56, 1999.
- [96] P. Hwang, "Wavenumber spectrum of intermediate-scale ocean surface waves," *IEEE Proceedings of Geoscience and Remote Sensing Symposium*, vol. 1, pp. 272-275, 2005.
- [97] J. Johnson, J. Toporkov, and G. Brown, "A numerical study of backscattering from time evolving sea surfaces: Comparison of hydrodynamic models," *IEEE Transactions on Geoscience and Remote Sensing*, vol. 39, pp. 2411 - 2420, November 2001.
- [98] M. Bachynski and M. Kingsmill, "Effect of obstacle profile on knife-edge diffraction," *IRE Transactions on Antennas and Propagation*, vol. 10, pp. 201 - 205, March 1962.



